Physics – Uspekhi **63** (12) 1188 – 1218 (2020)

REVIEWS OF TOPICAL PROBLEMS PACS numbers: 52.80.Tn, **52.90.+z**, 92.60.Pw

Relativistic runaway electron avalanche

L P Babich

DOI: https://doi.org/10.3367/UFNe.2020.04.038747

Contents

Abstract. Discussed are the genesis of the concept of the relativistic runaway electron avalanche (RREA) and its mechanism as an analog of the Townsend's avalanche, but capable of developing, unlike the latter, in weak thundercloud electric fields. Thanks to this, it was possible to overcome difficulties while interpreting results of observations of penetrating emission enhancements in thunderstorm atmospheres. The main inelastic interactions of high-energy electrons with atomic particles participating in the avalanche development are described; in terms of the drag forces, the essence of the runaway process is discussed; and methods of RREA numerical simulation are described. In approximate historical sequence, results of calculations of the spatial and temporal scales of the avalanche enhancement are analyzed and contemporary data on avalanche macroscopic characteristics are given, which is required for numerical simulations of the runaway electrons in the fluid approximation. As an extension to the relativistic range of the mechanism of the classical cathode-directed streamer, relativistic positive feedback is discussed, by means of which a generation of the RREA series, as a self-sustained process, is supported. Laboratory experiments on RREA modeling are described, in one of which the initial stage of the avalanche was produced.

Keywords: relativistic avalanche, runaway electrons, kinetic equation, Monte Carlo methods, macroscopic characteristics, positive feedback, laboratory experiments

The historical background of the issue is often more interesting than the results obtained.
I P Pavlov (1849–1936),
1904 Nobel Prize winner
in Physiology and Medicine

1. Introduction

Progress in gas discharge physics, a field of plasma physics, from which modern plasma science has been developed with all the wealth and variety of its processes, has been for many years limited to the concepts and results available in widely known monographs [1–4]. Further studies, in essence, have used the same concepts, whatever original approaches were used for their development and new results obtained (see [5–10] and references therein). These concepts are based on the conventional electric breakdown mechanisms: the Townsend and the streamer. The first mechanism, implying the generation of consecutive series of electron avalanches supported by cathode emission, operates at low pressures. The second, which is volumetric, is independent of the cathode emission and operates at high pressures; however, in both cases, the gas is 'dense,' i.e., the concentration of atomic particles N or the pressure P are so high that the free path length λ_e of an electron with energy ε in equilibrium to the electric field

L P Babich Russian Federal Nuclear Center – All-Russian Research Institute of Experimental Physics,
prosp. Mira 37, 607188 Sarov, Nizhny Novgorod region,
Russian Federation
E-mail: leonid.babich52@gmail.com, babich@elph.vniief.ru

Received 29 October 2019, revised 15 March 2020
Uspekhi Fizicheskikh Nauk **190** (12) 1261 – 1292 (2020)
Translated by L P Babich and V L Derbov

Table 1. Configurations and results of the first laboratory experiments in which the generation of accelerated electrons was observed at atmospheric pressure.*

Characteristics of experiment \ Reference	Frankel et al. [13]	Stankevich and Kalinin [16]	Noggle at al. [15]	Tarasova and Khudyakova [17]
Configuration of electrodes	Needle (−) – plane (+)	Rod (−) – plane (+)	Needle (−) – plane (+)	Rode (−) – plane (+)
d, cm	?	0.04	2 – 10	0.5 – 8.5
Cathode, r_{cath}		Cone with rounded top		Hemisphere, $r_{cath} = 6$ mm
Gas	Helium	Air	Helium	Air
τ_{idle}, ns	?	< 2	< 10	$\ll 0.6$
Δt_{idle}**		23 ns	≈ 50 μs	≈ 3 ns
U_{idle}, kV	17	40 – 52	≈ 300	≈ 300
N_{disch}	10^4	1	10,000	1
mR/pulse	< 0.04	0.4	< 0.04	Electrons

* The gas number density equals the Loschmidt number $N_L = 2.688 \times 10^{25}$ m^{-3}; τ_{idle}, Δt_{idle}, U_{idle} are the rise time, duration, and amplitude of the voltage pulse in the no-load mode, respectively; r_{cath} is the radius of curvature of the cathode working surface, d is the interelectrode spacing, N_{disch} is the number of discharges sufficient for reliable registration of radiation.
** Duration of the first oscillation of the decaying no-load voltage waveform.

strength E/N (or E/P) reduced to the concentration N (or pressure P) is much less than the interelectrode spacing d.

Electron motion in a medium under the action of electric force $-e\mathbf{E}$ is described by the Langevin equation:

$$\frac{\mathrm{d}\mathbf{p}}{\mathrm{d}t} = e\mathbf{E} - \boldsymbol{\Gamma}(\mathbf{p}), \tag{1}$$

where $\mathbf{p}$ is the electron momentum, $\mathbf{E}$ is the field strength vector, e is the elementary charge, and $\boldsymbol{\Gamma}(\mathbf{p})$ is the stochastic force responsible for the inelastic (excitation and ionization), elastic, and radiative interactions of the electron with atomic particles.

In the simplest case, Eqn (1) takes the following form:

$$\frac{\mathrm{d}\mathbf{p}}{\mathrm{d}t} = e\mathbf{E} - F(\varepsilon)\,\frac{\mathbf{p}}{p}, \tag{2}$$

where $F(\varepsilon)$ is the drag force caused by the interactions of the electron with atoms (see Section 2).

In the approximation $F(\varepsilon)(\mathbf{p}/p) = \nu m\mathbf{v}_d$, where m is the electron mass and $\nu \approx \sigma N v_e$ is the frequency of electron collisions, in a weak field, when the process develops so slowly that $|(\mathrm{d}\mathbf{p}/p)(v\,\mathrm{d}t)| \ll 1$, transport processes are described in terms of the drift motion of electrons, and the Drude formula follows from Eqn (2), $\mathbf{v}_d = -\mu_e\mathbf{E}$, where $\mu_e = e/(\nu m) = e/(\sigma N m v_e)$ is the mobility depending on velocity v_e of electrons and cross section σ of their collisions with atoms. According to the Drude formula, the drift speed $\mathbf{v}_d$ depends on the local value of E/N. All other average characteristics of the electron ensemble also depend locally on E/N: the average energy $\langle\varepsilon\rangle$, the frequency of ionization by electron impacts ν_{ion}, the Townsend ionization coefficient $\alpha_T = \nu_{ion}/v_d$, etc.

However, in sufficiently strong fields, it is necessary to take into account that the characteristics of the electron ensemble depend not only on the magnitude of E/N in the domain of the ensemble localization but also on its entire prehistory (see [11, 12] and references therein). Right up to the end of the 1960s, an opinion dominated, according to which the local relationship of the integral characteristics of a gas-discharge plasma with E/N is violated only in the range of extremely low pressure magnitudes ($P \ll 1$ atm). This opinion began to change after a few communications were published in the second half of the 1960s, describing the successful registration of penetrating radiation pulses from laboratory discharges in gases of atmospheric density (Table 1).

X-rays, as a manifestation of generating high-energy electrons, were first registered in 1966 by Frankel et al. from discharges in helium [13]. A bit later, Noggle et al., in experiments aimed at modeling electron acceleration in lightning discharges — according to Wilson's hypothesis [14] of the possibility of acceleration of electrons to high energies in thundercloud fields — observed X-rays from discharges in helium [15]. Attempts to detect the radiation from discharges in air were unsuccessful, as were attempts by Frankel et al. in neon.

Even before the publication by Noggle et al., Stankevich and Kalinin [16] observed X-rays as a result of the acceleration of electrons in discharges in the open atmosphere. They focused their attention on high overvoltages relative to the self-sustained breakdown voltage U_{self}. This approach, which turned out to be very productive in the long term, allowed studying high-energy phenomena in discharges in dense gases and discovering earlier unknown phenomena and gas-discharge dependences [11, 12].

The excitation of X-rays in the experiments performed by Frankel et al., Noggle et al., and Stankevich and Kalinin was, most likely, not purely a gas-discharge effect. Because of strongly nonuniform geometry [13, 15] or extremely small interelectrode spacing [16], the field emission electrons could accelerate up to the anode, where they generated bremsstrahlung in the X-ray range. In the paper by Tarasova and Khudyakova [17], the last in a series of four pioneering studies in the late 1960s, in discharges in the open atmosphere with rather long gas-discharge gaps (d up to 10 cm), electrons were accelerated self-consistently with discharge development, i.e., with gas ionization and the formation of

space charges [17]. Tarasova and Khudyakova also used high overvoltages achieved owing to the subnanosecond voltage rise-time; however, interference of emission electrons was excluded by a rather uniform field geometry due to the vast area of the cathode working surface (see Table 1). Subsequent experiments [18] showed that Tarasova and Khudyakova directly detected for the first time high-energy electrons rather than their bremsstrahlung, as in previous experiments [13, 15, 16], and the source of the electrons was the gas-discharge plasma itself, rather than the cathode emission. An electron pulse was generated during the breakdown development at the voltage pulse front. As confirmed by direct measurements, even for discharges in strongly nonuniform fields, when the interference of the field emission with the registered flux of high-energy electrons is possible, the latter, after all, is born in the gas-discharge plasma [19, 20].

In further experiments (see [11, 12, 19–26] and references therein), it was shown that the pulse of accelerated electrons, referred to as runaway (from collisions with atoms [28]) according to Eddington's terminology [27], are generated during the initial stage of discharges in dense gases. The pulse duration is extremely small: thus, discharges in the open atmosphere generate a pulse of runaway electrons (REs) with a duration of hundreds of picoseconds [11, 12, 19, 20, 25]. The RE pulse, via gas pre-ionization, creates conditions for the breakdown and development of a contracted spark channel at sufficiently small d or a volumetric diffuse discharge at large d [11, 12, 23, 24, 26]. The participation of REs in the breakdown leads, in particular, in the case of not too long gas-discharge gaps, to the amplitude of the voltage pulse $U_{\rm idle}$ in the no-load mode not being reached, because, already at the pulse leading edge, the conductivity current limits the voltage rise.

The participation of REs in the breakdown in dense gases, including the open atmosphere, at high overvoltages relative to the $U_{\rm self}$ has been proven in a large number of laboratory experiments [11, 12, 18–26]. In the open atmosphere, the transition of low-energy electrons to the runaway mode in fields whose strength is close to or, all the more so, smaller than the self-sustained breakdown field strength $E_{\rm self} = U_{\rm self}/d = 2.5-3$ MV m^{-1} is unreal. But electrons with sufficiently high initial energy can continue gaining energy in rather weak fields, e.g., according to Wilson's hypothesis [14], those of thunderclouds with a strength of $\approx 0.3-0.4$ MV m^{-1} [10, 29–33].

In the first half of the 1980s, Parks et al. [34] and McCarthy and Parks [35] registered aboard a plane inside a thundercloud rather prolonged (duration more than 1 s) X-ray emission (according to the modern terminology, the glow [36, 37]) with photon energies above 100 keV. The radiation preceded a lightning discharge and disappeared synchronously with the discharge. It was impossible to explain the recorded radiation intensity [29] in the framework of Wilson's hypothesis [14] as a result of the acceleration in a thundercloud field of secondary high-energy electrons produced in the atmosphere by cosmic rays [30] or, as Wilson assumed, as a result of the decay of atmospheric radionuclides.

Based on the observational data [34, 35], in particular, taking into account that the observed X-rays and, therefore, the generation of electrons responsible for them preceded the lightning discharges, and in view of the negative result of the analysis [29], Gurevich, Milikh, and Roussel-Dupré proposed and substantiated a mechanism of the runaway breakdown in atmosphere [30] in a relatively weak thundercloud field (referred to below as the GMR mechanism). It is known that, during the transport of relativistic electrons in a substance, secondary electrons are generally born in the low-energy range; therefore, extremely rare events with the production of high-energy electrons are usually ignored. Such events, however, can change the course of the ionization process in a large-scale electric field, such as that of thunderclouds, since sparse secondary electrons with sufficiently high energies also appear to be involved in the runaway mode. As predicted by Gurevich, Milikh, and Roussel-Dupré, this results in the development of a relativistic runaway electron avalanche (RREA), i.e., a process of an exponential rise of the number of high-energy electrons.

RREA development is followed by a reproduction, also exponential, of low-energy electrons, a corresponding growth of the conductivity, and, as a result, according to Gurevich, Milikh, and Roussel-Dupré, a breakdown in fields weaker ($E < E_{\rm self}$) than required for the usual breakdown with the participation of low-energy electrons at the tails of the electron distribution function (EDF) with energies above the ionization energy $\varepsilon_{\rm ion}$ of the gas atoms and molecules. This new process, as a development of the hypothesis by Wilson [14], was proposed by the authors of [30] to explain the phenomena in a thunderstorm atmosphere. From the first calculations, it became clear that the characteristic length $l_{\rm e}$ of the RREA e-fold enhancement is tens of meters and increases with a decrease in the concentration $N_{\rm mol}$ of air molecules, i.e., with altitude above sea level. Therefore, receiving an RREA in the laboratory is practically impossible because of the restricted sizes of high-voltage installations. But thundercloud fields are generated in such vast atmosphere domains that many-fold multiplication of an RREA is possible.

A fundamental difference between the avalanche processes and electric breakdown with REs observed in laboratory and RREAs from the GMR mechanism is that the former are developed in strong and superstrong fields with the strength $E \gg E_{\rm self}$, while the latter was predicted for relatively weak thundercloud fields, the observed magnitude of which, $E \approx 0.3-0.4$ MV m^{-1}, is by 10 times smaller than $E_{\rm self}$. The breakdown in gases at high overvoltages, occurred under the action of high-voltage pulses with sub-nanosecond and nanosecond leading edges, is initiated by the pulsed process of field emission [6, 8, 11, 12], while high-energy electrons, initiating atmospheric RREAs, are permanently generated by cosmic radiation.

It is worth noting that the breakdown according to the GMR mechanism substantially differs from that with REs participating in laboratory discharges also by the fact that, in the latter case, avalanches and streamers easily develop. Therefore, REs, generally speaking, are not necessary for the breakdown, though, of course, they significantly affect the discharge space-time characteristics, whereas, in the GMR mechanism, the REs are essentially required, because low-energy avalanches and streamers cannot develop in weak fields.

Observations of REs in laboratory discharges in strong fields is by no means a justification of the Wilson hypothesis [14] about the possibility of the acceleration of electrons to high energies in extended, but weak, thundercloud fields. On the contrary, the GMR mechanism is a direct development of Wilson's hypothesis. At present, it is a cornerstone of the physics of the high-energy processes in a thunderstorm atmosphere, which are responsible for the generation of the penetrating radiation observed in the thunderstorm atmosphere (see reviews [37–40] and references therein) and

predicted for the atmospheres of other planets in the Solar System [41, 42]. RREA development in a thundercloud in the cosmic radiation field is capable of creating conditions (preconditioning [30]) necessary for triggering lightning discharges [43–49].

The present paper is motivated by the growing interest in high-energy atmospheric electricity. The review is restricted to publications devoted to the RREA itself. Those studies in which the RREA characteristics are used to analyze and numerically simulate observational results on thunderstorm penetrating emissions and lightning discharges are not discussed. Reviews [37–40] are devoted to the results of experimental studies of high-energy processes in the thunderstorm atmosphere without a description of the RREA concept genesis or the history and methods of obtaining the RREA characteristics. The history of calculating the RREA characteristics is instructive and can engage the interested reader.

The review is organized as follows. In Sections 2 and 3, the main inelastic interactions of high-energy electrons with atomic particles are described in terms of the drag forces, and the essence of the runaway process is presented. In Section 4, the results of the first calculations of the characteristic time of RREA enhancement are analyzed. In Section 5, methods of RREA numerical simulation are described. The results of calculations of the RREA parameters are discussed in Sections 6 and 7 approximately in historical sequence. Section 8 discusses a mechanism of relativistic positive feedback capable of supporting the generation of a RREA series as a self-sustained process. Finally, in Section 9, laboratory experiments undertaken for RREA modeling are described.

2. Drag forces

High energy electrons in the media of atomic particles collide with nuclei and electron shells. As a result, they change the direction of their motion and lose kinetic energy $\varepsilon = (\gamma - 1)mc^2$, where $\gamma = (1 - \beta^2)^{-1/2}$, $\beta = v/c$, v is the electron velocity, and c is the speed of light, in inelastic (excitation and ionization) and radiative interactions, which in the physics of high-energy atmospheric electricity are usually described integrally in terms of the corresponding drag forces $F_{\rm in}(\varepsilon)$ and $F_{\rm rad}(\varepsilon)$ (Fig. 1).

The electron energy losses per unit of path due to inelastic interactions (historically called 'ionization') are calculated in terms of the effective drag κ [50], which in the range of small magnitudes of the momentum transfer $q^2/m = (p' - p)^2/m \ll mc^2$ (excitation and, partially, ionization of atomic shells) is as follows:

$$\kappa^{\rm small} = 2\pi \sum_i n_i Z_i r_{\rm e}^2 mc^2 \, \frac{\gamma^2}{\gamma^2 - 1} \ln\left[q \, \frac{m^2c^4(\gamma^2 - 1)}{2.73I^2} + \frac{1}{\gamma^2}\right], \tag{3}$$

where for molecular gases n_i is the number of atoms with charge Z_i constituting a molecule, $mc^2 \approx 0.511$ MeV is the electron energy at rest, $r_{\rm e} = e^2/(4\pi\varepsilon_0 mc^2) \approx 2.818 \times 10^{-15}$ m is the classical electron radius, and $I \approx 13.5\, Z_{\rm at}$ is the effective energy of the atomic shell ionization in a substance with atomic number $Z_{\rm at}$ (for air, the more accurate values are $I \approx 85.7$ eV [43, 44], $I \approx 80.5$ eV [51]).

In the range of large magnitudes of momentum transfer with the ionization of atomic shells ($q^2/m = (p' - p)^2/m \gg I$)

$$\kappa^{\rm large} = \sum_i n_i Z_i \int_{\varepsilon_1}^{\varepsilon/2} \varepsilon_{\rm s} \sigma_{\varepsilon'}(\varepsilon', \varepsilon_{\rm s}) \, {\rm d}\varepsilon_{\rm s}\,, \tag{4}$$

where $\varepsilon_{\rm s}$ is the energy transferred to a secondary electron, $\varepsilon_1 = q_1^2/m$, $I \ll q_1^2/m \ll mc^2$, i.e., ε_1 is within the overlapping range, and the Möller formula for the cross section of the electron scattering by an immobile free electron is used for the differential ionization cross section $\sigma_{\varepsilon'}(\varepsilon', \varepsilon)$ [50, 52, 53]:

$$\sigma_{\varepsilon'}(\varepsilon', \varepsilon) = 2\pi r_{\rm e}^2 mc^2 \, \frac{\gamma'^2}{\gamma'^2 - 1} \left[\frac{1}{\varepsilon^2} - \frac{1}{\varepsilon(\varepsilon' - \varepsilon)} \, \frac{(2\varepsilon' + mc^2)mc^2}{(\varepsilon' + mc^2)^2} + \frac{1}{(\varepsilon' - \varepsilon)^2} + \frac{1}{(\varepsilon' + mc^2)^2}\right]. \tag{5}$$

As a result, the sum $F_{\rm in}(p) = (\kappa^{\rm small} + \kappa^{\rm large})N_{\rm at} = F_{\rm ex}(p) + F_{\rm ion}(p)$ gives the formula [50, 52, 53] for the specific electron energy losses due to inelastic interactions with the atomic shells ('drag force'):

$$F_{\rm in}(\varepsilon) = \frac{2\pi r_{\rm e}^2 mc^2 N_{\rm at} \sum_i n_i Z_i}{\beta^2} \left[\ln\left(\frac{m^2c^4(\gamma^2 - 1)(\gamma - 1)}{2I^2}\right) - \left(1 + \frac{2}{\gamma} - \frac{1}{\gamma^2}\right)\ln 2 + \frac{1}{\gamma^2} + \frac{(\gamma - 1)^2}{8\gamma^2} - \delta(\gamma)\right], \tag{6}$$

where $N_{\rm at}$ is the atomic concentration, and $\delta(\gamma)$ is the correction due to the density effect, which for air is insignificant below 30 MeV and slowly increases in the range of higher energies.

In the ranges of low ($\gamma \to 1$) and high ($\gamma \gg 1$) energies, Eqn (6) reduces as follows [50, 52, 53]:

$$F_{\rm in}(\varepsilon) \approx \frac{2\pi r_{\rm e}^2 m^2 c^4 N_{\rm at} \sum_i n_i Z_i}{\varepsilon} \, \Lambda\,, \quad \Lambda = \ln \frac{\varepsilon e^{1/2}}{2I}\,, \quad \varepsilon \ll mc^2\,, \tag{7}$$

$$F_{\rm in}(\varepsilon) \approx 2\pi r_{\rm e}^2 mc^2 N_{\rm at} \sum_i n_i Z_i \, \frac{\gamma^2}{\gamma^2 - 1} \, \Lambda\,, \quad \Lambda = \ln \frac{\varepsilon^3}{2I^2 mc^2}\,, \quad \varepsilon \gg mc^2\,. \tag{8}$$

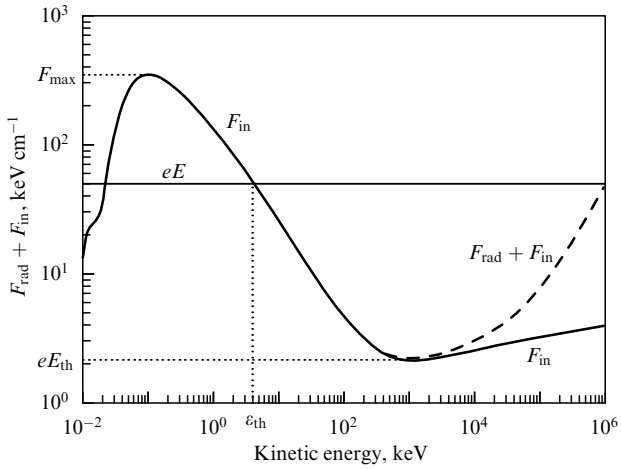

Figure 1. Dependence of electron drag force on kinetic energy in air under STP conditions [37]. $F_{\rm in}$ is the drag force due to excitation and ionization of atomic electron shells, $F_{\rm rad}$ is the force caused by bremsstrahlung, eE is the electric force, $\varepsilon_{\rm th}$ is the energy runaway threshold.

The radiation drag force $F_{\rm rad}(\varepsilon)$ owing to electron bremsstrahlung is described by a formula [52, 54], in which the kinetic energy ε and momentum p are in mc^2 and mc units, respectively:

$$F_{\rm rad}(\varepsilon) = N_{\rm at} r_{\rm e}^2 \alpha \sum_i n_i Z_i \, \Phi\varepsilon \,, \tag{9}$$

where

$$\Phi = \frac{12\varepsilon^2 + 4m^2}{3\varepsilon p} \ln\left(\frac{\varepsilon + p}{m}\right) - \frac{(8\varepsilon + 6p)m^2}{3\varepsilon p^2}\left(\ln\frac{\varepsilon + p}{m}\right)^2 - \frac{4}{3} + \frac{2m^2}{\varepsilon p}\int_0^x \frac{\ln(1+y)}{y}\,{\rm d}y \,, \tag{10}$$

$$x = \frac{2p(\varepsilon + p)}{mc^2} \,.$$

In frequently used limit cases of small and high energies, the formula for $F_{\rm rad}(\varepsilon)$ is significantly simplified [54]:

$$F_{\rm rad} = \frac{16}{3} N_{\rm at} r_{\rm e}^2 \alpha \sum_i n_i Z_i \varepsilon \,, \quad \varepsilon \ll m \,, \tag{11}$$

$$F_{\rm rad} = 4\alpha r_{\rm e}^2 N_{\rm at} \sum_i n_i Z_i \varepsilon \left(\ln\frac{2\varepsilon}{m} - \frac{1}{3}\right), \quad \varepsilon \gg m \,. \tag{12}$$

For a mixture of gases, in the formulas above it is necessary to perform a summation over fractions Δ_j of the components:

$$\sum_j \Delta_j \sum_i n_{j,i} Z_{j,i} \quad \text{and} \quad \sum_j \Delta_j \sum_i n_{j,i} Z_{j,i}^2 \,. \tag{13}$$

For dry air, disregarding the contribution of argon and other minor components and assuming $N_{\rm at} = 2N_{\rm mol}$, we can replace the first of these sums with $Z_{\rm at} \approx 7.25$ [30, 38, 43–45] and the second with the corresponding value of $Z_{\rm at}^2$.

The force $F_{\rm in}$ dominates in the range of relatively low energies, whereas $F_{\rm rad}$ becomes dominating in the energy range significantly exceeding the value [52, 54]

$$\varepsilon_{\rm bound} \approx 1600 \frac{mc^2}{Z_{\rm at}} \,, \tag{14}$$

at which $F_{\rm in} = F_{\rm rad}$; thus, for air ($Z_{\rm at} \approx 7.25$), $\varepsilon_{\rm bound} \approx$ 110 MeV.

3. Elementary idea of the electron runaway process

A rigorous description of the electron runaway effect is possible only within stochastic approaches (see, e.g., [55–57]). Qualitatively, it is possible to clarify the conditions under which an electron moves in a gas medium under the action of an electric force not uniformly in the drift mode but with continuous acceleration, within a deterministic model [11, 12, 23, 24, 58, 59] based on of an equation for the variation in the electron kinetic energy along the coordinate x in the direction of the electric force $\mathbf{e} = -\mathbf{E}/E$:

$$\frac{{\rm d}\varepsilon}{{\rm d}x} = eE\langle\mu\rangle - F(\varepsilon) \,, \tag{15}$$

which is obtained by multiplying Eqn (2) by $\mathbf{p}$. Here, $\langle\mu\rangle$ is the mean cosine of the angle θ between the directions of the vectors $\mathbf{p}$ and $\mathbf{e}$, $F(\varepsilon) = F_{\rm in}(\varepsilon) + F_{\rm rad}(\varepsilon)$ (see Fig. 1).

Function $F_{\rm in}(\varepsilon)$ at the electron kinetic energy $\varepsilon_{\max} \approx 1.36\,I$ reaches a maximum of

$$F_{\rm in}^{\max} = \frac{2\pi r_{\rm e}^2 (mc^2)^2 Z_{\rm at} N_{\rm at}}{2.718\,I} \,,$$

and then, at the energy

$$\varepsilon_{\min} = (\gamma - 1)\,mc^2 \approx 2.39\,mc^2 \approx 1.22 \text{ MeV} \,, \tag{16}$$

passes through a minimum

$$F_{\rm in}^{\min} \approx 21.7 \times 2\pi r_{\rm e}^2 Z_{\rm at} N_{\rm at}\, mc^2 \,, \tag{17}$$

after which it experiences a logarithmic rise (Fig. 1). In air ($N_{\rm at} \approx 2N_{\rm mol}$, $Z_{\rm mol} \approx 2Z_{\rm at} \approx 14.5$ [30, 43–45, 60]) under STP conditions ($N_{\rm mol} = N_{\rm L} \approx 2.688 \times 10^{25}$ m^{-3}), $F_{\rm in}^{\max} \approx$ 23.1 MeV m^{-1}, $\varepsilon_{\max} \approx 110$ keV, $F_{\rm in}^{\min} \approx 217$ keV m^{-1}, $\varepsilon_{\min} \approx 1.22$ MeV. According to semiempirical formulas [61] (see also [11, 12, 59]), which are more accurate in the low-energy range than Eqn (6), $F_{\rm in}^{\max} \approx 35.6$ MeV m^{-1} and $\varepsilon_{\max} \approx 150$ keV. Both estimates of $F_{\rm in}^{\max}$ exceed by more than an order of magnitude the strength of the uniform self-breakdown field $E_{\rm self} = U_{\rm self}/d$ under STP conditions (in different sources 2.5–3 MV m^{-1} [7–10]). Allowing for the angular scattering increases the drag force; thus, $F_{\max}$ increases by approximately 1.5 times [28] and $F_{\min}$ increases by 20–25% [56, 57, 62], the minimum position $\varepsilon_{\min}$ being shifted towards higher energies to approximately 5 MeV [56, 62], which is extremely important for switching on the relativistic positive feedback (see Section 8.3). For electrons with energies below $\varepsilon_{\max}$ to be capable of overcoming the maximum $F_{\rm in}^{\max}$, multiple overvoltages relative to $E_{\rm self}$ are required, such as in the experiments by Tarasova and Khudyakova [17] and in subsequent studies (see [11, 12, 18–26] and references therein).

As seen in Fig. 1, unlike the function $F_{\rm in}(\varepsilon)$, which has two extrema, the radiation losses $F_{\rm rad}(\varepsilon)$ monotonically grow with the energy, and in air, as noted above, they dominate in the range of electron energies above ≈ 110 MeV.

If $eE < F_{\rm in}^{\max}/\langle\mu\rangle$, then the equation

$$eE - \frac{F(\varepsilon)}{\langle\mu\rangle} = 0 \tag{18}$$

has three roots, $\varepsilon_1 < \varepsilon_2 < \varepsilon_3$, from which ε_1 (in the range of the lowest energies) and ε_3 (in the high-energy range) correspond to the steady states of the electronic ensemble, whereas ε_2 corresponds to an absolutely unstable state (Fig. 1) [59]. If $eE > F_{\rm in}^{\max}/\langle\mu\rangle$ and even more so $eE \gg F_{\rm in}^{\max}/\langle\mu\rangle$, electrons of all energies are runaway. If $eE < F_{\rm in}^{\max}/\langle\mu\rangle$, only those electrons whose energies exceed the runaway threshold $\varepsilon_{\rm th}$, which is approximately determined as the second root of Eqn (18), are runaway [11, 12, 30, 51, 59].

4. Spatial and temporal avalanche enhancement scales

RREA, as well as Townsend's avalanche of low-energy electrons [1–8], after a short-term stage of disordered development, comes to a steady exponential rise of the electron number in space and time:

$$N_{\rm e}(t) = N_{\rm e}(t=0) \exp\frac{t}{t_{\rm e}} \,, \tag{19}$$

$$N_e(x) = N_e(x=0)\exp\frac{x}{l_e}\,, \tag{20}$$

where $N_e(t=0)$ and $N_e(x=0)$ are the values of the number of relativistic REs at the initial moment of time and at the origin of the axis x directed along the vector $\mathbf{e} = -\mathbf{E}/E$, respectively; t_e and l_e are the temporal and spatial scales of the avalanche enhancement by e times.

In the steady-state mode, in addition to t_e and l_e, it is also possible to attribute to the avalanche such average macroscopic parameters as the average energy of high-energy electrons $\langle\varepsilon\rangle$, speed $\mathbf{v}_{re}$ along the vector $\mathbf{e}$, and coefficients of diffusion along, $D_\parallel$, and across, $D_\perp$, the direction $\mathbf{e}$. It is conventional to calculate the RREA parameters as functions of the so-called overvoltage [30, 43, 44], i.e., the ratio of the module of electric force eE acting on an electron to the minimum F_{in}^{min} of the drag force $F_{in}(\varepsilon)$ (17) (see Fig. 1):

$$\delta = \frac{eE}{F_{in}^{min}} = \frac{E\,[\mathrm{kV\ m^{-1}}]}{217\,P\,[\mathrm{atm}]}\,. \tag{21}$$

This 'overvoltage' should not be confused with the real overvoltage U_{max}/U_{self} relative to the voltage of the self-sustained breakdown U_{self} [7, 9, 11, 12]; here, U_{max} is the amplitude of a high-voltage pulse reached before the breakdown, which can greatly exceed U_{self}, but is less than the supply voltage in the no-load mode [11, 12].

In the physics of high-energy atmospheric electricity, t_e and $l_e = t_e v_{re}$ are of particular importance, since the inverse quantities $1/t_e$ and $1/l_e$ are relativistic analogs of the ionization frequency ν_{ion} and Townsend's ionization coefficient α_T in low-energy avalanches [1–8]. Due to the need to interpret the results of field observations of thunderstorm-induced penetrating radiation and to localize their sources, the main focus was initially on functions $l_e(\delta)$ and $t_e(\delta)$; the other parameters ($\langle\varepsilon\rangle$, $\mathbf{v}_{re}$, $D_\parallel$, $D_\perp$) were calculated later with the improvement in models of high-energy processes in a thunderstorm atmosphere.

The length l_e, corresponding to the scales of thunderstorm fields, is so great that measuring is impossible; therefore, it remains only to calculate this length from the results of a theoretical analysis and computer simulations. The dependence of l_e on δ was first calculated analytically in the pioneering work [30]. Analytical studies were carried out after that, including those based on the kinetic equation (KE). At the same time, substantially more accurate approaches were developed. The function $t_e(\delta)$ was calculated based on the numerical solution of the KE, for the first time reported in [43], with the ionization integral $J_{ion}(\varepsilon,\mu)$ responsible for producing secondary high-energy electrons [38, 43, 44, 58, 60, 63–66]. It was computed from the results of numerical simulation by the particle-in-cell (PIC) method [67] and the Monte Carlo (MC) technique [63, 65, 68–74], the most adequate for the stochastic nature of the runaway process. In particular, the VNIIEF standard code ELIZA [75] (see Section 5.2.1) was used, which allows for all the variety of electron interactions with atomic nuclei and electron shells, as well as the back effect of the products of these reactions (bremsstrahlung, positrons) on avalanche development [63, 65, 69–72]. A simplified MC (SMC) technique was developed, which is restricted to the description of inelastic interactions by means of drag force $F_{in}(\varepsilon)$ (6) and a stochastic description of the angular scattering and the production of REs [58, 65, 69, 70] (see Section 5.2.3). Values of $t_e(\delta)$ calculated under STP conditions are presented in Table 2. Recalculation to any pressure P or concentration $N_{mol}(z)$ of molecules at a given altitude z is carried out as follows:

$$t_e(P) = \frac{t_e\,(1\ \mathrm{atm})}{P\,(\mathrm{atm})} = t_e(N_L)\,\frac{N_L}{N_{mol}(z)}\,. \tag{22}$$

The original version of the ELIZA code [75] was tested many times in modeling laboratory and field experiments at VNIIEF. Therefore, the results of calculations using the updated version of the code, which includes the electric field and increased accuracy of the elementary interactions description [63, 65, 69–72], were initially considered the most accurate. The ELIZA code can be used to calibrate less full but timesaving computer codes implementing the MC or KE methods. However, to avoid the subjective factor effect, which, as shown below, has negatively manifested itself in the first calculations aimed to refine the results of analysis [30], the results of numerical simulations of $t_e(\delta)$ using the full MC codes and KE solution should be compared with those obtained by methods that are substantially less accurate but transparent, as in Ref. [30].

In Ref. [30], based on the equations (consequences of Eqn (2)) for the module of the electron speed $\mathbf{v}$ and the cosine μ of the angle between the vectors $\mathbf{v}$ and $\mathbf{e}$, including the nonrelativistic expression (7) for the drag force $F_{in}(\varepsilon)$ with $\Lambda = \ln[2\varepsilon/(Z\varepsilon_{ion})]$, where $\varepsilon_{ion} \approx 15$ eV, the following formula was derived:

$$l_e(\delta) = \frac{u_{s0}(\delta)}{2\pi r_e^2 Z_{mol} N_{mol}} \approx 50\,u_{s0}(\delta)\,\frac{N_L}{N_{mol}}\ [\mathrm{m}]\,, \tag{23}$$

in which $u_{s0} = 2\varepsilon_0(\delta)/(mc^2)$, $\varepsilon_0(\delta)$ is the minimum energy of a secondary electron sufficient for the runaway (threshold ε_{th}), and an average charge of $Z_{mol} = 14.5$ is assumed for the nuclei of diatomic nitrogen and oxygen molecules [30].

Equation (23) was derived ignoring the angular scattering of electrons under the assumption that the momentum $\mathbf{p}$ of a secondary electron is orthogonal to the momentum $\mathbf{p}'$ of the primary RE, and F_{in}^{min} is expressed as $F_{in}^{min} = 4\pi r_e^2 mc^2 Z_{mol} N_{mol} a$, which, with the accepted value of $a \approx 10$ [30], practically coincides with Eqn (17). Later values of $a \approx 11$ [38, 60] and 11.2 [44] were obtained, apparently, for other values of Z_{mol} and ε_{ion} in the formula for Λ.

The function $u_{s0}(\delta)$ was plotted in [30] in the range $2 \leqslant \delta \leqslant 5$, corresponding to overvoltages in thundercloud fields using which, in Eqn (23), the values of l_e were first estimated. Thus, at $\delta = 2, 3, 5$, the values of the length $l_e \approx 45$, 30, 18.5 m or the time $t_e \approx l_e/c \approx 150$, 100, 62 ns were obtained. It is seen from Table 2 that the values of $t_e(\delta)$ at $\delta = 3$ and 5 exceed the data computed by the ELIZA code (the first row) by less than two times; on the contrary, at $\delta = 2$, the value of $t_e(\delta)$ obtained using the ELIZA code is greater, but only by 1.26 times. However, the time scales $t_e(\delta)$, calculated by the ELIZA code without the angular scattering (second row of Table 2), i.e., as in Ref. [30], are from two to four times smaller than those in Ref. [30].

After results of analysis [30] were published, the further 'fate' of the function $t_e(\delta)$ was unfortunate. In studies implementing more perfect approaches, the accuracy of the calculated values of $t_e(\delta)$ worsened, as was found later [58, 63–65, 68, 69, 71, 72]. Thus, the values of $t_e(\delta)$ obtained from the KE solution allowing for the angular scattering [43, 44], but with an incorrectly calculated ionization integral (35),

Table 2. Time of e-fold avalanche enhancement t_e (ns) reduced to the molecular concentration for different overvoltages δ under the STP conditions $N_L \approx 2.688 \times 10^{25}$ m^{-3} (1 atm).

Reference	Method	Overvoltage δ									
		1.4	1.8	2	2.5	3	5	8	10	12	15
[71, 72]	ELIZA (1)	1236	270	189.7	110	77.6	34.3	17.8	13.3	10.45	
[71, 72]	ELIZA (2)	201	99.3	81		41.4	16.1	10.7	8.0	6.4	
[63, 69]	ELIZA (1)			400			50	26			
[65]	ELIZA (1)			440			54	27.5			
[74]	REAM	988			105		34.3	18.5		11.2	
[74]	Eqn (66)	975		174	102	73	33.6	18.6	14.5	9.17	
[69]	SMC			445			43	22			
[65, 77, 78]	SMC			200			35.6	18.6			
[58]	SMC			174.4			33.2	17.3	12.9	10.04	7.59
[30]	Analyses (2)			150		100	62				
[76]	Analyses (2)			≈ 11		≈ 9.4	≈ 5.6	≈ 2.8			
[68]	Analyses (3)			200							
[38, 60]	Analyses (4)	147	101	86.3		47.0	21.8	10.8	7.7	5.9	
[58]	Eqn (50)			185			35	18.3	13.6	10.75	8.11
[65]	Analyses			145			31.4	16.7			
[43, 44]	KE (5)			14			3.5	1.5			
[63]	KE (5)			81.8			11.7	5.38			
[64]	KE (5)			96			13	6			
[65] LANL	KE (5)			161			34.4	18.9			
[65] VNIIEF	KE (6)			197			39.9	21.2			
[67]	PIC						26	12.5			

(1) Full MC code ELIZA (Sections 5.2.1 and 7).
(2) Without allowing for the angular scattering of electrons.
(3) Statement of the angular scattering problem.
(4) Equation (58) (see Section 6) without allowing for the angular scattering of electrons.
(5) Solution of KE with the ionization integral (35), (39) (see Section 5.1).
(6) Solution of the KE divergent form (40) with the ionization integral (35), (39) (see Section 5.1).

turn out to be underestimated by an order of magnitude (see Table 2). Due to an erratum specified in Section 5.2.1, the improved MC code ELIZA yielded greatly overestimated values of $t_e(\delta)$ (third row of Table 2). In Ref. [76], based on the analysis the function $t_e(\delta)$, improved in comparison with the Ref. [30] though still without the angular scattering, was calculated in the range $0 \leqslant \delta \leqslant 10$ for the altitude $z = 5$ km ($N_{mol}(z) \approx 1.5 \times 10^{25}$ m^{-3}) (see Fig. 3 in Ref. [76]). The values of $t_e(\delta)$ reduced to the STP conditions (see Table 2) are 10 times less than in Ref. [30] and are close to the underestimated values obtained from the KE solution [43, 44].

5. Methods of avalanche numerical simulations

The MC and KE methods described below can be used not only to analyze high-energy thunderstorm processes in planetary atmospheres. They are applicable to solving problems of transport of high-energy electrons in dense gaseous media, both with and without an electric field. These include a description of the electron–positron component of extensive air showers, numerical simulation of high-voltage discharges in dense gases with the participation of REs and nonsustained gas discharges supported by electron beams, including those intended for pumping gas lasers, calculating the propagation of relativistic electron beams in the atmosphere, describing the kinetics of Compton electrons produced by nuclear explosion in the atmosphere, etc.

5.1 Kinetic equation. Collision operators

Soon after the introduction of the GMR mechanism in the physics of atmospheric electricity [30], the RREA theory was developed based on the KE for the EDF $f(t, p, \mu)$, where p is the momentum module and μ is the cosine of the angle θ between the momentum vector **p** and a unit vector **e** in the electric force direction [43–45, 63–65]:

$$\frac{\partial f(t,p,\mu)}{\partial t} - eE\left(\frac{1-\mu^2}{p}\frac{\partial}{\partial \mu} + \mu\frac{\partial}{\partial p}\right) f(t,p,\mu) = \mathrm{St}\left\{f(t,p,\mu)\right\}. \quad (24)$$

Consistent derivation of the collisional operator $\mathrm{St}\{f(t, p, \mu)\}$ for high-energy electrons in a medium with a uniform external electric field specifying the direction **e** was executed much later [66] following the procedure developed

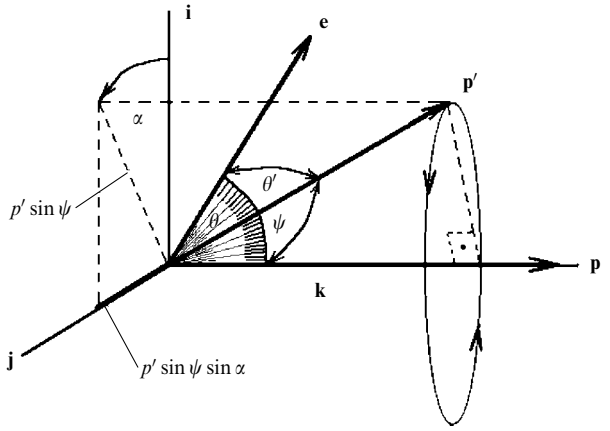

Figure 2. Electron scattering geometry: **e** is the electric force direction, $\mathbf{p}'$ and **p** are the electron momenta before and after the interaction, ψ is the scattering angle [66].

by Holstein [79] for the collision operator in a nonrelativistic gas-discharge plasma, with a description of all approximations. The operator consists of rigorous balance components responsible for elastic collisions $\mathrm{St}_{\mathrm{el}}$, excitation $\mathrm{St}_{\mathrm{ex}}$, and ionization $\mathrm{St}_{\mathrm{ion}}$:

$$\mathrm{St}\,\{f\} = \mathrm{St}_{\mathrm{el}}\,\{f\} + \mathrm{St}_{\mathrm{ex}}\{f\} + \mathrm{St}_{\mathrm{ion}}\,\{f\}\,. \tag{25}$$

The geometry of the electron scattering is presented in Fig. 2 with a system of coordinates defined by the unit vectors [79]:

$$\begin{aligned}\mathbf{i} &= \frac{\mathbf{p}\times[\mathbf{e}\times\mathbf{p}]}{p^2\sin\theta} = \frac{\mathbf{e}p^2 - \mathbf{p}(\mathbf{pe})}{p^2\sin\theta}\,,\\ \mathbf{j} &= \frac{\mathbf{p}\times\mathbf{e}}{p\sin\theta}\,,\quad \mathbf{k} = \frac{\mathbf{p}}{p}\,,\end{aligned} \tag{26}$$

where $\mathbf{p}(p,\theta,\varphi)$ is the electron momentum vector after the scattering. In this set, **k** is the polar axis, the scattering angle $\psi\in[0,\pi]$ is a polar angle, and the angle $\alpha\in[0,2\pi]$ between **j** and the direction of the projection of the momentum $\mathbf{p}'(p',\theta',\varphi')$ before the scattering on the plane $\mathbf{p}=0$ is the azimuthal angle.

The formula relating the angles α and ψ with the angles θ' and θ between **e** and the electron momentum directions before $\mathbf{p}'(p',\theta',\varphi')$ and $\mathbf{p}(p,\theta,\varphi)$ after the scattering,

$$\cos\theta' = \cos\theta\cos\psi + \sin\theta\sin\psi\cos\alpha\,, \tag{27}$$

was derived in [79] (Eqn (19b) of Ref. [79]) assuming $p'\approx p$, which is violated in the case of inelastic interactions and appears excessive. Relation (27) can be obtained without the assumption $p'\approx p$, multiplying the decomposition of the vector $\mathbf{p}'$ in the basis $(\mathbf{i},\mathbf{j},\mathbf{k})$ by **e** [66]:

$$\begin{aligned}\mathbf{p}' = \frac{\mathbf{p}}{p}\,p'\cos\psi + \frac{\mathbf{p}\times\mathbf{e}}{p\sin\theta}\,p'\sin\psi\sin\alpha\\ + \frac{\mathbf{p}\times[\mathbf{e}\times\mathbf{p}]}{p^2\sin\theta}\,p'\sin\psi\cos\alpha\,.\end{aligned} \tag{28}$$

The variation in p' is particularly great in ionizing interactions, because not only is energy ε' of the primary electron decreased by the value of ionization threshold $\varepsilon_{\mathrm{ion}}$, but the remaining energy $(\varepsilon'-\varepsilon_{\mathrm{ion}})$ is shared by two free electrons. The correct relation between the angles θ' and θ is of key importance in the problem of relativistic REs multiplication, because the runaway energy threshold depends on the angle, at which the electron moves relative to the **e** direction [66]; this relation determines whether both electrons, the primary and secondary, or only one of them, would occur in the runaway mode.

The operator, deduced by Holstein, was reduced to the differential form, convenient for calculations, using the Lorentz approximation valid for weakly anisotropic EDFs. However, in the high-energy range, the interactions with small variations of the momentum direction and magnitude dominate, so that, using this circumstance, components $\mathrm{St}_{\mathrm{el}}$ and $\mathrm{St}_{\mathrm{ex}}$ are reduced to the differential form with an accuracy up to the square terms in the EDF decomposition in terms of μ' [66]. As a result, the following representation of the full collision operator (25) is obtained, where the lower limit in the ionization integral is equal to the correct value $\varepsilon+\varepsilon_{\mathrm{ion}}$, unlike $2\varepsilon+\varepsilon_{\mathrm{ion}}$ in the first papers [43, 44]:

$$\begin{aligned}\mathrm{St}\left\{f(p,\mu,t)\right\} &= \frac{1}{p^2}\,\frac{\partial}{\partial p}\,p^2\\ &\times\left(F_{\mathrm{ex}(1)}(p) + \frac{m}{M}\,N_{\mathrm{mol}}\,\frac{p^2}{m}\sum_j \Delta_j n_j \sigma_{\mathrm{tr}}^{(j)}(p)\right) f(p,\mu,t)\\ &+\left[N_{\mathrm{mol}}\,\frac{\beta c}{2}\left(\sum_j \Delta_j n_j\left(\sigma_{\mathrm{tr}}^{(j)}(p)+\sigma_{\mathrm{ex,tr}}^{(j)}(p)\right)\right)\right]\hat{L}_\mu f(p,\mu,t)\\ &+N_{\mathrm{mol}}\beta c\left(\sum_j \Delta_j n_j \sum_i \int_{\varepsilon+\varepsilon_{\mathrm{ion}}^{(i)}}^{\infty} \mathrm{d}\varepsilon'\left(\sigma_{\varepsilon'}(\varepsilon',\varepsilon)\right)_{\mathrm{ion}}^{(j,i)}\right.\\ &\times\left.\frac{\gamma'^2-1}{\gamma^2-1}\int_0^{2\pi}\frac{\mathrm{d}\alpha}{2\pi}\,f(p',\mu',t) - \sigma_{\mathrm{tot}}(\varepsilon)f(p,\mu,t)\right),\end{aligned} \tag{29}$$

where $\mu=\cos\theta$; $\mu'=\cos\theta'$; $\varepsilon=(\gamma-1)mc^2$ is the electron kinetic energy; M is the average mass of the nuclei of gas mixture components; j is a component of the gas mixture with a fraction Δ_j; $\sigma_{\mathrm{ex}}^{(j,i)}$ is the excitation cross section of a state (i) with the excitation energy $\varepsilon_{\mathrm{ex}}^{(j,i)}$ (bound–bound transitions);

$$\sigma_{\mathrm{tr}}^{(j)} = 2\pi\int_{-1}^{1}(1-\xi)\sigma_{\mathrm{el}}^{(j)}(p,\xi)\,\mathrm{d}\xi$$

is the transport cross section; $\sigma_{\mathrm{el}}^{(j)}(p,\xi)$ is the elastic scattering cross section; $\xi=\cos\psi$;

$$\sigma_{\mathrm{ex,tr}}^{(j)}(p) = \sum_i 2\pi\int_{-1}^{1}\mathrm{d}\xi\,(1-\xi)\sigma_{\mathrm{ex}}^{(j,i)}(p,\xi)\,;$$

$$\hat{L}_\mu = \frac{\partial}{\partial\mu}\,(1-\mu^2)\,\frac{\partial}{\partial\mu}$$

is the angular part of the Laplace operator in spherical coordinates;

$$\sigma_{\mathrm{tot}}^{(j,i)}(\varepsilon) = \int_0^{(\varepsilon-\varepsilon_{\mathrm{ion}}^{(j,i)})/2}\left(\sigma_\varepsilon(\varepsilon,\varepsilon')\right)_{\mathrm{ion}}^{(j,i)}\mathrm{d}\varepsilon'$$

is the cross section and $\varepsilon_{\mathrm{ion}}^{(j,i)}$ is the ionization threshold of the electron shell (i); $(\sigma_{\varepsilon'}(\varepsilon',\varepsilon))_{\mathrm{ion}}^{(j,i)}$ is the differential ionization cross section (symmetric relative to the secondary electron energy $\varepsilon_{\mathrm{s}}=(\varepsilon'-\varepsilon_{\mathrm{ion}}^{(j,i)})/2$); and

$$\sigma_{\mathrm{tot}}(\varepsilon) = \sum_j \Delta_j \sum_i n_{j,i}\,\sigma_{\mathrm{tot}}^{(j,i)}(\varepsilon)$$

is the total ionization cross section. The quantities μ' and μ are related as $\mu' = \mu\mu_0 + (1-\mu_0^2)^{1/2}(1-\mu^2)^{1/2}\cos\alpha$, which

is a consequence of Eqn (27) and the energy and momentum conservation law $\xi - \mu_0(\varepsilon', \varepsilon) = 0$, where for $\mu_0(\varepsilon', \varepsilon)$ under the approximation $\varepsilon, \varepsilon' \gg \varepsilon_{\text{ion}}^{(i)}$ [38, 43, 44, 50, 60] the following formula is valid:

$$\mu_0^2(\varepsilon', \varepsilon) = \frac{\varepsilon(\varepsilon' + 2mc^2)}{\varepsilon'(\varepsilon + 2mc^2)} . \tag{30}$$

The primes label the quantities before the interaction events. As the electrons are indistinguishable, for definiteness, an electron with lower energy is considered secondary.

The drag force caused by the energy losses due to the excitation of the atomic shells is introduced in operator (29):

$$F_{\text{ex}(1)} = N_{\text{mol}}\, 2\pi \sum_j \Delta_j n_j \sum_i \varepsilon_{\text{ex}}^{(j,i)} \int_{-1}^{1} \sigma_{\text{ex}}^{(j,i)}(p, \xi)\, \mathrm{d}\xi . \tag{31}$$

The ionization integral in operator (29) is obtained without any restrictions except those imposed by the conservation laws. Its description accuracy is determined by function (30) and the differential ionization cross section. When using for this cross section the Möller formula (5), the integral accuracy is limited by condition $\varepsilon', \varepsilon, \varepsilon_{\text{s}} \gg \varepsilon_{\text{ion}}^{(i)}$ for the energies of primary electron ε' before and after ε the collision and the secondary electron energy ε_{s}. In problems where considering the kinetics in the energy range on the order of $\varepsilon_{\text{ion}}^{(i)}$ is required, it is necessary to use the corresponding set of differential cross sections $(\sigma_{\varepsilon'}(\varepsilon', \varepsilon))_{\text{ion}}^{(i)}$ and an accurate formula for $\mu_0(\varepsilon', \varepsilon)$, allowing for the binding of atomic electrons.

After extracting part of the ionization integral in the range $[\varepsilon + \varepsilon_{\text{ion}}^{(j,i)}; 2\varepsilon + \varepsilon_{\text{ion}}^{(j,i)}]$ in operator (29), an operator for the dominating 'weak' ionizing interactions is obtained, in which the primary electron loses a small part $\Delta\varepsilon^{(j,i)} = \varepsilon_{\text{s}} + \varepsilon_{\text{ion}}^{(j,i)} \ll \varepsilon, \varepsilon'$ of its energy, and the secondary electron populates the low-energy range [66]:

$$\begin{aligned} \text{St}_{\text{ion}}^{\text{weak}} &= N_{\text{mol}}\, \beta c \sigma_{\text{tot}}(\varepsilon) f(p, \mu, t) \\ &+ \frac{1}{p^2} \frac{\partial}{\partial p} p^2 F_{\text{ion}}(\varepsilon) f(p, \mu, t) + \frac{F_{\text{ion}}(\varepsilon)}{2\gamma p} \hat{L}_\mu f(p, \mu, t) , \end{aligned} \tag{32}$$

where the ionization drag force is introduced:

$$F_{\text{ion}}(\varepsilon) = N_{\text{mol}} \sum_j \Delta_j n_j \sum_i \int_0^{(\varepsilon - \varepsilon_{\text{ion}}^{(j,i)})/2} \Delta\varepsilon^{(j,i)} \left(\sigma(\varepsilon, \varepsilon_{\text{s}})\right)_{\text{ion}}^{(j,i)} \mathrm{d}\varepsilon_{\text{s}} . \tag{33}$$

The full drag force, as the sum $F_{\text{in}}(\varepsilon) = F_{\text{ex}(1)}(\varepsilon) + F_{\text{ion}}(\varepsilon)$, is described by Eqn (6) for inelastic energy losses.

The remaining part of the ionization integral with the lower limit $2\varepsilon + \varepsilon_{\text{ion}}^{(i)}$ is responsible for rare events with the production of a high-energy secondary electron populating the RREA. As a result, the full operator is as follows:

$$\begin{aligned} \text{St}\left\{f(p, \mu, t)\right\} &= \frac{1}{p^2} \frac{\partial}{\partial p} p^2 \\ &\times \left(F_{\text{in}}(p) + \frac{m}{M} N_{\text{at}} \frac{p^2}{m} \sum_j \Delta_j \sigma_{\text{tr}}^{(j)}(p) \right) f(p, \mu, t) \\ &+ \left[N_{\text{mol}} \frac{\beta c}{2} \left(\sum_j \Delta_j n_j \left(\sigma_{\text{tr}}^{(j)}(p) + \sigma_{\text{ex, tr}}^{(j)}(p) \right) \right) + \frac{F_{\text{ion}}(p)}{2\gamma p} \right] \\ &\times \hat{L}_\mu f(p, \mu, t) + J_{\text{ion}}(\varepsilon, \mu) , \end{aligned} \tag{34}$$

where

$$\begin{aligned} J_{\text{ion}}(\varepsilon, \mu) &= N_{\text{mol}}\, \beta c \sum_j \Delta_j n_j \sum_i \int_{2\varepsilon + \varepsilon_{\text{ion}}^{(j,i)}}^{\infty} \mathrm{d}\varepsilon' \left(\sigma_{\varepsilon'}(\varepsilon', \varepsilon)\right)_{\text{ion}}^{(j,i)} \\ &\times \frac{\gamma'^2 - 1}{\gamma^2 - 1} \int_0^{2\pi} \frac{\mathrm{d}\alpha}{2\pi} f(p', \mu', t) . \end{aligned} \tag{35}$$

For molecules consisting of two identical atoms ($N_{\text{at}} Z_{\text{at}}^2 = 2N_{\text{mol}}(Z_{\text{mol}}/2)^2 = N_{\text{mol}} Z_{\text{mol}}^2/2$), using the results of Ref. [80], but taking into account the contribution of Mott's multiplier in the cross section σ_{tr}, the following formula is obtained:

$$\frac{\beta c}{2} N_{\text{at}} \sigma_{\text{tr}}(\gamma) = \frac{Z_{\text{mol}}}{2\gamma p} F(\gamma)\, \Gamma(\gamma, I, Z_{\text{at}}) , \tag{36}$$

where the function $\Gamma(\gamma, I, Z_{\text{at}})$ is weakly dependent on γ, increasing in air from 0.262 to 0.271 at an energy variation from 51 keV to 1.53 MeV [80]. If, according to the arguments [66] based on the analysis of the elementary cross sections, we omit the second terms in the first and second components of operator (34) and assume $F_{\text{in}}(p) = F_{\text{ion}}(p)$, which is valid for small Z_{mol} and $(\gamma - 1)mc^2 \gg \varepsilon_{\text{ion}}^{\max}$, then, with relation (36) taken into account, the following operator is obtained:

$$\begin{aligned} \text{St}\left\{f(p, \mu, t)\right\} &= \frac{1}{p^2} \frac{\partial}{\partial p} p^2 F_{\text{in}}(p) f(p, \mu, t) \\ &+ \frac{\left(Z_{\text{mol}} \Gamma(\gamma, I, Z_{\text{at}}) + 1\right) F(\varepsilon)}{2\gamma p} \hat{L}_\mu f(p, \mu, t) + J_{\text{ion}}(\varepsilon, \mu) , \end{aligned} \tag{37}$$

the first component of which describes a flux in the momentum space and the second one describes the angular diffusion due to scattering by atomic electrons and dominating elastic scattering by the nuclei (the component with the factor $Z_{\text{mol}} \Gamma(\gamma, I, Z_{\text{at}})$). The production of high-energy electrons is described by the ionization integral (35).

Operator (37) is similar to the operator in Refs [43, 44], where the factor before the Laplace operator is reduced to the form

$$\frac{(Z_{\text{mol}}/2 + 1)\, F_{\text{in}}(p)}{4\gamma p} , \tag{38}$$

obtained using the results of the analysis in [80]; apparently, the value $\Gamma = 0.25$ is assumed, with which the factor before the Laplace operator in Eqn (37) is equal to

$$\frac{(Z_{\text{mol}}/2 + 2)\, F_{\text{in}}(p)}{4\gamma p} , \tag{39}$$

i.e., differs by the term 2 in the numerator, which increases the contribution of scattering by atomic electrons, which, however, should not greatly affect the results of the KE solution in view of $Z_{\text{mol}}/2 \gg 1$.

Operator (37) implies an important simplification, namely, the Fokker–Planck decomposition in the approximation of small-angle scattering domination and small energy loss: $\Delta\varepsilon^{(j,i)} = \varepsilon_{\text{s}} + \varepsilon_{\text{ion}}^{(j,i)} \ll \varepsilon, \varepsilon'$. Energy and momentum are conserved within an accuracy of the decomposition order and only on average: the real energy losses in individual collisions are replaced with the average losses when using the continuous drag force, the average change in the direction of the primary electron momentum due to collisions being equal to zero, because $\mathbf{F}_{\text{in}} \uparrow\downarrow \mathbf{p}$. KE considers neither the fluctuations of energy losses, nor the angular fluctuations, which are

automatically taken into account by the MC technique, where the conservation laws are fulfilled in each individual collision, and statistical data for many collisions are accumulated.

To eliminate the contribution of unphysical sources of electrons in the solution using the finite-differences technique, it is expedient to use the divergent form of the KE (24) [58, 63–65]:

$$\frac{\partial f}{\partial t}+\frac{1}{p^2}\frac{\partial}{\partial p}\left[p^2 f(\mu eE-F_{\rm in})\right]+\frac{\partial}{\partial \mu}\left(eE\,\frac{1-\mu^2}{p}\,f\right)-\frac{(Z+2)F_{\rm in}}{8\gamma p}\,\frac{\partial}{\partial \mu}\left[(1-\mu^2)\,\frac{\partial f}{\partial \mu}\right]=J_{\rm ion}(\varepsilon,\mu)\,. \tag{40}$$

If, following the arguments of [66], based on the analysis of elementary cross sections, we omit in operator (29) the first component and the term containing $\sigma_{\rm ex,\,tr}(p)$ in the second component, then two terms will remain, responsible for ionization and scattering by nuclei:

$$\mathrm{St}\left\{f(p,\mu,t)\right\}=N_{\rm mol}\,\frac{\beta c}{2}\sum_j \Delta_j n_j \sigma_{\rm tr}^{(j)}(p)\,\hat{L}_\mu f(p,\mu,t)+N_{\rm mol}\beta c\left(\sum_j \Delta_j \sum_i n_{j,i}\int_{\varepsilon+\varepsilon_{\rm ion}^{(j,i)}}^{\infty}\mathrm{d}\varepsilon'\left(\sigma_{\varepsilon'}(\varepsilon',\varepsilon)\right)_{\rm ion}^{(j,i)}\times\frac{\gamma'^2-1}{\gamma^2-1}\int_0^{2\pi}\frac{\mathrm{d}\alpha}{2\pi}\,f(p',\mu',t)-\sigma_{\rm tot}(\varepsilon)f(p,\mu,t)\right). \tag{41}$$

This operator is simpler than operator (37). It differs in the lower limit of the ionization integral and the term responsible for the angular scattering. Scattering by nuclei is described by the transport cross section $\sigma_{\rm tr}(p)$, while scattering by atomic electrons stays in the ionization integral. Therefore, when describing the ionization events, it is not necessary to restrict oneself to the Möller formula (5) for the ionization cross section, in contrast to previous papers [43, 44, 58, 60, 63–65], where the derivation of the ionization integral is based on Eqn (5).

A consistent reduction procedure allowed automatic extraction of the differential component, responsible for angular scattering by atomic electrons, from the ionization integral. It is absent in [43, 44], where the process was considered on a plane and the EDF $f(p',\mu',t)$ was fixed for two values of μ'. As a result, the possibility of expanding the EDF in a series in μ' was missed: the integration over the azimuthal angle was replaced with a quadrature using the trapezoid rule $(f(t,\varepsilon',\mu'_+)+f(t,\varepsilon',\mu'_-))/2$ with $\mu'_\pm=\mu\mu_0\pm[(1-\mu^2)(1-\mu_0^2)]^{1/2}$. This shortcoming, leading to a substantial overestimation of the RE generation rate, was pointed out in a report (reference [10] in paper [65]) and in papers [58, 66]. It is also worth noting that Eqn (27), derived using the instant set of coordinates with the basis vector $\mathbf{k}=\mathbf{p}/p$, is significantly simpler than the corresponding expressions in [38, 43, 44, 58] with $\mathbf{e}$ as one of the basis vectors (see Eqn (52) in Section 6). The small quantity $\Delta\mu$, used to expand EDF in series, is obtained directly from Eqn (27).

The ionization integral is deduced under the assumption $\varepsilon',\varepsilon,\varepsilon_{\rm s}\gg\varepsilon_{\rm ion}^{(j,i)}$; therefore, in computer calculations, $\varepsilon_{\rm ion}^{(i)}$ can be ignored, and if ε' and ε are large compared to the binding energies of atomic electrons, the summation by (i) can be replaced with multiplication by $Z_{\rm mol}$ when using the Möller formula (5) for the differential cross section of ionization.

5.2 Monte Carlo codes

5.2.1 ELIZA code. The ELIZA method and code developed by E N Donskoy [63, 65, 69–72, 75] implement the MC technique to solve the set of linear nonstationary Boltzmann equations

$$\frac{\partial f^\ell(\mathbf{r},\boldsymbol{\varepsilon},t)}{\partial t}+\mathbf{v}^\ell(\varepsilon)\,\frac{\partial f^\ell(\mathbf{r},\boldsymbol{\varepsilon},t)}{\partial \mathbf{r}}+\sigma^\ell(\mathbf{r},\varepsilon)v^\ell(\varepsilon)f^\ell(\mathbf{r},\boldsymbol{\varepsilon},t)=\int\sum_{\ell'}f^{\ell'}(\mathbf{r},\boldsymbol{\varepsilon}',t)\sigma^{\ell'}(\mathbf{r},\varepsilon')v^{\ell'}(\varepsilon')K^{\ell'\ell}(\mathbf{r};\boldsymbol{\varepsilon}'\to\boldsymbol{\varepsilon})\,\mathrm{d}\boldsymbol{\varepsilon}'+g^\ell(\mathbf{r},\boldsymbol{\varepsilon},t)\,, \tag{42}$$

where $f^\ell(\mathbf{r},\boldsymbol{\varepsilon},t)$ is the distribution function of particles of type ℓ by energy ε and directions $\boldsymbol{\omega}$ ($\boldsymbol{\varepsilon}=\varepsilon\boldsymbol{\omega}$, $\mathbf{v}^\ell=v^\ell\boldsymbol{\omega}$) at time t and point $\mathbf{r}$; v^ℓ is the velocity of the particles; $\sigma^\ell(\mathbf{r},\varepsilon)$ is the total interaction cross section; $K^{\ell'\ell}(\mathbf{r};\boldsymbol{\varepsilon}'\to\boldsymbol{\varepsilon})$ is the transition kernel for the interaction producing type ℓ particles; and $g^\ell(\mathbf{r},\boldsymbol{\varepsilon},t)$ is the source of the particles.

The motion of electrons and positrons in the electric field along each section of a trajectory between collisions is described by the equation

$$\frac{\mathrm{d}\mathbf{p}}{\mathrm{d}t}=e\mathbf{E}(\mathbf{r})\,, \tag{43}$$

where $\mathbf{r}$ is the radius vector of a spatial point.

In the spherical coordinates with the axis $z\uparrow\uparrow\mathbf{e}$ after replacing differentiation with respect to t by differentiation along a path, $\mathrm{d}s=c\beta\,\mathrm{d}t$, Eqn (43) is reduced to the following set of equations:

$$\frac{\mathrm{d}\varepsilon}{\mathrm{d}s}=eE_z\mu\,,\quad \frac{\mathrm{d}\mu}{\mathrm{d}s}=\frac{eE_z(1-\mu^2)}{pc\beta}\,,\quad \alpha=\cos\varphi=\mathrm{const}\,, \tag{44}$$

where $\mu=\cos\theta$ is the cosine of the angle between the direction of electric force $\mathbf{e}$, acting on the electron or positron, and the direction $\boldsymbol{\omega}$ of the particle motion. The set of equations (42) for electrons $(-)$ and positrons $(+)$ is reduced as follows:

$$\frac{\partial f^\pm(\mathbf{r},\boldsymbol{\varepsilon},t)}{\partial t}+\frac{\partial\left(\mathbf{v}^\pm f^\pm(\mathbf{r},\boldsymbol{\varepsilon},t)\right)}{\partial \mathbf{r}}+e\,\frac{\partial}{\partial\varepsilon}\left(E_z\mu v^\pm(\varepsilon)f^\pm(\mathbf{r},\boldsymbol{\varepsilon},t)\right)+e\,\frac{\partial}{\partial\mu}\left(E_z\,\frac{1-\mu^2}{p}\,f^\pm(\mathbf{r},\boldsymbol{\varepsilon},t)\right)+\sigma^\pm(\mathbf{r},\varepsilon)v^\pm(\varepsilon)f^\pm(\mathbf{r},\boldsymbol{\varepsilon},t)=\int\sum_{\ell'}f^\pm(\mathbf{r},\boldsymbol{\varepsilon}',t)\sigma^{\ell'}(\mathbf{r},\varepsilon')v^{\ell'}(\varepsilon')K^{\ell'\pm}(\mathbf{r};\boldsymbol{\varepsilon}'\to\boldsymbol{\varepsilon})\,\mathrm{d}\boldsymbol{\varepsilon}'+g^\pm(\mathbf{r},\boldsymbol{\varepsilon},t)\,. \tag{45}$$

The upgraded ELIZA code is based on the libraries of the cross sections of the photon, electron, and positron interactions with matter developed using the libraries EPDL92 (photons), EEDL92 (electrons), EADL92 (shell relaxation), and literature data (see references in [72, 81]). For photons, the following processes are considered: incoherent (Compton) scattering with the bound state of atomic electrons taken into account; coherent (Rayleigh) scattering; photoabsorption with the emission of fluorescence photons and Auger electrons taken into account; and production of electron–positron pairs and triplets. Elastic scattering by nuclei, ionization and excitation of atomic shells, and bremsstrahlung are taken into account for electrons. Elastic scattering by nuclei and free electrons, bremsstrahlung, and two-photon

annihilation are taken into account for positrons. Photoabsorption is modeled individually for nine atomic subshells: K, L1, L2, L3, M1, M2, M3, M4, and M5. In the shell relaxation model, all transitions to these subshells with the emission of fluorescence photons and Auger electrons are taken into account. The ionization of each subshell is modeled separately, and this process, as well as photoabsorption, is followed by the relaxation of the atomic shells. Atomic shell excitation is taken into account. The modeled energy range is limited from below by 1 keV; from above, there are no restrictions.

Unfortunately, when introducing the external electric field into the updated version of the code, a regrettable erratum was made, $E_z = E|\mu|$ in the first of Eqns (44), underestimating the electric force on average by 15–20%, which led to overestimation of $t_e(\delta)$ (third and fourth lines in Table 2) [63, 65, 69, 70]. After correction, new calculations of $t_e(\delta)$ were carried out taking into account (first line in Table 2) and not taking into account (second line in Table 2) the angular scattering of electrons and positrons [71, 72].

5.2.2 REAM code. The Runaway Electron Avalanche Model (REAM) code implementing the MC technique, developed by Dwyer for numerical simulations of the RREA [42, 73, 74, 82], allows for the main interactions of electrons: ionization and excitation of atoms, Möller scattering (5), and elastic scattering modeled by means of the screened Coulomb potential. The generation and transport of bremsstrahlung are modeled taking into account the photoelectric effect, Compton scattering, pair production, and Rayleigh scattering. In the course of the transport of positrons, two-photon annihilation and bremsstrahlung are taken into account. Production of high-energy electrons, capable of initiating an RREA via scattering of positrons, Compton scattering, and absorption of high-energy photons, is separately calculated.

5.2.3 Simplified Monte Carlo codes. In the simplified Monte Carlo (SMC) technique, the motion of high-energy electrons is described by Eqn (1) with the force $\mathbf{\Gamma}(\mathbf{p})$ divided into two parts: the deterministic one is described by the drag force $F_{in}(\varepsilon)$ (6) and the other one, responsible for the elastic collisions, remains stochastic and is modeled using the MC technique [58, 65, 69, 70, 77, 78]. Despite the high frequency of elastic collisions, it is possible to use a time step Δt greatly exceeding the time between the collisions, since the average scattering angle remains extremely small. The modeling is conducted as follows. Electrons with energy ε' are injected at an angle θ relative to the vector $\mathbf{e}$. The range of the simulated energies is limited from below by a small energy ε_{min}, e.g., 1 keV [65, 69, 77, 78] and 2 keV [58]. Electrons with higher energies are separated via interactions with molecules, so that a part of them is slowed down below ε_{min}, while the others are involved in the runaway mode, thus forming the RREA. In the SMC codes, the possibility of switching off the changes of the primary electron energy and momentum vector in the course of ionization impacts is provided [69]. This corresponds to a violation of the conservation laws in the KE (see Section 5.1).

In the first developed SMC version [69], the electron between the consecutive collision events moves according to Eqn (2) under the combined action of the electric force and drag force (6). Elastic scattering is described in the framework of the diffusion approximation as a process of multiple scattering into small angles in terms of the differential cross section of the electron scattering by a nucleus with charge Z, for which, as a rule, the screened Rutherford cross section is used [52, 58, 78, 83, 84]:

$$\frac{d\sigma_{el}}{d\Omega} = \frac{r_e^2 Z^2 (1-\beta^2)}{\beta^4 (1-\cos\theta + 2\eta)^2}\,, \qquad \eta = 1.7\times 10^5\, Z^{2/3}\,\frac{1-\beta^2}{\beta^2}\left(1.13 + 3.76\,\frac{\alpha^2}{\beta^2}\right), \tag{46}$$

where $d\Omega$ is the solid angle element and η is the shielding parameter.

According to (46), the scattering into small angles of the order of $\eta^{1/2}$ dominates. The average scattering angle is estimated as $\langle\psi^2\rangle \approx \psi_{min}^2\, n_{col}$, where n_{col} is the number of elastic collisions experienced by the electron. The theory is not quite adequate for the RE case. Though the cross section of elastic scattering into large angles is rather small, the probability of such events can be high because of the long trajectories of REs.

The avalanche enhancement length and time are calculated integrating the Möller cross section (5):

$$l_e(\varepsilon', \varepsilon_{th}) = \left(N_{mol}\int_{\varepsilon_{th}}^{\varepsilon'/2} \sigma(\varepsilon, \varepsilon')\, d\varepsilon\right)^{-1}, \quad t_e = \frac{l_e}{c}\,. \tag{47}$$

In Section 3, the deterministic definition of the runaway threshold ε_{th} is given, but, because of the stochastic origin of the runaway process, an exact definition of the threshold is impossible. Therefore, in Eqn (47), the threshold ε_{th} is assumed to be a certain effective energy, above which the RE fraction Δ tends to one.

Using the SMC method, the dependence of the RE fraction Δ on the initial energy ε' and injection angle θ of the simulated electron was calculated [69]. The obtained fraction Δ varies extremely slowly with the variation in θ within the limits $0-\pi/2$. With the further growth of θ, Δ sharply decreases. The energy at which $\Delta \approx 70-80\%$ was accepted as the runaway threshold: $\varepsilon_{th} = 650$, 120, and 65 eV at $\delta = 2$, 5, and 8, respectively. With the angular scattering switched off, the threshold magnitudes ε_{th}, thus defined, decrease several-fold. For two greatly differing values of ε' (2 and 10 MeV) using the calculated ε_{th}, the values of $l_e(\varepsilon, \varepsilon_{th})$ and $t_e \approx l_e/c$ were calculated using Eqn (47). The values of $t_e(\delta)$ for $\varepsilon' = 2$ MeV are presented in Table 2. The results differ by two times from the final results of the full ELIZA code (first line in Table 2), which, according to [69], is due to the estimative character of calculating the threshold ε_{th} and by the fact that instead of averaging over the entire distribution of electrons, the history of a monoenergetic beam was traced. After removing these unjustified simplifications in the SMC, the calculated values of t_e [65, 77, 78] (Table 2) became close to those calculated with the ELIZA code (first line in Table 2).

In the SMC developed by Lehtinen et al. [58], the energy losses of electrons and change in their motion direction due to elastic collisions in the energy range below $\varepsilon_{min} = 2$ keV are described in terms of drag force $F_{in}(\varepsilon)$ (6) and angular diffusion, respectively. Ionization processes with the production of electrons with energy $\varepsilon' > 2$ keV are calculated explicitly; therefore, the corresponding energy losses

$$N_{mol} Z_{mol} \int_{\varepsilon_{min}}^{\varepsilon/2} \varepsilon' \sigma_\varepsilon(\varepsilon, \varepsilon')_{ion}\, d\varepsilon'$$

are eliminated from F_{in}. The scattering into angles ψ is described by the diffusion equation for the probability distribution function of the random number $\omega = \cos\psi$ at the time step Δt, which in the two-term approximation for the Legendre polynomial expansion has the form

$$f(\omega, \Delta t) = \frac{1}{2D\Delta t} \exp\left(\frac{\omega - 1}{2D\Delta t}\right), \quad D = \frac{1}{4}\frac{\mathrm{d}\langle\psi^2\rangle}{\mathrm{d}t}. \qquad (48)$$

In the case of scattering into very small angles, the fixed change in the scattering angle is used:

$$\Delta\psi \equiv \sqrt{\frac{\mathrm{d}\langle\psi^2\rangle}{\mathrm{d}t}\,\Delta t}\,, \qquad \frac{\mathrm{d}\langle\psi^2\rangle}{\mathrm{d}t} = \frac{4\pi r_e^2 c^4 N_{\text{mol}} Z_{\text{mol}}^2}{v^3\gamma^2} \log\left(\frac{164.7}{Z_{\text{mol}}^{1/3}}\frac{p}{mc}\right), \qquad (49)$$

with the rate of change of the mean square of the scattering angle ψ taken from book [83] and the maximum and minimum values of the angle taken from report [80] and book [84], respectively.

In the formula $P = N_{\text{mol}} Z_{\text{mol}} \sigma_{\text{tot}}(\varepsilon) v \Delta t$ for the probability of high-energy ($\varepsilon' > 2$ keV) electron production within the time step Δt, the total ionization cross section is calculated by integrating the Möller cross section (5) within the limits $[\varepsilon_{\min}, \varepsilon/2]$.

To confirm the results of the SMC calculations, the authors of Ref. [58], proceeding from a KE written in the divergent form (40), derived a formula, which at $v \to c$ is reduced as follows:

$$t_e = 2\pi r_e^2 c N_{\text{mol}} Z_{\text{mol}} \frac{\varepsilon_{\text{th}}}{mc^2}, \qquad (50)$$

where the runaway threshold ε_{th} is defined by Eqn (18). Among the calculated values $\varepsilon_{\text{th}} = 549$, 103, 54, 41, 32, 24 keV at $\delta = 2$, 5, 8, 10, 12, 15, the first three are smaller than the above-mentioned values of ε_{th} determined by the fraction of REs but somewhat exceed the values calculated using Eqn (60) (see Section 7).

The values of t_e calculated in Ref. [58] by the SMC method and with formula (50) are presented in Table 2. They are seen to be close to the final t_e values obtained using the ELIZA code (the first line of Table 2). In the range of small δ, the values of t_e calculated using Eqn (50) are closer to the t_e values calculated using the ELIZA code than to those calculated in [58] using the SMC: e.g., at $\delta = 2$, $t_e = 174.4$ ns (SMC), 185 ns (Eqn (50)), and 189.7 ns (ELIZA, the first line of Table 2). It should be noted that the values of t_e at $\delta = 5$ and 8, calculated with the SMC in [65], almost coincide with those predicted by Eqn (50). Discussing the results, the authors of [58] emphasize that, within the earlier kinetic and analytical models [43, 44, 85–88], the RREA development rate was overestimated by more than an order of magnitude.

The SMC code developed by Celestin and Pasko is intended to simulate the electron kinetics in an extremely wide energy range from fractions of an electronvolt to a few GeV [89, 90]. This is achieved by using the differential cross section of ionization by electron impact according to the relativistic binary encounter Bethe (RBEB) model [91, 92]. The cross section is presented in the analytical form, which is a combination of the Möller cross section and the dipole part of the Bethe cross section. For the RREA problem, the simulated energy range is extremely wide, 0.01–200 MeV,

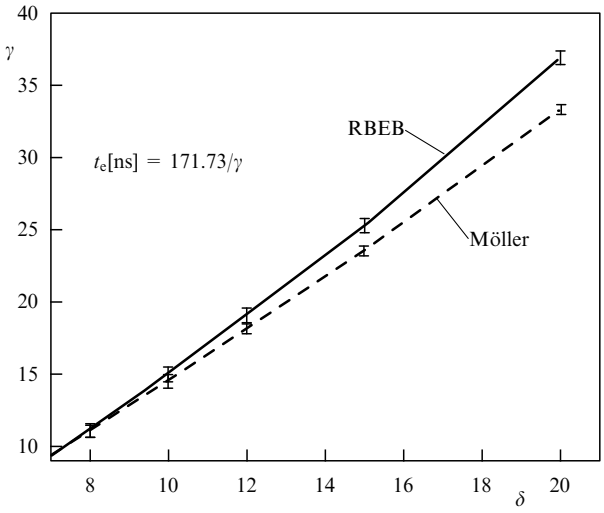

Figure 3. Dependence of the characteristic RREA enhancement time on the overvoltage calculated with the SMC code using the conventional approach (Möller) and the RBEB model by Silisten and Pasko [92].

and only the elastic scattering of electrons and ionization by electron impact are taken into account in the diffusion approximation. The angle between vectors of primary and secondary electrons is calculated by solving the equations for the momentum and energy conservation laws. As the simulated energy range extends up to 200 MeV, the radiation drag force is allowed for. Photons and positrons are not simulated.

Figure 3 presents the dependences of the RREA development rate on overvoltage δ, calculated using the RBEB model and the conventional model with the integration of the Möller cross section (see (47)). It is seen that, in the range of the δ values approximately below $\delta = 10$, both models give close rate values, and for small δ typical of thundercloud fields identical rates are predicted. With the growth of δ, the discrepancy significantly increases, and in the field with very high δ, typical of discharges at overvoltages high relative to the field strength E_{self} in a self-sustained breakdown [11, 12, 17–26], a large discrepancy is to be expected.

In general, the final $t_e(\delta)$ values, calculated by SMC codes, are in good agreement with the results using the ELIZA code (first line in Table 2). Thus, the SMC method, considering only inelastic interactions (deterministic) and elastic scattering (stochastic) of electrons is efficient for numerical simulations that, unlike full MC codes, do not require much computer time.

6. Calculations of the avalanche enhancement time scale based on the kinetic equation

To improve the description of the RREA kinetics and to calculate more precise functions $t_e(\delta)$ and $l_e(\delta)$, the authors of the GMR mechanism addressed the KE [43, 44], in which the electron scattering in elastic collisions is taken into account, which is the only difference from the elementary processes considered in analysis [30]. The KE (24) with collision operator (37), (38), including ionization integral (35), is solved. The values of t_e and, therefore, $l_e \approx ct_e$ calculated in [43, 44] decreased by more than an order of magnitude in comparison with results of analytical calculations [30] (see Table 2). Arguments in favor of a positive role of the angular

scattering in the avalanche development rate are presented in report [43].

However, for heuristic reasons, it is clear that the inclusion of additional interactions of electrons, competing with the ordering action of the electric field, inevitably enhances the randomization of electron momenta. The electrons and secondary particles (gamma photons and positrons), experiencing elastic scattering by the atomic nuclei and electron shells, move away from the field lines. Therefore, to counterbalance the effective drag force, a stronger electric force is required. As a result, $t_e(\delta)$ increases.

The negative role of elastic scattering in the RREA development is demonstrated in report [68], and then in the detailed analysis performed in Ref. [69]. Using the SMC technique, it is shown that minimum possible values of $t_e(\delta)$ exceed several-fold those computed in [43, 44] (Table 2). In particular, to analyze the experiment by McCarthy and Parks [35], for $\delta = 2$, the runaway threshold was calculated as $\varepsilon_{th} = 600$ keV, with which, according to Eqn (47), at an altitude of 5 km the length $l_e(\delta = 2) \approx 120$ m was obtained. This value corresponds to the time $t_e(\delta = 2) = 200$ ns at sea level (see Table 2) and is in good agreement with the result of the final calculations using the ELIZA code (first line in Table 2).

Later, with the purpose of coordinating the results given by different methods, a detailed analysis on the KE basis (24) was executed [38, 60] with the collision operator including the radiation force F_{rad}:

$$\begin{aligned}\mathrm{St}\left\{f(p,\mu,t)\right\} &= \frac{1}{p^2}\,\frac{\partial}{\partial p}\,p^2(F_{in}+F_{rad})f(p,\mu,t)\\ &+\frac{F_{in}\sum_i Z_i^2/Z}{4\gamma p}\,\hat{L}_\mu f(p,\mu,t)\\ &+N_{mol}\,\beta c\,\frac{2\pi Ze^4}{mc^2}\int_\varepsilon^\infty \frac{\gamma'^2-1}{\gamma^2-1}\left[\varepsilon^{-2}+(\varepsilon'+mc^2)^{-2}\right]\\ &\times\int\frac{\mathrm{d}\varphi}{2\pi}\int f(\varepsilon',\mu',\varphi)\,\delta(\mu_1-\mu_0)\,\mathrm{d}\mu_1\,\mathrm{d}\varepsilon'\,, \end{aligned} \tag{51}$$

where $\delta(\mu_1 - \mu_0)$ is the Dirac delta-function, φ is the angle between $\mathbf{p}'$ and $\mathbf{e}$, and the relation between the angles is expressed as

$$\mu' = \frac{\mu\mu_1 \pm (1-\mu_1^2)^{1/2}\sin\varphi\sqrt{\mu_1^2-\mu^2+(1-\mu_1^2)\sin^2\varphi}}{\mu_1^2+(1-\mu_1^2)\sin^2\varphi}\,. \tag{52}$$

Formulas (8) for F_{in} with $\Lambda = 11$ and (12) for F_{rad} are used in the energy range $\varepsilon \ll mc^2$.

To coordinate the results of calculating $t_e(\delta)$ by KE and MC techniques, it was supposed that "at high energies the main role in the runaway breakdown process is played not by ionization Coulomb collisions, but by much more stronger bremsstrahlung effect" [60]. However, first, this process is included in the ELIZA code, and, second, the radiation losses in air are compared to the ionization ones according to Eqn (14) only at the electron energy of 110 MeV, which, according to simulations of RREA using the MC technique, is not attained. The authors of Ref. [38] believe that "the ionization plays a major role at low energy $\leqslant 5$ MeV. At the energy $\geqslant 5$ MeV the dominating role belongs to the bremsstrahlung force." Apparently, they meant that, beginning at the energy ≈ 5 MeV, the F_{rad} component contributes to the drag force, $F = F_{in} + F_{rad}$. However, F_{rad} becomes dominating in the energy range greatly exceeding the boundary magnitude of 110 MeV. Indeed, from the equality $F_{in} = F_{rad}$ at $\gamma^2 \gg 1$ (see Eqns (8) and (12)) with $Z_{at} \approx 7.25$ and $\Lambda = 11$, the equation for the boundary energy is obtained,

$$\begin{aligned}\gamma_{bound} - 1 &= \frac{\varepsilon_{bound}}{mc^2} = \frac{\pi\Lambda}{\alpha Z_{at}\ln\left[2\varepsilon_{max}/(mc^2)\right]}\\ &\approx \frac{653}{\ln\left[2\varepsilon_{max}/(mc^2)\right]}\,,\end{aligned} \tag{53}$$

yielding $\varepsilon_{bound} \approx 120$ MeV, which is close to the estimate of 110 MeV (14).

The direct contribution of the RREA's own bremsstrahlung to its development, including gas ionization by positrons and photons produced by e^+e^- annihilation, is obviously overestimated (see Section 8.1). The secondary emissions are important for maintaining the RREA series via relativistic positive feedback (RFB) (see Section 8.2).

From the equality $eE = F_{rad}(\varepsilon_{max})$ a formula follows for the maximum energy available to REs [60]:

$$\frac{\varepsilon_{max}}{mc^2} = \frac{\pi a}{\alpha Z_{eff}\ln(2\gamma)}\,\delta \approx \frac{653\,\delta}{\ln(2\gamma)}\,, \tag{54}$$

from which the values $\varepsilon_{max} = 430$ and 850 MeV are obtained for $\delta = 5$ and 10, respectively [38], which are quite accurate, as they greatly exceed ε_{bound}, i.e., belong to the domain of radiation force domination. However, in view of the exponential RE energy distribution with the average energies given in Table 3, the RE portion in the energy range above ε_{bound} is extremely small, $\approx (0.7-3)\times 10^{-8}$ for $5 \leqslant \delta \leqslant 10$, and the RFB [42, 73] limits the RREA enhancement to the magnitude of $\approx 10^5$ (see Section 8.3).

The exponential increase in the RE number follows from the asymptotic behavior of the EDF at high energies, $\exp(\lambda t)$, with the increment

$$\lambda \approx 0.065\,\delta^{3/2}\ [38]\,,\quad \lambda \approx \frac{0.6}{a}\,\delta^{3/2} \approx 0.055\,\delta^{3/2}\ [38, 60]\,. \tag{55}$$

The second formula in (55) is obtained with $a = 11$ [60] as a solution to the eigenvalue problem formulated based on the KE. With the use of time scale $t_0 = (4\pi r_e^2 cZN_{mol}\Lambda)^{-1}$ [38] at $\Lambda = a = 11$, from Eqn (55), it follows that

$$t_e = \frac{t_0}{\lambda} = \frac{\delta^{-3/2}}{2.4\,c\pi r_e^2 N_{mol} Z_{mol}}\,, \tag{56}$$

which differs by the coefficient in the denominator from the formula in Ref. [60]:

$$t_e = \frac{\delta^{-3/2}}{1.4\,c\pi r_e^2 N_{mol} Z_{mol}}\,. \tag{57}$$

With the numerical values of the quantities for air at a pressure of 1 atm ($N_{mol} = N_L$) and $Z_{mol} = 14.5$, Eqn (57) yields

$$t_e\,[\mathrm{ns}] \approx 244\,\delta^{-3/2}\,. \tag{58}$$

The values of t_e calculated using Eqn (58) greatly exceed the data from [43, 44] and agree rather well with the values of t_e computed using the ELIZA code with the angular

scattering of electrons switched off [71, 72] (se Table 2). This is particularly true in the range of high values of δ, in spite of the fact that Eqn (58) was derived with the simplified description of interactions. Therefore, the analytical calculations can be used to test calculations with the MC codes.

The values of t_e obtained with the ELIZA code, taking into account the angular scattering of electrons (the first line of Table 2), significantly differ from those computed with the scattering ignored both in the ELIZA code and in Eqn (58). In the range $\delta \geqslant 2$, the former exceeds the latter by approximately 1.5–2 times, but in the domain of weak fields (approximately $\delta \leqslant 2$), when the scattering effect is stronger, the discrepancy increases and attains an order of magnitude at small δ, apparently, testifying to the fact that the magnitude $\delta \approx 2$ is critical in the RREA development.

In further studies, to eliminate the difference between t_e values obtained by the MC and KE techniques, the KE solution procedures were improved. Consent was attained in Refs [63–65] by solving the divergent form of the KE (40), in which the ionization process was described not on the plane as in [43, 44], but in the 3D geometry. Moreover, the description of the kinetics of secondary electrons after an ionization event was improved by increasing the approximation accuracy of the integration over the azimuthal angle α in the ionization integral (35). The values of the function $t_e(\delta)$ [64, 65] computed solving the KE are presented in Table 2. It is seen that the values of t_e, obtained by different groups using full MC codes [71, 72, 74] and SMCs [58, 65, 77, 78] and solving the KE [65] with angular scattering included are in good agreement.

The ELIZA code is intended to solve problems with the joint transport of electrons, positrons, and photons, taking into account all elementary processes described in terms of the corresponding cross sections. In other approaches, including SMC ones, only the ionization and elastic interactions of electrons with atomic particles are taken into account, using the drag force to describe the average effect of the weak ionizing collisions. These distinctions, most likely, are responsible for the remaining disagreement.

7. Fundamental macroscopic characteristics of an avalanche

Numerical simulations of discharges with RREA participation are conducted in terms of the drift-diffusion equations describing the kinetics of all charged particles in the framework of the fluid approximation, the RE kinetics being described by the following equation (see, e.g., [93–96]):

$$\frac{\partial n_{re}}{\partial t} + \operatorname{div}\left(n_{re}\mathbf{v}_{re} - D_{\perp}\left(\nabla n_{re} - \frac{\mathbf{v}_{re}(\mathbf{v}_{re}\nabla n_{re})}{v_{re}^2}\right) - \frac{D_{\parallel}\mathbf{v}_{re}(\mathbf{v}_{re}\nabla n_{re})}{v_{re}^2}\right) = \nu_{re} n_{re} + S_{re}^{ext}\,, \tag{59}$$

where n_{re} is the RE concentration, ν_{re} is the runaway electron multiplication rate, $\mathbf{v}_{re} = -v_{re}\mathbf{e}$ is the vector of the directed RE velocity, $v_{re} = |\mathbf{v}_{re}|$, $D_{\parallel}$ and $D_{\perp}$ are the coefficients of RE diffusion, longitudinal and transverse relative to the vector $\mathbf{e}$, respectively, and S_{re}^{ext} is the external RE source. To solve Eqn (59), the dependences of v_{re}, $D_{\parallel}$, $D_{\perp}$, and ν_{re} on the overvoltage δ are required. These dependences, obtained from the results of numerical simulations of the RREA by means of the ELIZA [71, 72, 97, 98] and REAM [73, 74, 82, 99] MC codes, are given below. The simulations were executed for the STP conditions in the cylindrical coordinates $\mathbf{z} \uparrow\uparrow \mathbf{e}$ and $\mathbf{r} \perp \mathbf{e}$.

The simulations with the ELIZA code were carried out with a statistical error of less than 1–2% as follows. At the initial moment of time, electrons with kinetic energy ε_0 were injected along the direction $\mathbf{e}$. The calculations were executed for two greatly differing values, $\varepsilon_0 = 2$ and 10 MeV. Though a majority of electrons are produced in the low-energy range, including the range below the runaway threshold ε_{th}, these electrons relax down to thermal energies, so that their contribution to the RREA is negligible. The dependences of the electron number $N_e(t)$ on time for various δ are the primary result of the simulations. The exponential RREA mode, obeying the law $\partial \ln(N_e(t)/N_e(t=0))/\partial t \approx \text{const}$, stabilizes during the time interval, a few times shorter than the avalanche enhancement time $t_e(\delta)$. The effect of the initial energy ε_0 on the RREA dynamics manifests itself at $\delta < 2$, and the time required for the RREA to enter the exponential mode is decreased with the growth of ε_0. For $\delta < 2$, this time increases with the reduction in δ, so that only electrons with high ε_0 are capable of entering the runaway mode.

The results of calculations using the ELIZA code are presented in Table 3 for a wide range of δ values, including, along with small δ typical of thunderous fields, the range of high δ attained in laboratory discharges generating REs [11, 12, 17–26]. Recall that at $\delta \approx 14$ a usual self-sustained breakdown in air is developed driven by low-energy electrons. The characteristics at the moment of time $t_{run} \gg t_e(\delta)$ corresponding to the end of the simulation are defined as follows.

(1) The time $t_e = t_{run}/\ln(N_e(t_{run})/N_e(t=0))$ is determined by the linear segment of function $\ln(N_e(t_{run})/N_e(t=0))$.

(2) The module of the directed velocity is $v_{re} = \langle z\rangle/t_{run}$.

(3) The spatial scale (enhancement length) is $l_e = t_e v_{re}$.

(4) The average electron energy is

$$\langle\varepsilon\rangle = \left(N_e(t_{run})\right)^{-1}\sum_{i=1}^{N_e(t_{run})}\varepsilon_i\,.$$

(5) The coefficients of longitudinal and transverse diffusion are $D_{\parallel} = \langle(z - \langle z\rangle)^2\rangle/(2t_{run})$ and $D_{\perp} = \langle r^2\rangle/(\pi t_{run})$, respectively. Here,

$$\langle z\rangle = \sum_{i=1}^{N_e(t_{run})}\frac{z_i}{N_e(t_{run})}$$

is the mean value of coordinate z of the electron swarm,

$$\left\langle\left(z - \langle z\rangle\right)^2\right\rangle = \sum_{i=1}^{N_e(t_{run})}\frac{\left(z_i - \langle z\rangle\right)^2}{N_e(t_{run})}$$

is the mean square deviation of the coordinate z from $\langle z\rangle$,

$$\langle r^2\rangle = \sum_{i=1}^{N_e(t_{run})}\frac{r_i^2}{N_e(t_{run})}$$

is the mean square coordinate r.

(6) The energy runaway threshold ε_{th}, a conditional quantity, as the runaway process is stochastic, is defined by the relation

$$\frac{1}{l_e(\delta)} = N_L\int_{\varepsilon_{th}(\delta)}^{\langle\varepsilon\rangle/2}\sigma_{\varepsilon'}\left(\langle\varepsilon\rangle,\varepsilon\right)\mathrm{d}\varepsilon\,, \tag{60}$$

Table 3. Dependences on overvoltage δ under STP conditions of characteristic time t_e of avalanche enhancement, magnitude of directed velocity v_{re}, enhancement length $l_e = v_{re}t_e$, average electron energy $\langle\varepsilon\rangle$, runaway threshold ε_{th}, and coefficients of longitudinal $D_\parallel$ and transverse $D_\perp$ diffusion [72, 97, 98].

δ	t_e, ns*	$v_{re}\times10^{-8}$, m s^{-1}	l_e, m	$\langle\varepsilon\rangle$, MeV	ε_{th}, keV	$D_\parallel$, m^2 s^{-1}	$D_\perp$, m^2 s^{-1}
1.3	8905						
1.4	1236/201						
1.5	696.4	2.69	187.33	6.75	1400	1.52×10^8	6.27×10^8
1.6	447.2/133						
1.8	270.1/99.3						
2	189.7/81.0	2.64	50.81	6.74	470	7.73×10^7	2.88×10^8
2.5	109.8						
3	77.6/41.4	2.65	16.56	6.79	160		
4	47.5/27.1	2.65	12.59	6.83	116		
5	34.3/16.1	2.66	9.12	6.87	90	1.49×10^7	4.88×10^7
6	26.4/15.7	2.66	7.02	6.79	70		
7	21.3/12.8	2.67	5.69	6.68	56		
8	17.8/10.7	2.68	4.77	6.61	47	7.14×10^6	2.05×10^7
10	13.3/8.0	2.69	3.58	6.41	35	5.13×10^6	1.34×10^7
12	10.45/6.36	2.69	2.81	6.15	28	3.94×10^6	9.44×10^6
14	8.56/5.48	2.69	2.30	5.99	23	3.21×10^6	6.99×10^6
16	5.80	2.68	1.55	5.38	15.5	2.10×10^6	3.70×10^6
50	1.52	2.66	0.40	4.35	5.5	7.63×10^5	6.40×10^5
100	0.60	2.65	0.16	3.46	1.6	3.82×10^5	1.66×10^5

*With/without angular scattering taken into account.

where in cross section (5) the energy ε' of the primary electron is set equal to $\langle\varepsilon\rangle$.

For comparison, note that in Table 3, the runaway threshold values $\varepsilon_{th}(\delta=2)=470$ keV and $\varepsilon_{th}(\delta=8)=47$ keV are close to or slightly differ from the values $\varepsilon_{th}(\delta=2)=470$ keV and $\varepsilon_{th}(\delta=8)=67$ keV, estimated using equation $eE\langle\mu(\varepsilon_{th},\delta)\rangle=\langle F_{in}^{min}\rangle$, where $\langle F_{in}^{min}\rangle$ is the average minimum of the drag force (6), and the values 549 keV and 54 keV [58] and 650 keV and 65 keV [69] are calculated by SMC codes (see Section 5.2.3).

Enhancement time t_e and length l_e. It is seen in Table 3 that time t_e decreases from 8905 ns to 0.6 ns with the increase in δ from 1.3 to 100. The sharp increase in t_e in the range $\delta<2$, apparently, testifies to the proximity of the value $\delta\approx2$ to the critical one, below which too low a number of electrons is capable of entering the runaway mode; due to this reason, the corresponding t_e magnitudes are computed with significant uncertainty. The value $\delta=1.3$ according to Eqn (21) corresponds to the critical (threshold) field strength $E_{th}\approx270-284$ kV m^{-1} at STP [56, 57, 73], when l_e sharply increases to several km. It is assumed in Ref. [30] that the range $1\leqslant\delta\leqslant2$ (corresponding to $E_{th}\approx2-4$ kV m^{-1}) is critical. For δ values of interest for the physics of high-energy atmospheric electricity, the results of simulations executed using the ELIZA code are approximated as follows:

$$t_e\,[\mathrm{ns}]=\exp\left(\frac{7.11}{\delta^{0.441}}\right)\pm5\%\,,\qquad \delta\in[2,10]\,. \tag{61}$$

In the range of high δ values, which are of interest for studies of laboratory discharges in strong fields [11–26], the data on $l_e(\delta)$ in Table 3 are approximated as follows [97, 98]:

$$l_e(\delta)=(0.063\,\delta-0.72)^{-1}\ [\mathrm{m}],\qquad \delta\geqslant20\,, \tag{62}$$

with the corresponding time

$$t_e\,[\mathrm{ns}]\approx\frac{l_e}{c}\approx10\,(0.189\delta-2.16)^{-1}\,. \tag{63}$$

Dwyer [73] while introducing the RFB mechanism (see Section 8.2) simulated the RREA using the REAM MC code. An approximation was proposed for the obtained dependence of l_e on E, which in terms of the overvoltage $\delta=eE/F_{in}^{min}$ with $F_{in}^{min}\approx217$ keV m^{-1} is described by the following function:

$$l_e\,[\mathrm{m}]\approx33.18\,(\delta-1.26)^{-1}\,,\qquad 1.38\leqslant\delta\leqslant11.52\,, \tag{64}$$

with the corresponding time

$$t_e\,[\mathrm{ns}]\approx\frac{l_e}{c}\approx1.1\,(\delta-1.26)^{-1}\,. \tag{65}$$

For the results of the subsequent calculations with the REAM code [74], approximations for t_e and l_e are proposed, which in terms of δ with $F_{in}^{min}\approx217$ keV m^{-1} are as follows:

$$t_e\,[\mathrm{ns}]=\frac{125.8}{\delta-1.276\,N_L/N(z)}\,,\quad l_e\,[\mathrm{m}]=\frac{33.64}{\delta-1.272\,N_L/N(z)}\,, \tag{66}$$

where $N(z)$ is the concentration of molecules at altitude z and an average electron energy of 7.3 MeV is assumed [74].

As seen in Table 2, the values of t_e calculated using the MC technique [74] and Eqn (66) in the range of approximately $\delta\geqslant2-2.5$ are quite close to those computed using the ELIZA code (the first line of Table 2) and are much less than the latter in the range of smaller δ.

Energy spectra of high-energy electrons. Through numerical simulations using the ELIZA code, an evolution of the electron energy distribution was studied. The time required for the distribution to achieve the steady state, defined as the time after which the distribution does not vary except for part of the high-energy 'tail' containing a portion of electrons fewer than $10^{-4}-10^{-5}$, amounts to $t_{st}\approx(4-6)\,t_e$. The steady-state values of the average energy $\langle\varepsilon\rangle$ monotonically and weakly decrease with the rise of δ because of the threshold ε_{th} decrease. With δ increasing from 1.5 to 100, energy $\langle\varepsilon\rangle$ decreases only twofold. In the range $\delta=1.5-14$, the values of $\langle\varepsilon\rangle$ slightly differ from each other, varying in the range of $\approx7-6$ MeV (see Table 3). Similar results are obtained with the KE solution [65].

It is possible to estimate the average energy $\langle\varepsilon\rangle$ by the energy gained by the RE before the production of a secondary RE:

$$\langle\varepsilon\rangle\approx v_{re}(\delta-1)\,F_{in}^{min}\,t_e(\delta)+\varepsilon_0\,. \tag{67}$$

According to this formula, the weak dependence of $\langle\varepsilon\rangle$ on δ is due to a competition of two processes, namely, the energy gain in the field (factor $(\delta-1)$) and the production of secondary low-energy ($\ll\langle\varepsilon\rangle$) electrons ($v_{re}F_{in}^{min}\,t_e(\delta)$). The higher δ, the more efficient the energy gain, but the more intense the reproduction of low-energy electrons.

The weak dependence of $\langle\varepsilon\rangle$ on δ testifies to the closeness of the corresponding steady-state energy distributions. In Fig. 4, the energy distributions at different moments of time

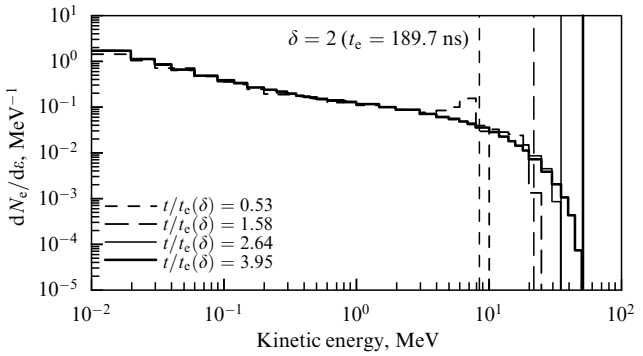

Figure 4. Electron energy distribution normalized to unity at various moments of time for overvoltage $\delta = 2$ calculated with the ELIZA code. The vertical lines mark the maximum values of energy attained by the primary electron at moment of time t [72].

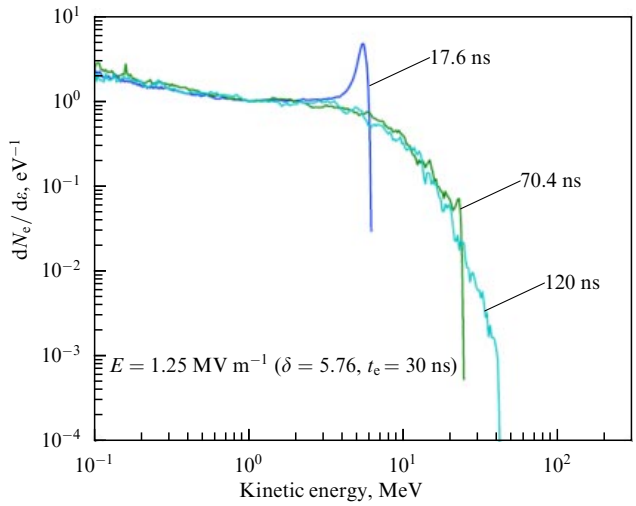

Figure 5. Process of establishing electron energy distribution at overvoltage $\delta = 5.76$. Numerical simulations with the RBEB model [89].

are illustrated for $\delta = 2$. The vertical lines correspond to the maximum energy values $\varepsilon_{max} = v_{re}(\delta - 1)F_{in}^{min}\, t + \varepsilon_0$ attained by the primary electron at moment of time t. This means that in the distribution there are primary electrons moving along the vector **e**. According to Eqn (54), the energy ε_{max}, which is an almost linear function of δ, is equal, e.g., to 430 MeV at $\delta = 5$ and 850 MeV at $\delta = 10$ [38].

For comparison, Fig. 5 illustrates the process of establishing the energy distribution, as simulated by Silisten and Pasko at $\delta = 5.76$ with the SMC code, which is quite consistent with the establishment process obtained with the ELIZA code.

Figure 6 illustrates the steady-state energy distributions of RREA electrons computed with the ELIZA code [72]. Obviously, the distributions are close to each other and weakly depend on δ. So, the maximum difference between distributions in the range $\delta = 2-8$ and in the energy range of 0.01–40 MeV does not exceed 15%. This universal distribution is approximated by the function

$$\exp\left(-1.08\times10^{-5}u^6 - 4.2\times10^{-6}u^5 + 9.76\times10^{-6}u^4 + 1.265\times10^{-2}u^3 - 5.64\times10^{-2}u^2 - 0.433u - 2.1185\right), \quad (68)$$

where $u = \ln(\varepsilon\,[\text{MeV}])$.

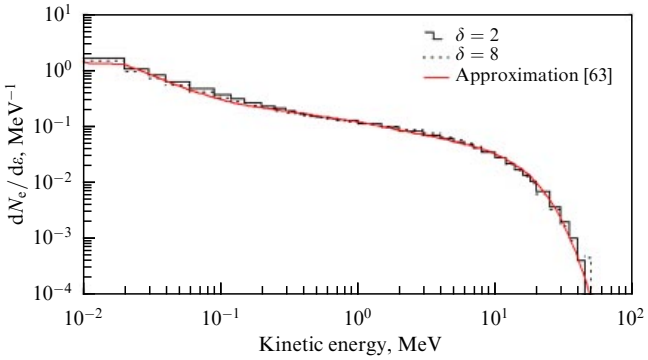

Figure 6. Steady-state electron energy distribution normalized to unity for overvoltage magnitudes $\delta = 2$ and 8 calculated with the ELIZA code [72].

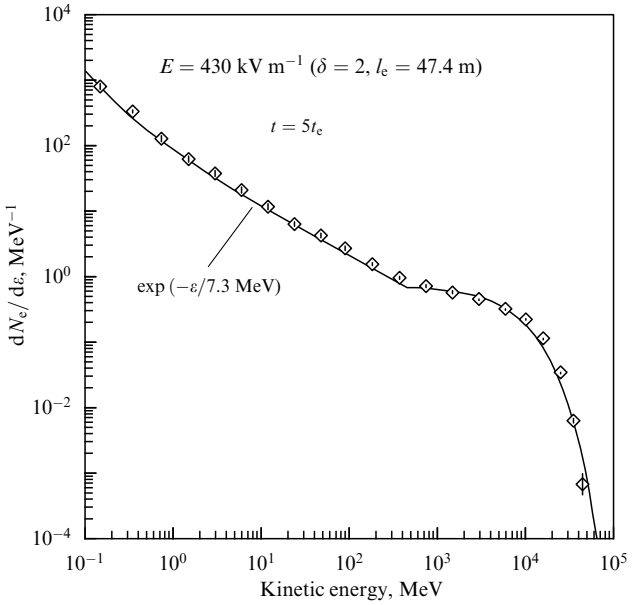

Figure 7. Electron energy distribution normalized to unity at the overvoltage $\delta = 2$ calculated using the REAM code (diamonds) and simple analytical model (curve) [74].

The steady-state electron energy distributions in the range of 100 eV–60 MeV are calculated with the REAM code [73, 74]. For these distributions, under the assumption that $\langle\varepsilon\rangle = 7.3$ MeV, a simpler universal approximation is offered:

$$f_{re} \approx \frac{1}{7.3\text{ MeV}} \exp\left(-\frac{\varepsilon}{7.3\text{ MeV}}\right), \quad (69)$$

which is valid in the range from one hundred keV to several tens of MeV, independent of the field strength and the concentration of air molecules. This distribution at $\delta = 2$ is illustrated in Fig. 7.

For comparison, Fig. 8 illustrates the steady-state distribution calculated by Silisten and Pasko at $\delta = 10$ using the SMC code [92], which is quite consistent with the distributions calculated with the ELIZA and REAM codes.

Angular distributions of high-energy electrons [72]. Steady-state electron angular distributions significantly depend on the overvoltage δ, with an increase in which they become more extended along **e**, i.e., an increasing part of the electrons is dragged by the field as it strengthens. These distributions

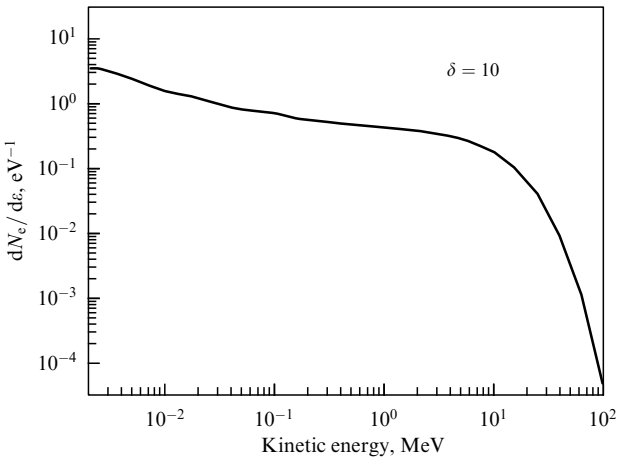

Figure 8. Steady-state electron energy distribution normalized to unity at the overvoltage $\delta = 10$ calculated with the RBEB model [92].

are approximated by the following function (ELIZA):

$$g(\mu, b) = \frac{1-b^2}{2\pi(1-b\mu)^2}\,, \qquad 2\pi\int_0^1 g(\mu, b)\,\mathrm{d}\mu = 1\,, \tag{70}$$

where $b = 0.91$ for $\delta = 2$ and $b = 0.97$ for $\delta = 8$. The error in approximation (70) is maximal at values of μ close to 1, e.g., 12% for $\delta = 2$ and 34% for $\delta = 8$.

The steady-state electron angular-energy [MeV] distributions can be written as a product (ELIZA):

$$f(\varepsilon, \mu) = f_1(\varepsilon)\, f_2(\mu|\varepsilon)\,, \tag{71}$$

where $f_1(\varepsilon)$ is the normalized energy distribution (68) and $f_2(\mu|\varepsilon)$ is the steady-state angular distribution of electrons with energy ε, normalized similarly to (64), which can be approximated as follows:

$$\ln f_2(\mu|\varepsilon) = \begin{cases} y_1(\varepsilon) - k_1(\varepsilon)(1-\mu)\,, & \mu \geqslant 0\,, \\ y_2(\varepsilon) + k_2(\varepsilon)(\mu+1)\,, & \mu < 0\,, \end{cases} \tag{72}$$

where, for $\delta = 2$,

$$y_1(\varepsilon) = 0.5756\,\ln(0.9\varepsilon) - 0.46\,, \quad k_1(\varepsilon) = 1.24(14\varepsilon)^{0.5} - 0.92,$$
$$y_2(\varepsilon) = -2.76(2.3\varepsilon)^{0.48} - 2.53\,, \quad k_2(\varepsilon) = 0.557\ln\varepsilon + 2.91\,, \tag{73}$$

and, for $\delta = 8$,

$$y_1(\varepsilon) = 0.6178\ln\varepsilon + 0.4145\,, \quad k_1(\varepsilon) = 3.224(5\varepsilon - 0.07)^{0.57}\,,$$
$$y_2(\varepsilon) = -7.6(4\varepsilon)^{0.31} - 0.6\,, \quad k_2(\varepsilon) = 0.8858\ln\varepsilon + 5.142\,. \tag{74}$$

Figure 9 shows the normalized electron angular distributions in the energy groups $\varepsilon_1 - \varepsilon_2$: 40–60 keV, 250–300 keV, 0.8–1 MeV, 5–6 MeV, and 20–25 MeV [72]. The approximation curves are calculated assuming an electron energy equal to $\varepsilon = (\varepsilon_1 + \varepsilon_2)/2$. It is seen that Eqns (71)–(74) approximate the results of numerical calculations well in a wide energy range. For each energy group, the average cosine $\langle\mu\rangle$ is calculated, which is approximated by the function

$$\langle\mu(\varepsilon, \delta)\rangle = a(\delta)\frac{\varepsilon}{1 + a(\delta)\,\varepsilon} \tag{75}$$

with a marginal error $\leqslant 0.06$ at $a(\delta = 2) = 2.7$ MeV^{-1} and $a(\delta = 8) = 12$ MeV^{-1}.

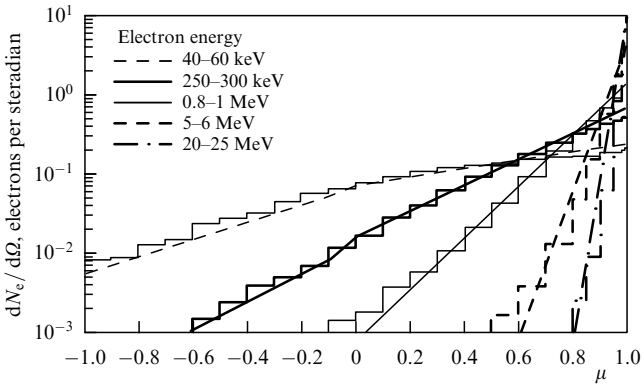

Figure 9. Normalized angular electron distributions in various energy ranges $[\varepsilon_1; \varepsilon_2]$ for $\delta = 8$. Histograms are the results of calculations with the ELIZA code, curves are the results of the approximation (71)–(74) [72].

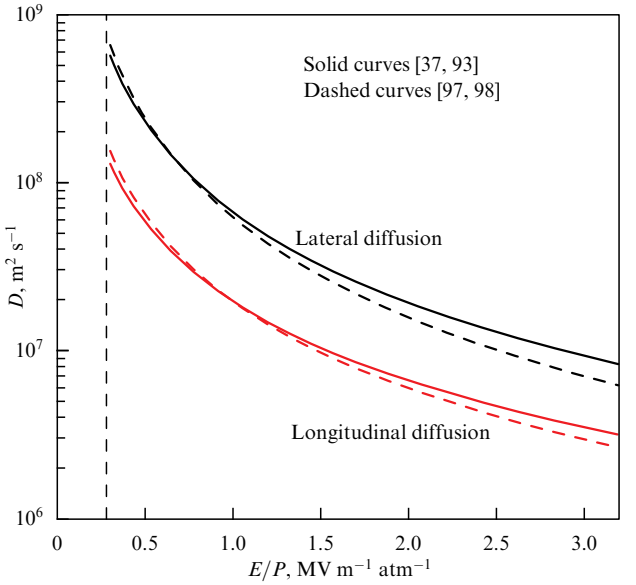

Figure 10. Dependences on the field strength of the coefficients of longitudinal and transverse diffusion relative to the vector calculated with the REAM [37, 93] and ELIZA [97, 98] codes.

Diffusion of high-energy electrons. Extremely important is the conductivity magnitude at the expense of low-energy electrons produced during the RREA development. The low-energy conductivity is directly proportional to the concentration of low-energy electrons, which depends on the spatial distribution of the high-energy electrons, which, in turn depends, in particular, on the diffusion. The role of the longitudinal diffusion in lightning inception by the runaway breakdown was for the first time analyzed by the authors of the GMR mechanism [76]. In connection with this analysis, it was noted in review [37] that the diffusion, as predicted in [76], is 15–40 times weaker than obtained by numerical simulation using the REAM code [93], which is because the angular scattering is allowed for in the latter, and doubt was expressed concerning the enhanced conductivity magnitude predicted in Ref. [76].

The dependences of the diffusion coefficients $D_\parallel$ and $D_\perp$ on the field strength E calculated with the REAM [37, 93] and ELIZA [97, 98] codes are compared in Fig. 10. In the range of low E magnitudes typical of thunderstorm fields, the coefficients are almost identical, but with the rise of E the

calculations with the REAM code predict slightly stronger diffusion than with the ELIZA code. However, even in the range of E magnitudes close to the strength of the usual self-sustained breakdown field $E_{\rm self}$, the difference does not exceed a few percent ($D_{\parallel}$) or a few tens of percent ($D_{\perp}$).

8. Relativistic positive feedback

8.1 Contribution of the intrinsic bremsstrahlung of the avalanche to its enhancement

The electron energy in low-energy Townsend avalanches spent on the excitation of atoms and molecules, seemed to be lost forever, in many cases is returned backward, thus contributing to the Townsend ionization coefficient $\alpha_{\rm T}$. Thus, in gas mixtures, if the excitation energy of atom A exceeds the ionization energy of atom B, reactions occur similar to the Penning reaction $A^* + B \to A + B^+ + e^-$, responsible for the ionization of atom B, or destroying the negative ions (see, e.g., [5, 7, 100–102]). The photons emitted due to the deactivation of atoms A^* are also capable of ionizing atoms of component B.

Similarly, the energy spent by RREA on the bremsstrahlung, some portion of which is spent further on the production of secondary positrons, partially comes back, contributing to the avalanche population via the ionization of air by high-energy bremsstrahlung photons, positrons and photons produced by e^+e^- annihilation. Numerical simulation of the RREA with the MC technique using such codes as ELIZA includes the backward contribution of the processes with the participation of the RE bremsstrahlung and positrons to the RE production rate, which is reflected in the calculated RREA enhancement time $t_{\rm e}(\delta)$. At high enough overvoltages δ, the generation of REs by direct impact ionization dominates, and the relative contribution of processes with the participation of photons and, hence, of positrons is small and decreases with the growth of δ; however, at small δ ($\lesssim 2$) typical of thundercloud fields, it becomes substantial.

To check the contribution of bremsstrahlung to the RREA enhancement rate and to speed up simulations at small δ, it was proposed to divide the process into a sequence of generations of electron and photon avalanches [81]. In the i-th generation, the electrons produced by high-energy impact ionization are simulated, and the contribution of photons is ignored. Using the steady-state angular and energy distributions of the i-th generation of electrons, the bremsstrahlung of the i-th generation is simulated, which in the following cycle produces secondary electrons (and positrons) of the $i+1$-th generation, which, in turn, generate photons of the $i+1$-th generation, and so on.

Ideologically, this approach goes back to the independence of the RREA bremsstrahlung characteristics of whether they are computed self-consistently with the avalanche development or obtained from already calculated steady-state electron energy distributions [103]. In the first approach, the angular and energy distributions of the radiation are computed self-consistently with the avalanche development. In the second approach, for each δ, first, the steady-state electron angular and energy distributions are calculated, and then the bremsstrahlung characteristics in the subsequent moments of time are computed. It turns out that the bremsstrahlung obeys the same laws as the parent RREA: the radiation flux is amplified exponentially with the same characteristic time scale $t_{\rm e}$ as the RREA, and in a wide δ range there is a universal steady-state energy distribution of the bremsstrahlung independent of δ.

The time dependence of the number of electrons in the n-th generation is obtained repeating the specified procedure n times:

$$N_{\rm e}^{(n)}(t) = N_{\rm e}(0)\,\frac{1}{n!}\left(\frac{c_{\rm in}t}{t_{\rm e}}\right)^n \exp\frac{t}{t_{\rm e}}\,, \tag{76}$$

where $N_{\rm e}(0)$ is the initial number of high-energy electrons.

The total avalanche population at moment of time t is the sum of high-energy electrons of all generations:

$$N_{\rm e}^{\infty}(t) = N_{\rm e}(0)\exp\frac{t(1+c_{\rm in})}{t_{\rm e}}\,, \tag{77}$$

where $c_{\rm in} = c_\gamma c_{\gamma{\rm e}} t_{\rm e}$, $c_{\gamma{\rm e}}$ is the average number of electrons capable of entering the runaway mode, which are generated per unit time by one photon of the steady-state spectrum; c_γ describes the growth of the number of photons in the steady-state mode, so that $N_{\rm e}(0)c_\gamma$ is the initial number of photons in this mode. The coefficient c_γ is given by the formula

$$c_\gamma = t_{\rm e}\int_{\{\varepsilon\}} f_{\rm e}(\varepsilon)\Sigma_{\rm brem}(\varepsilon)v_{\rm e}(\varepsilon)\,{\rm d}\varepsilon \int_{\varepsilon_{\gamma\,\min}}^{\varepsilon}\sigma_{\rm brem}(\varepsilon,\varepsilon_\gamma)\,{\rm d}\varepsilon_\gamma \times M_{\{\varepsilon_\gamma\}}\left[1-\exp\left(-\frac{\min\bigl(t,\tau(\varepsilon_\gamma)\bigr)}{t_{\rm e}}\right)\right], \tag{78}$$

in which $f_{\rm e}(\varepsilon)$ is the steady-state electron energy distribution normalized per electron, $\Sigma_{\rm brem} = N\sigma_{\rm brem}$ is the total macroscopic bremsstrahlung cross section, $v_{\rm e}(\varepsilon)$ is the electron velocity, $\sigma_{\rm brem}(\varepsilon,\varepsilon_\gamma)$ is the bremsstrahlung cross-section differential with respect to photon energy ε_γ and normalized to unity ($\int_{\varepsilon_{\gamma\,\min}}^{\varepsilon}\sigma_{\rm brem}(\varepsilon,\varepsilon_\gamma)\,{\rm d}\varepsilon_\gamma = 1$), $M_{\{\varepsilon_\gamma\}}$ is the mathematical expectation along trajectories of photons with the initial energy ε_γ, and $\tau(\varepsilon_\gamma)$ is the lifetime of a photon with energy ε_γ.

Since $1-\exp\left[-\min\left(t,\tau(\varepsilon_\gamma)\right)/t_{\rm e}\right]$ increases with δ, but more slowly than $t_{\rm e}$ decreases, c_γ decreases with the rise in δ, and the ratio $c_\gamma/t_{\rm e}$ increases. Instead of the simplest exponential mode of avalanche enhancement with the time scale $t_{\rm e}$, as given by Eqn (19) in Section 4, according to Eqn (77), the mode is realized (formally at $t\to\infty$) with the time scale

$$\frac{t_{\rm e}}{1+c_{\rm in}}\,. \tag{79}$$

Using numerical simulation, the steady-state angular and energy distributions of electrons and bremsstrahlung photons, time dependences of the electron and photon numbers, and spatial electron distributions along and perpendicular to the electric force were found for the first four generations at $\delta = 1.5$ [81]. The calculated value of the parameter $c_{\rm in}$ with an accuracy of 1% is within the interval 0.1845–0.19455, to which the interval for the limit enhancement time $t_{\rm e}^{\infty} = t_{\rm e}/(1+c_{\rm in}) \in (597.14; 603.23)$ ns corresponds, even the upper boundary of which is significantly less than $t_{\rm e} = 696.4$ computed without splitting into generations (see Table 3).

8.2 Concept of relativistic positive feedback

Long ago, it was discovered [1–9] that photons with energy ε_γ above the gas ionization threshold $\varepsilon_{\rm ion}$ and photoelectric effect threshold $\varepsilon_{\rm ph}$ on the cathode, radiated from the gas discharge volume and ionized by the primary electron avalanche and streamer, produce free electrons as a result of

the gas ionization and photoelectric effect on the cathode. This also happens in the volume directly between the positive avalanche (streamer) trail and the cathode, so that secondary avalanches are initiated, extending towards the primary avalanche (streamer) and thus facilitating the propagation of the cathode-directed streamer. Thus, positive feedback is realized as a sequence of generations of electron avalanches and photons forming an ionized channel, propagating self-consistently with the emission of photons with energies $\varepsilon_\gamma \geqslant \varepsilon_{\text{ion}}$ towards the cathode, i.e., against the direction of the electric force vector **e**. Unlike the simple exponential electron multiplication $\exp(\alpha_T x)$ along the gas-discharge gap, with the feedback taken into account, the number of electrons increases according to the following law [1–5]:

$$n_e(x) = \frac{n_0 \exp(\alpha_T x)}{1 - \gamma_T\left[\exp(\alpha_T x) - 1\right]}, \tag{80}$$

where γ_T is the second Townsend coefficient responsible for the generation of secondary electrons outside the primary avalanche (streamer) volume. Generally, coefficient γ_T also accounts for both the potential and kinetic emission of electrons from the cathode due to bombardment by positive ions. The discharge in a gap with interelectrode spacing d becomes self-sustained under the condition [1–5]

$$\gamma_T\left[\exp(\alpha_T d) - 1\right] = 1. \tag{81}$$

By analogy, Dwyer proposed a mechanism of relativistic positive feedback (RFB) including consecutive generations of high-energy electrons, bremsstrahlung photons, and positrons [73]. In this mechanism, the bremsstrahlung of the primary RREA, secondary positrons, their bremsstrahlung, and e^+e^- annihilation photons, creating secondary high-energy electrons in the volume that includes — which is of primary importance — the regions beyond the main volume of the primary avalanche, support a series of relativistic avalanches. Without RFB, the process fades out, because, according to Dwyer, the ionization by the external sources (cosmic rays; products of atmospheric radon disintegration; electrons accelerated during lightning discharges) is insufficient for the initiation of consecutive generation of relativistic avalanches. The external sources only deliver the initiating REs. Instead of Eqn (19) from Section 4, Dwyer suggests that the rise in the RREA electron population obeys the following law:

$$N_e(t) = N(0)\gamma_D^{t/\tau} \exp\frac{L}{l_e}, \tag{82}$$

where $L = vt$ is the vertical length of the domain with a sufficiently strong electric field, in which with velocity v the ascending relativistic avalanches propagate. The time τ is defined as the delay between the moment when the initial relativistic electron, produced in processes involving some portion of the avalanche bremsstrahlung flux propagating against the direction **e** of the electric force acting on electrons, appears at the border of the strong field domain, and the end of the cycle, when the next batch of feedback electrons enters this domain. The following estimates are obtained for air at ground level [73]:

$$\begin{aligned} &\tau < 10\ \mu\text{s} \quad \text{for} \quad E > 350\ \text{kV m}^{-1}, \\ &\tau < 3\ \mu\text{s} \quad \text{for} \quad E > 500\ \text{kV m}^{-1}. \end{aligned} \tag{83}$$

The coefficient γ_D, as a relativistic analog of the second Townsend coefficient γ_T ('amplification factor' [73]), is defined as the number of feedback REs generated in the considered volume with electric field per initial RE that entered this volume from the outside [73].

Figure 11 illustrates three mechanisms of high-energy electron generation initiated by one high-energy particle in a thunderstorm atmosphere [37]. In the figure, for clarity, the trajectories of positrons and photons propagating against the vector **e** and initiating new avalanches (blue arrows) are displaced to the right; actually, as was shown by numerical simulation, they generally lie within the initial avalanche volume [37, 42]. The RFB mechanism increases the RE number by almost $\approx 10^{13}$ times, in contrast to the simple RREA mechanism, which provides an increase in the RE number by $\approx 10^5$ times relative to that in the simple Wilson acceleration mechanism.

Unlike classical formula (80), which was derived using the Townsend coefficient, time τ and coefficient γ_D in Eqn (82) are introduced by analogy without justification. Assuming $c_{\text{in}} = (t_e/\tau)\ln\gamma_D$ in Eqn (77) and taking into account that $L = vt$ and $l_e = vt_e$, it is possible to obtain Eqn (82). However, the physical sense of the coefficient $c_{\text{in}} = c_\gamma c_{\gamma e} t_e$, derived rigorously to consider the bremsstrahlung contribution to the avalanche enhancement as a continuous process, does not correspond to the sense of the parameters τ and γ_D, introduced artificially to describe the same process of avalanche development.

Despite the obvious genesis of the RFB mechanism, doubts have been expressed concerning its efficiency. Thus, Milikh and Roussel-Dupré [104, 105] consider the RFB insignificant in many cases. Objecting, Dwyer and Rassoul [106], in particular, note that the production rate of positrons should be compared not to the full RE generation rate, as Milikh and Roussel-Dupré do on the basis of their own estimations, but to the generation rate of the initiating particles that would correspond to the RFB process. Dwyer and Rassoul note that already in the first studies [73, 107] it was shown that the RFB can really be applied to thunderclouds, limiting the electric field strength to the magnitude $E_{\text{th}} \approx 284$ kV m^{-1} and, thereby, the maximal achievable RREA enhancement. The threshold magnitude of the thunderstorm field strength, at which the RFB becomes self-sustained, i.e., the equality $\gamma_D = 1$ holds, depends on the strong field configuration, of major importance being the horizontal size of the domain with the field on which, in particular, the RFB due to long-range photons is dependent [82, 108].

The avalanche electrons with the highest energies move in the directions close to the electric force direction . The angular distribution of the photons with energies sufficient to generate secondary REs is close to the angular distribution of the parent electrons [99, 103, 108, 109]. Therefore, the secondary electrons are produced in processes with the participation of the photons generally near the RREA symmetry axis. As the velocities of photons and relativistic electrons are virtually the same, a majority of secondary electrons should be generated by photons in the same space domain that is occupied by high-energy electrons, and, therefore, doubts about the RFB mechanism efficiency could arise.

However, the photon free path length between two consecutive events of elementary interactions is large in comparison with the free path length of electrons having the

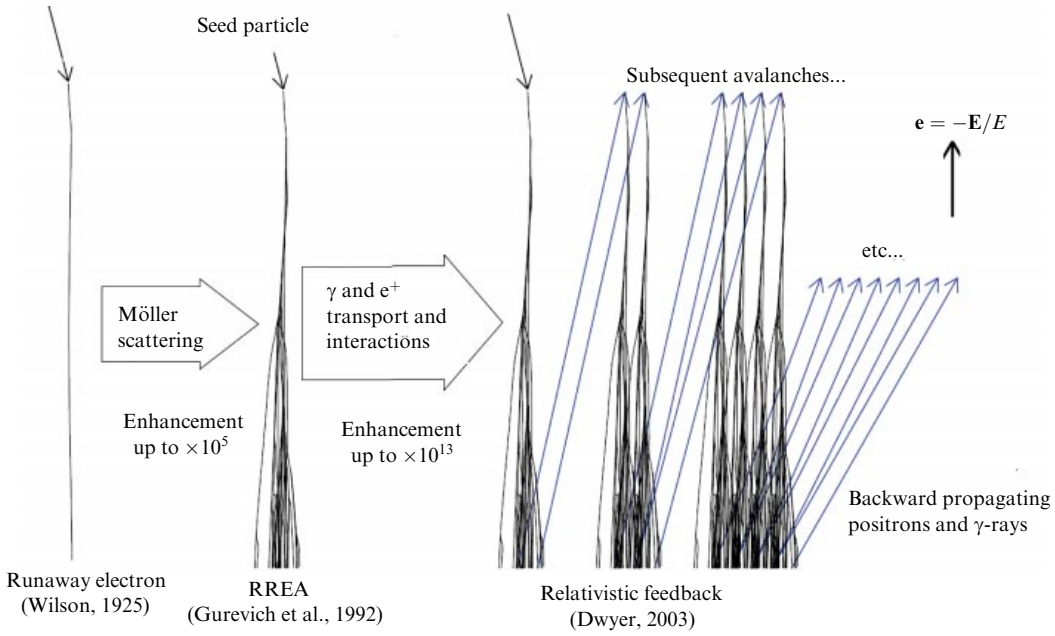

Figure 11. Comparison of the efficiency of RE generation mechanisms: by Wilson [14] (acceleration of electrons to high energies), by Gurevich et al. [30] (RREA according the GMR mechanism, enhancement by 10^5 times relative to the Wilson mechanism), and by Dwyer [73] (RREA with RFB, enhancement by 10^{13} times relative to the GMR mechanism) [37].

same energy, and the field does not affect their motion. Therefore, some portion of secondary REs is generated by photons far away from the main electron bulk, and thus is capable of initiating new avalanches. Indeed, according to results of numerical simulations at $\delta = 1.5$, during avalanche development, the main part of it, containing almost $\approx 99\%$ of the electrons, moves along the **e** direction, so that the avalanche dimensions grow, but its volume as a whole remains rather small. Nevertheless, a small number ($\approx 1\%$) of electrons leave the main volume of the avalanche, and with avalanche development, these electrons can lag more and more behind the bulk [81]. As the relativistic avalanches extend over distances of tens of kilometers, and the discharges caused by them develop in volumes up to 1000 km^3, the RFB mechanism, including the production of secondary high-energy electrons in the processes involving photons and positrons far away from the primary avalanche, can be efficient, and the generation of a series of consecutive avalanches is supported not only by air preionization due to cosmic rays, as was believed when paper [30] was published, in which the estimates are executed based on the flux of 1 cm^2 s^{-1} of secondary cosmic rays with an energy > 1 MeV at the altitude of 10 km [110], but also by the RFB mechanism.

8.3 Mechanism of relativistic positive feedback

In further studies [42, 80, 108], Dwyer develops the RFB mechanism. Using numerical simulations with the REAM code, the mechanism is analyzed by tracing the trajectories of a series of generations of electrons and photons crossing a plane located at mid-height of the domain with size L with the electric field in which the simulated RREA is being developed. The initial REs and photons are marked as particles of the first generation. The number of the RE generation which produced a new particle is attributed to all secondary electrons, photons, and positrons, irrespective of the birth mechanisms. As soon as an electron moving along vector **e** crosses the middle plane, the number of its generation is increased by 1. The RFB coefficient γ_D is defined as the ratio of the number of REs in the generation $N + 1$ crossing the middle plane to the number of REs in generation N crossing the same plane.

The relative contributions of the RFB mechanisms are illustrated in Fig. 12. In the range of high field strength magnitudes, feedback at the expense of the RE bremsstrahlung dominates. To switch the RFB on, the effective attenuation length λ_{at} along the vector **e** of the RFB mediators, i.e., high-energy photons and positrons, should exceed the RREA amplification length l_e. Thus, with the increase in the number of l_e lengths and, therefore, with the increase in the number of REs, the number of the feedback electrons crossing the middle plane can also increase relative to the initial number of REs. In weak fields, length l_e exceeds the attenuation length λ_{at} of the photons due to Compton scattering, so that the RFB is switched off when the field strength is less than ≈ 750 [kV m^{-1}] N_{mol}/N_L. As the length of the runaway positron flux attenuation due to e^+e^- annihilation amounts to hundreds of meters, in the range of low field strength magnitudes the RFB is carried out due to annihilation. On the other hand, in the range of stronger fields, the length l_e is so small that the probability of pair production is less than the probability of the RFB at the expense of the bremsstrahlung [42].

In the range of small field strength magnitudes, the most typical for thundercloud fields, the process is poorly affected by the reduction in the longitudinal (along the height) size L of the domain with the field, as the positrons are generated generally near the primary avalanche. This is illustrated in Fig. 13, where a dependence on L of the maximum field strength E_{max}, required for the fulfilment of the condition $\gamma_D = 1$, is given for three values of the ratio of the transverse size R of the domain with the field to the length L [42].

Dwyer notes that the field strength E_{th} [kV m^{-1}] = 284 (N_{mol}/N_L), being a threshold for RREA development, is

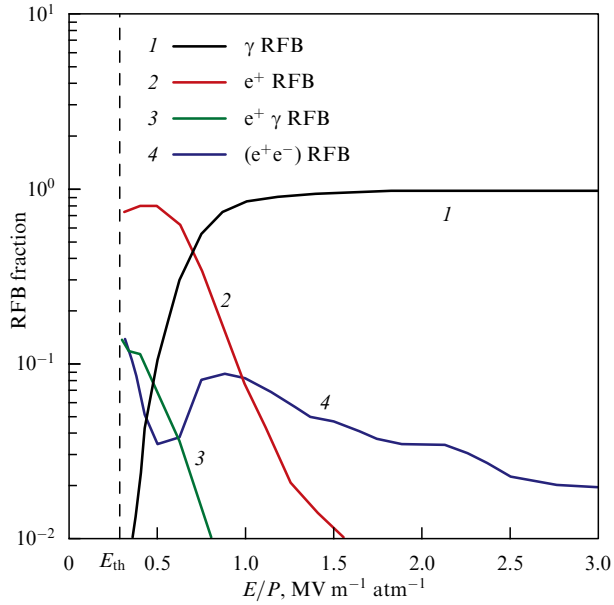

Figure 12. Relative contribution of electron bremsstrahlung (*1*), positrons (*2*), positron bremsstrahlung (*3*), and e^+e^- annihilation (*4*) to the total relativistic feedback in air for $R \gg L$, where R and L are the transverse and longitudinal (vertical) dimensions of the domain with field strength E exceeding the threshold $E_{th} = 284$ kV m^{-1} atm^{-1} [73] of RREA development (vertical dashed line) [42].

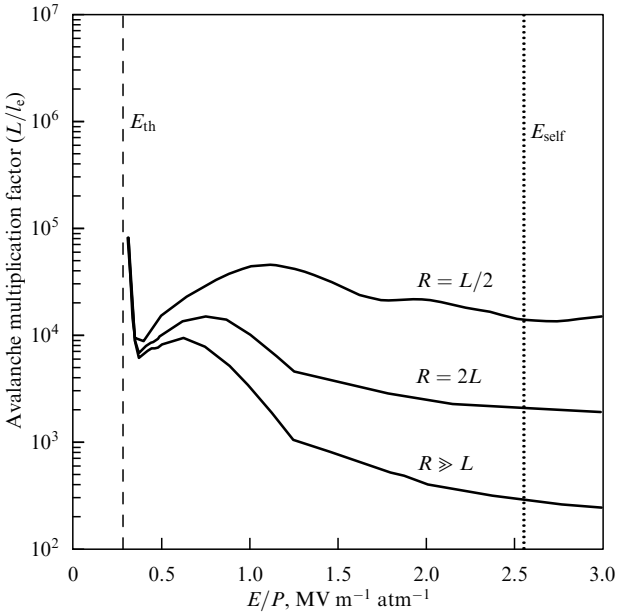

Figure 14. Dependence of the highest possible RREA enhancement factor $\exp\xi$ on the reduced field strength for air. Vertical lines show the threshold magnitudes of the field strength required for RREA development E_{th} and the ordinary breakdown E_{self} [42].

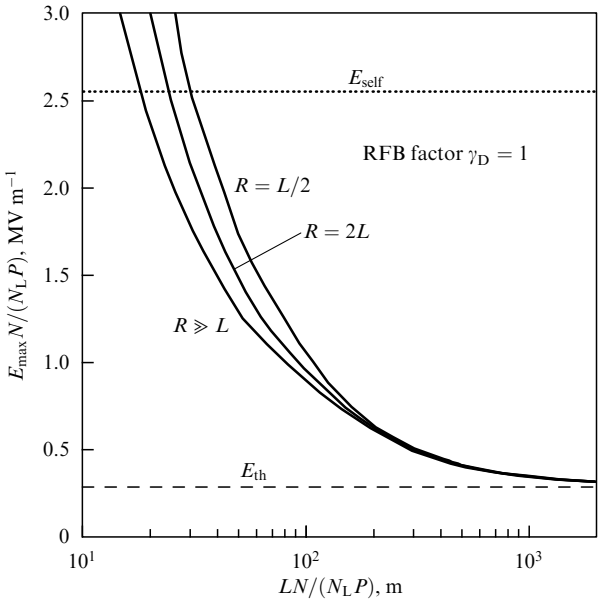

Figure 13. Maximal static electric field strength achievable in air for various ratios of the vertical L and horizontal R dimensions of the domain occupied by the field. The dotted and dashed lines show the threshold values of the usual breakdown E_{self} and RREA development E_{th}, respectively [42].

not marginal, because the rate of ionization only by relativistic avalanches is not necessarily sufficient to discharge the thundercloud field under the conditions of active cloud electrification. Really, the measured magnitudes of the thunderstorm field strength [31, 32] often significantly exceed E_{th}. The RFB mechanism imposes the upper limit on the large-scale electrostatic field strength, achievable in the atmosphere. If this limit is exceeded, the RE flux increases exponentially, the conductivity is raised, and, as a result, the strength quickly decreases below this limit. The polarization of the gas-discharge plasma, formed during the development of the RREA series, weakens the field, and the generation of avalanches is terminated.

Dwyer calculates the RE flux during the time t_{dis} of discharge development with the RFB participation, defined as the time during which the field strength at the end of avalanche development is decreased by e times. At atmospheric pressure with the field strength rise from a magnitude near the threshold $E_{th} \approx 284$ kV m^{-1} to $E \approx 500$ kV m^{-1}, the time t_{dis} sharply decreases from about 134 μs to about 20 μs, and then slowly decreases to ≈ 17 μs with the growth of E, the self-breakdown field strength being $E_{self} \approx 2.5-3$ MV m^{-1}. The RE flux increases by orders of magnitude up to 10^{19} m^{-2} s^{-1} with the increase in field strength from E_{th} to $E \approx 500$ kV m^{-1}, and then slowly increases to $\approx 2 \times 10^{19}$ m^{-2} s^{-1} at $E \approx 3$ MV m^{-1}. For other pressures, the results are scaled as $E(N_L/N)$, depending on LN/N_L.

The RFB imposes a restriction on the field strength and, therefore, on the enhancement of a single RREA. Figure 14 illustrates the highest possible RREA enhancement factor $\exp\xi = \exp\int_0^L dz/l_e(z)$ as a function of the field strength, reduced to the pressure, for several values of the ratio L/R of the dimensions of the domain in which the avalanche develops. It is seen that, irrespective of L/R, the enhancement factor does not exceed 10^5, but even in this extreme case the required size L is so great that $\exp\xi = 10^5$ cannot be applied to thunderstorms, especially taking into account that the distances are scaled inversely proportional to the molecule concentration (altitude) [42]. One relativistic RE per m length produces $\approx 10^5$ secondary low-energy electron–ion pairs, so that the screening of the field by polarizing plasma limits the RE fluence to the order of 10^{10} m^{-2}, produced before the field significantly weakens [73].

On the other hand, the RFB enhances RE generation. Assuming that the RFB is switched off at the moment of time t_{dis}, the ratio of the maximal RE and bremsstrahlung fluxes computed with the RFB taken into account and according to the RREA standard model was calculated. The ratio is equal to 10^9 near the threshold $E_{th} \approx 284$ kV m^{-1}, 10^{11} at $E \approx 500$ kV m^{-1}, and 10^{13} at $E \approx 3$ MV m^{-1} [42].

Dwyer defines the gas-discharge process in a thunderstorm field with RFB participation as a unique mechanism, different from the mechanism of a single RREA, capable of generating $10^{16}-10^{17}$ REs, depending on the source altitude. To produce REs in such numbers, a transverse avalanche size of 100 m is sufficient, which is much less than the sizes of thunderstorm domains with a strong field [82]. The above values of $t_{dis} \approx 17-134$ μs [42] correspond to $t_{dis} \approx 0.1-1$ ms at altitudes of ≈ 15 km, which is consistent with the frequently recorded rise times of terrestrial gamma-ray flashes (TGFs).

In Dwyer's opinion, the term 'runaway breakdown' frequently applied to the standard model of a single RREA is erroneous, since according to several criteria RREA is not a true breakdown. He emphasizes that, according to the classical definition, the breakdown gives rise to a new state of the system, which is independent of further external influences [1–4]. The breakdown and the subsequent discharge necessarily lead to the field collapse in the absence of a sufficiently high-power external source of voltage (current). In the standard RREA model, after the removal of an external source of high-energy seed electrons, avalanche development is sharply terminated. During RREA development, the conductivity of the gas medium is raised due to an increase in the low-energy (a few eV) electron population. This, however, does not necessarily lead to the field collapse, especially since the predicted rate of ionization by high-energy electrons leading to "anomalous growth of conductivity" [38, 11, 112] is strongly overestimated, as shown in analysis [99].

8.4 Self-sustained avalanches in the lightning leader transverse field

The RFB effect is clearly illustrated by the example of the development of consecutive RREA generations in the lateral vicinity of a lightning leader [113, 114]. Since, in this case, owing to the field geometry, the RFB threshold is significantly decreased, an analysis of the RFB in the leader transverse field is of undoubtful interest.

Conditions required for the development of RREA consecutive generations in the transverse field of a positively charged leader are found in Ref. [114]. To model this process using the ELIZA code, numerical simulations of the electron, photon, and positron trajectories were executed under STP conditions in the transverse field of an infinitely long circular cylinder (Fig. 15) with the radius r_{min}. The cylinder carried a surface ($E(r) = 0$, $r < r_{min}$) or volume charge ($E(r) = \lambda r/(2\pi\epsilon_0 r_{min}^2)$, where ϵ_0 is the permittivity of free space. Outside the cylinder ($r \geqslant r_{min}$), the field strength was $E(r) = \lambda/(2\pi\epsilon_0 r)$ in both cases. Here, r is the distance from the cylinder axis and λ is the linear charge density. The field strength distribution in the region $r < r_{min}$ is inessential, as the main voltage drops in the range $r \geqslant r_{min}$. The domain of RREA enhancement is restricted to the interval $[r_{min}, r_{max}]$, such that at the radius $r_{min} = \lambda/(2\pi\epsilon_0 E_{self})$ the self-breakdown field strength $E_{self} = 30$ kV cm^{-1} is attained, and at $r_{max} = \lambda/(2\pi\epsilon_0 \delta_{th} F_{min} P)$ the RREA threshold overvoltage $\delta(r_{max}) = 1.3$ is achieved. The simulation was performed in

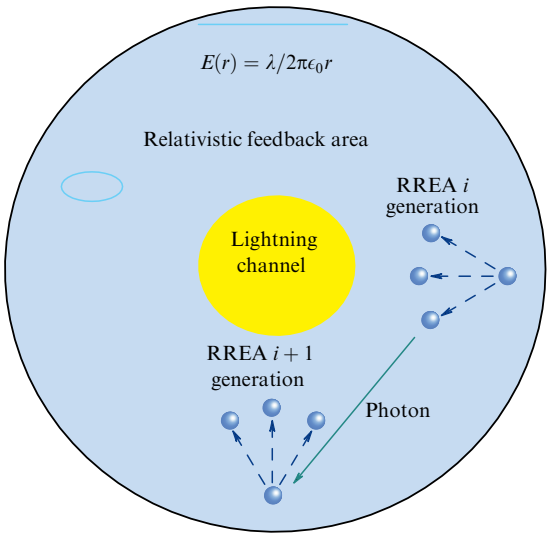

Figure 15. Schematic diagram of the relativistic feedback in the transverse field of a lightning leader [114].

terms of RE generation with the number of electrons N_i, where i is the generation number. N_0 seed electrons constitute the zero generation. The REs which are produced only by ionizing collisions of the REs themselves constitute an avalanche of the i-th generation. The avalanche of the $i+1$-th generation is initiated by a photon emitted by the avalanche of the i-th generation. To switch the RFB on, the sequence of the numbers N_i, beginning with some number i, should obey the geometrical progression law with the geometric ratio $q(\lambda) = N_{i+1}/N_i \geqslant 1$. The calculations are executed for charge densities in the range of $[\lambda_1, \lambda_2] = 1-2$ mC m^{-1}, corresponding to the magnitudes of $r_{min}(\lambda)$ and $r_{max}(\lambda)$.

The results obtained are as follows: $q(\lambda_1) \approx 0.1$, $q(\lambda_2) \approx 10$, the threshold magnitude $q(\lambda_{th}) \approx 1$ being attained at the density $\lambda_{th} \approx 1.5$ mC m^{-1}, typical of leaders [10, 33, 115], $r_{min} = 9$ m, and $r_{max} \approx 100$ m. In the region $[r_{min}, r_{max}]$, where the potential difference

$$\Delta\varphi_{th} = \frac{\lambda_{th}}{2\pi\epsilon_0} \ln \frac{r_{max}}{r_{min}} \approx 65 \text{ MV}$$

is common to thunderstorm fields [10, 33], the RREA is enhanced only 270 times. Note that λ_{th} and $\Delta\varphi_{th}$ are independent of the voltage. For a uniform volume charge distribution in the domain $r < r_{min}$, the results are as follows: $q(\lambda_1) \approx 0.1$, $q(\lambda_2) \approx 10$, threshold magnitude $q(\lambda_{th}) \approx 1$ being attained at density $\lambda_{th} = 1.1$ mC m^{-1} ($r_{min} = 6.5$ m, $r_{max} \approx 70$ m), which is close to $\lambda_{th} = 1$ mC m^{-1} obtained by Carlson [113].

The RREA enhancement limit of 10^5 (see Section 8.3), required for self-sustained discharge ignition, was obtained by Dwyer when initiating secondary avalanches by photons emitted 'backward' (against the vector $\mathbf{e} = -\mathbf{E}/E$) [42, 73], but the probability of 'backward' high-energy photon emission is much less than the probability of 'forward' photon emission. In the transverse field of the leader, the threshold enhancement and, accordingly, the required potential difference decrease. In the case of a positively charged leader, it is due to the fact that the electrons, attracted to the leader, emit high-energy photons mainly towards the leader. The contribution of positrons moving against the vector $\mathbf{e}$ is, most likely, similar in both cases.

9. Relativistic runaway electron avalanche in laboratory experiments

Undoubtedly, the observation of the full-scale RREA in laboratory would be of great interest, especially under conditions close to the STP. When modeling in the laboratory the process characteristic of the thunderstorm atmosphere, experimental conditions, most of all the field strength, degree of its nonuniformity, and air density, should not differ considerably from those in nature. Unfortunately, the spatial restriction is the main shortcoming of any imaginable laboratory experiment for RREA modeling in fields with the strength significantly below the self-breakdown magnitude $E_{\rm self} \approx 3$ MV m^{-1} ($\delta \approx 14$) in the atmosphere, because, at small values of δ, the length $l_{\rm e}$ multiply exceeds any reasonable spatial scale of the laboratory experiment. Three laboratory experiments with the purpose of observing the RREA [116–119] and demonstrating the runaway breakdown [116, 119] were carried out. The first two experiments were performed in 1996–1998 at the Lebedev Physical Institute (LPI) of the Russian Academy of Sciences [116] and VNIIEF [117, 118] in cooperation with the Los Alamos National Laboratory (LANL); the third experiment was executed at the Institute of Electrophysics of the Ural Branch of the Russian Academy of Sciences in cooperation with LPI [119].

9.1 Experiment of the Lebedev Physical Institute

The first experiment on the observation of the runaway breakdown according to the GMR mechanism was carried out with microwave discharge in a quasi-spherical chamber with a diameter of $d_{\rm cham} = 45$ cm with a superimposed external magnetic field with induction $B = 400-1200$ G (0.04–0.12 T) [116]. The discharge was initiated by injecting a 30-ns-long electron pulse with the maximal electron energy $\varepsilon_{\max} \approx 300$ keV, for which the length of the Larmor orbit is 23–7.5 cm. The observed X-ray generation was interpreted as a manifestation of the runaway breakdown. But the experiment was carried out in a deep vacuum ($P = 5 \times 10^{-6}$ Torr, i.e., $\approx 6.7 \times 10^{-9}$ atm), so that the ionization free path length of electrons even with an energy ≈ 100 eV, i.e., near the position of the maximum $\sigma_{\rm ion,\,max} \approx 2.6 \times 10^{-20}$ m^2 of the ionization cross section of the air molecules [120], $\lambda_{\rm ion,\,max} = (\sigma_{\rm ion,\,max} N_{\rm L} P)^{-1} \approx 200$ m, exceeded by several orders of magnitude the chamber diameter. For $\varepsilon_{\max} \approx 300$ keV, the cross section is $\sigma_{\rm ion} \approx 10^{-23}$ m^2; hence, the free path $\lambda_{\rm ion}$ of the injected electrons is longer by approximately three orders of magnitude. Apparently, a multipactor microwave discharge (see, e.g., [121, 122] and references therein) developed, in which electrons produced on the chamber walls were energized in the microwave field and, while colliding with the walls, generated X-rays, which, therefore, could not be evidence of RREA development in a gas volume. The experiment, undoubtedly, is of interest for the physics of microwave discharges in connection with X-ray generation but has no relation to the breakdown problem driven by relativistic avalanches.

9.2 Experiment of the Russian Federal Nuclear Center VNIIEF

9.2.1 Concept of the experiment. Unlike classical Townsend's avalanches [1–5, 123], including electrons of all energies, the RREA is amplified only at the expense of electrons with energies above the runaway threshold $\varepsilon_{\rm th}$. Consequently, the idea of experiment [117, 118] was to inject into a long air gap with spacing d between flat electrodes a pulse containing a sufficiently large number of electrons $N_{\rm inj}(0, \varepsilon \geqslant \varepsilon_{\rm th})$ with energies exceeding $\varepsilon_{\rm th}$ and to measure at the gap exit the number $N(d, \varepsilon \geqslant \varepsilon_{\rm th})$ of electrons in the range $\varepsilon \geqslant \varepsilon_{\rm th}$ or the relative increase in their number. Executing such an experiment is a great challenge because of the inevitable production of a huge number of electrons with energies $\varepsilon \ll \varepsilon_{\rm th}$, the necessity to select the high-energy electrons against the background of electrons with under-threshold energies, the need to conduct measurements of small quantities in an unfavorable electromagnetic environment, etc. To exclude the outflow of the high-energy electrons from the acceleration domain because of the scattering in air, the areas of the electrodes should be rather vast to correspond to the long interelectrode spacing d.

The VNIIEF experiment was planned in cooperation with LANL in 1995, based on greatly underestimated values of RREA enhancement length $l_{\rm e}$ [43, 44]. It was supposed that, using rather high overvoltage δ in a meter-scale air gap, it would be possible to create at least one amplification by e times of the avalanche in the open atmosphere. However, because of the real $l_{\rm e}$ magnitudes, it was possible to observe only an initial stage of RREA development.

Table 4 presents a few values of overvoltage δ and the corresponding voltages $U_{\rm appl} = \delta F_{\rm in}^{\min} P$ to be applied to electrodes at atmospheric pressure. For the chosen values of δ, the values of the runaway threshold $\varepsilon_{\rm th}$, the average energy of electrons $\langle\varepsilon\rangle$, time $t_{\rm e}$, and length $l_{\rm e}$ of the RREA enhancement are given. Apparently, it is not easy to elaborate an experimental configuration corresponding to the length $l_{\rm e}$ of the RREA enhancement in a rather weak thundercloud field ($\delta < 2-3$). To decrease the runaway threshold and, therefore, to increase the RE numbers in both the injected and secondary beams, high voltages $U_{\rm appl}$ are required, which, however, are limited by electric breakdowns in air and along the surface of the solid dielectric isolating the electrodes. To avoid interference, the injected beam duration is to be much less than $t_{\rm e}$. It is imaginable to create a stressed gap with length d in the meter range, and, in view of the inequalities $l_{\rm e} \gg d$ and $eU_{\rm appl} \ll \langle\varepsilon\rangle$, it was expected to observe only an initial stage of the RREA.

In the initial part of the trajectories ($\ll d$), the injected electrons are separated into decelerated (thermalizing) and runaway ($\varepsilon \geqslant \varepsilon_{\rm th}$). The ratio of the number of primary (injected) electrons to the number of secondary REs is practically independent of the initial energy $\varepsilon_{\rm inj}$ of the injected high-energy electrons, as, beginning from $\varepsilon_{\rm inj} > (3-4)\,\varepsilon_{\rm th}$, the secondary electron production probability per unit length in the range $\varepsilon \geqslant \varepsilon_{\rm th}(\delta)$ weakly depends on the energy of the primary electrons. This significantly reduces the requirement for accuracy in measuring the energy spectrum of the injected electrons.

The small overlapping of the spectra of injected and secondary high-energy electrons, decreasing with the growth of δ, is one more important circumstance that, in principle, allows estimating the avalanche enhancement from the experimental results. In the course of avalanche multiplication, not only does the number of the REs increase, but also the energy distribution in the range $\varepsilon \geqslant \varepsilon_{\rm th}(\delta)$ changes. In the electric field, the distribution of primary electrons shifts to higher energies, but a low and extended plateau appears in the lower-energy part ($\varepsilon \geqslant \varepsilon_{\rm th}(\delta)$) of the distribution of secondary REs. Before the direct execution of the experiment, it was required to create registration methods, in which the specified

Table 4. Dependence on the overvoltage δ of the voltage U_{appl} to be applied to the air gap under STP conditions, and the RREA characteristics (see Table 3) for the realizable values of δ.

δ	U_{appl}, MV	ε_{th}, keV	$\langle\varepsilon\rangle$, MeV	t_{e}, ns	l_{e}, m
1.5	0.33	1400	6.75	696.4	187.3
2	0.44	470	6.74	189.7	50.8
3	0.65	160	6.79	77.6	16.6
4	0.87	116	6.83	47.5	12.6
5	1.09	90	6.87	34.3	9.1

peculiarities of the electron distribution would be revealed. The avalanche-like reproduction of relativistic electrons in the open atmosphere in fields with strength below the threshold E_{self} of the self-sustained breakdown could be proven by comparing the results of measuring these peculiarities with the expected results predicted by numerical simulation.

9.2.2 Experimental configuration. The experimental setup included the following units: (1) field-forming system (FFS) modeling the environment in the thunderstorm atmosphere; (2) high-voltage power supply feeding the FFS; (3) injector of nanosecond pulses of relativistic electrons; (4) trigger and synchronization unit.

The FFS is a chamber having the shape of a truncated cone with flat electrodes (Fig. 16). The electrodes are isolated by a hollow solid insulator partitioned by gradient rings with a compulsory distribution of the potential along the insulator to provide field uniformity. The diameter of the top electrode with high potential is equal to 0.6 m and the diameter of the grounded bottom electrode is 1 m. The interelectrode spacing is $d = 1$ m. The voltage is restricted to 1.2 MV by the breakdowns along the insulator surface. The experiments were executed with $U_{\text{appl}} = 1$ MV ($\delta \approx 5$) (see Table 4). Since at such values of d and U_{appl} the enhancement is $\approx \exp(d/l_{\text{e}}) \approx 1 + d/l_{\text{e}}$ or $\approx \exp(U_{\text{appl}}/\langle\varepsilon\rangle) \approx 1 + U_{\text{appl}}/\langle\varepsilon\rangle$, and according to the data in Table 4, at the FFS exit an increase of 10% in the number of electrons with $\varepsilon \geqslant \varepsilon_{\text{th}}$ was expected. A voltage pulse produced by the MIG-5000 generator [124] of the ORION-1 accelerator [125] with a rise time of 6 μs was applied to the FFS electrodes. A nanosecond electron beam was injected into the FFS at the maximum voltage.

The transportable MIN-1 accelerator [126] with an IA-9 acceleration tube [127] was used as the injector. A weakly diverging electron beam slightly nonuniform in the cross section with a diameter of 16 mm was generated. The electrons were injected via a 50-μm-thick titan anode of the tube with a diameter of 30 mm. The maximum magnitude of the beam current pulse outside the anode of the tube was $I_{\max} \approx 2$ kA, and the pulse duration was $\tau_{0.5} \approx 7$ ns. The electrons were distributed in the energy interval up to $\varepsilon_{\max}^{\text{inj}} \approx 670$ keV $\gg \varepsilon_{\text{th}}(\delta = 5) = 90$ keV (see Table 4). The beam was injected through a hole with a diameter of 20 cm in the high-voltage electrode covered with a metal mesh with a transparency of 0.7.

The absolute energy distribution of the injected electrons was calculated as $\Delta N/\Delta\varepsilon \approx I(t)\Delta t/(e^2 U(t))$ using the oscilloscope traces of current $I(t)$ and voltage $U(t)$ at the injector acceleration tube with a timing accuracy of the traces of no worse than 1 ns. The energy distribution of the electrons on the anode surface normalized to unity is given in Fig. 17. Also presented here is the distribution of electrons at the exit from the anode calculated using the ELIZA code. A similar

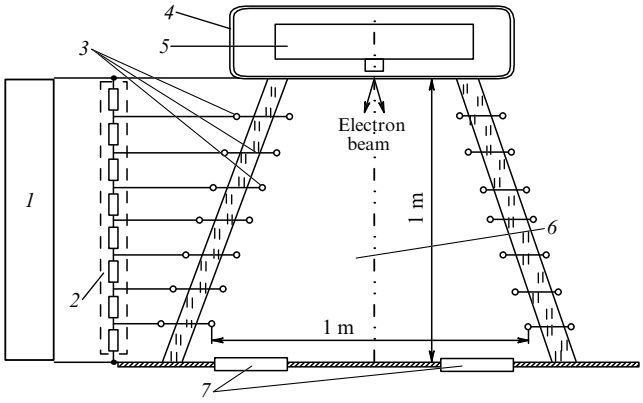

Figure 16. Schematic diagram of an experiment on the observation of the RREA initial stage. *1* — generator of the voltage pulses (MIG-5000 of the ORION accelerator), *2* — voltage divider, *3* — gradient rings, *4* — high-voltage electrode, *5* — injector of the electron beam (MIN-1), *6* — field-forming chamber, *7* — detectors [118].

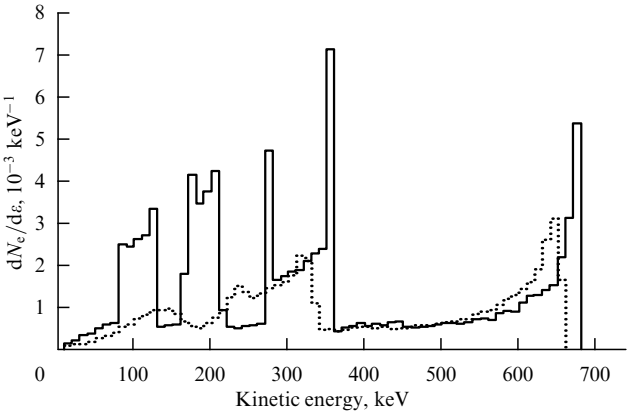

Figure 17. Energy distribution of electrons generated by the MIN-1 injector. The solid line is the distribution on the internal surface of the anode of the injector acceleration tube, the dotted line is the distribution at the output of a 50-μm-thick titanium window [118].

distribution with two groups of electrons near 300 and 650 keV was also measured with the magnetic spectrometry method. The calculated number of electrons on the internal surface of the anode was $\approx 9 \times 10^{13}$. About 30% of the electrons were absorbed in the anode; the distribution in the range below 300 keV experienced the greatest changes. The calculated total number of electrons at the tube outlet was $\approx 6 \times 10^{13}$.

9.2.3 Detectors for measuring the electron energy distribution in wide-aperture beams. Since an extremely small enhancement of the electron flux was expected, an adequately sensitive method of detecting electrons at the FFS exit was required. After analyzing the possibilities and testing several methods, the popular method of charge spectrometers with absorbing filters providing a fairly complete picture of the energy distribution of wide-aperture beams was chosen. In such spectrometers, metal collectors of various thicknesses with a rather vast collecting surface operate as detecting units. The basic design of collector detectors is illustrated in Fig. 18. The aluminum electron collector *2* is located in the metal thick-walled case *1*. Capacitors *5* increase the capacity between the case and the collector. In the top part of the case, there is a window covered with aluminum foil *3*.

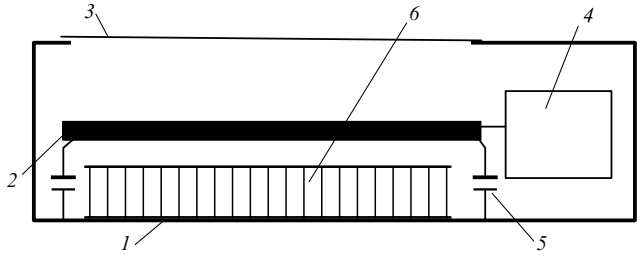

Figure 18. Collector detector intended for the measurement of electron energy spectra. *1* — case; *2* — collector; *3* — 50-μm-thick filter; *4* — recorder; *5* — additional capacitors; *6* — lattice of wells for reducing the effect of scattered electrons [118].

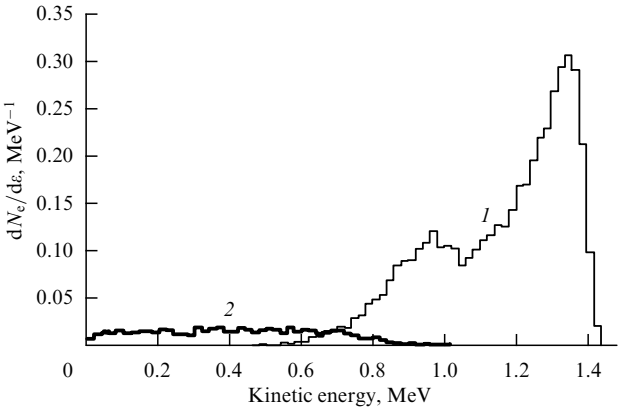

Figure 19. Electron energy distribution on the surface of a disk modeling the collector. The distribution is normalized to a fraction (0.107) of the total number of electrons on the internal surface of the injector anode (9×10^{13}). *1* — primary electrons, *2* — secondary electrons. $U = 1$ MV, $E \approx 1.1$ MV m^{-1}. The fraction of secondary electrons is 11.7%. Numerical simulation with the ELIZA code [117, 118].

Commonly, filters *3* of various thicknesses implement the selection of electrons by energies, while the collectors have one thickness meeting the condition of full absorption of electrons with the maximal expected energy. Large errors in the case of thin filters, when the detector readings are so close to each other that it is impossible to select with the required accuracy the secondary electrons making the major contribution to the readings of thin filters are an obvious shortcoming of such a configuration.

Essentially new opportunities are offered by a different version of the method, in which the collector operates as both the electron energy selector and the recorder [117, 118]. In such a version, the thickness of filter *3*, which only shields the detector from electromagnetic disturbances, is invariable, while the collectors of various thicknesses are used. In comparison with the conventional technique, one more advantage of using collectors of various thicknesses not shading each other is the considerably reduced effect of the scatter of the voltage on the collectors in different pulses on the distribution of electrons in the low-energy part of the region $\varepsilon \geqslant \varepsilon_{\rm th}$, extracted from the results of voltage measurements on the collectors.

The registration is carried out as follows (see Fig. 18). The part of the beam which passed through the filter *3* is partially absorbed in collector *2*. The voltage arising at capacitors *5* is proportional to the charge, i.e., to the number of electrons absorbed in collector *2*. The maximal voltage magnitude is recorded by the electronic circuit. The effect of electromagnetic noise did not exceed 5% of the useful signal, and the charge leakage from the collector due to air ionization within the detector volume was insignificant. To reduce the electron scattering from the bottom of the detector case, a lattice of 1-mm-thick aluminum plates with a height of 20 mm was used. Plates spaced 15 mm apart cross each other at right angles. The lattice placed under the collector on the grounded detector case (Fig. 18) reduced reflection from 12% to 1–2%, thereby, in essence, eliminating the registration of the scattered electrons. The method was implemented with the use of 8 identical detectors, each with area $S_{\rm col} = 329$ cm^2. They were evenly arranged around the FFS grounded electrode at the same distances from the FFS symmetry axis.

9.2.4 Observation of the initial stage of an avalanche. Table 5 presents the results of measuring the charges collected by the collectors in one of the pulses and the results of numerical simulations taking into account the electrons reflected from the FFS anode. The relative measurement error is estimated as ±10%, taking into account normalization to the thickest collector absorbing electrons of all energies. The error is mainly caused by random deviations of the beam from the symmetry axis of the system, because of which in different pulses different numbers of electrons arrive at the collectors.

Figure 19 illustrates the electron energy distribution expected at $U_{\rm appl} = 1$ MV on the surface of a disk modeling the collector, normalized to a fraction of 0.107 of the total number of electrons on the internal surface of the injector anode (9×10^{13}). In this distribution, the number of secondary electrons is 11.7%. To show that the RREA was really observed, it was necessary to compare the results of measurements and calculations of the expected collector indications (see Table 5). In addition to calculating the contribution of all electrons to the collector indications, the contributions of the primary (injected) and secondary electrons were calculated separately. A comparison of the experimental data with the normalized results of calculations assuming a zero portion of secondary electrons (fifth line in Table 5), i.e., considering only the contribution of primary electrons to the expected collector indications, lead to the conclusion that the number of generated secondary electrons in the runaway range $\varepsilon \geqslant \varepsilon_{\rm th}$ was rather large.

It should be noted that the expected indications of detectors calculated without allowing for the electrons reflected from the FFS anode significantly differ from the indications of thin collectors. However, the expected collector indications calculated allowing for the reflection of electrons from the FFS anode practically coincide with the measurement results, as is seen comparing the third and fourth lines in Table 5. Therefore, the enhancement of the flux of relativistic electrons in an electric field was implemented, i.e., the RREA initial stage was observed in the open atmosphere in a field nearly three times weaker than $E_{\rm self}$ required for the self-sustained breakdown by electrons with an energy of a few electronvolts.

Experiments with higher voltage have been planned. Numerical simulation predicts that with the increase in $U_{\rm appl}$ to 1.7 MV the fraction of secondary electrons with $\varepsilon \geqslant \varepsilon_{\rm th}$ would increase to 22%.

9.3 Experiment of the Institute of Electrophysics of the Ural Branch of RAS

As pointed out in the Introduction, discharges in the open atmosphere at high overvoltages relative to the self-sustained

Table 5. Calculated expected collector indications allowing for the reflection from the FFS anode (see the distribution in Fig. 19) and experimental collector indications normalized to the indications of collector no. 8.

Collector number		1	2	3	4	5	6	7	8
Collector thickness, mm		0.2	0.4	0.6	0.8	1.0	1.2	1.5	5
Experiment, $U = 1$ MV		0.055	0.13	0.21	0.37	0.50	0.67	0.78	1
Calculation	11.7% secondary + 88.3% primary electrons	0.051	0.10	0.21	0.36	0.50	0.68	0.82	1
	0% secondary + 100% primary electrons	0.010	0.039	0.14	0.28	0.44	0.64	0.80	1

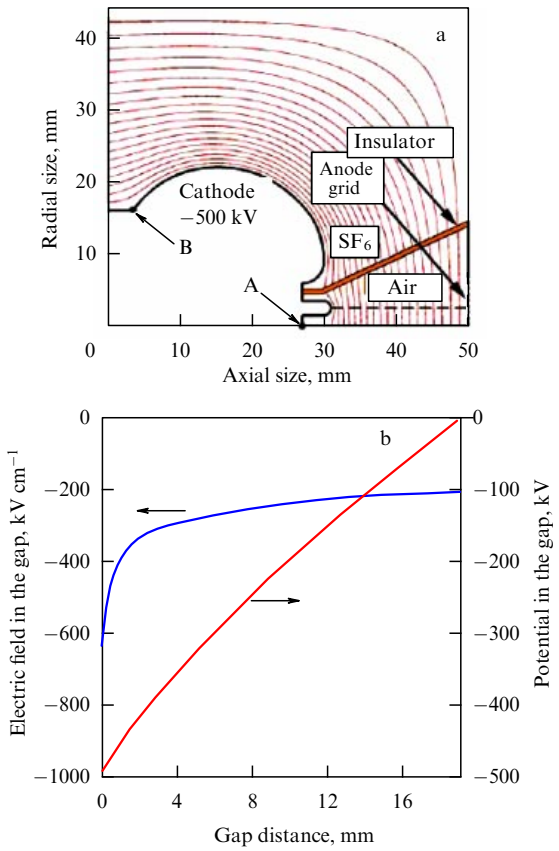

Figure 20. (a) Geometry of an electrode unit with an equipotential map. (b) Calculated distributions of the electric field strength and potential along the dashed line in Fig. (a) [119].

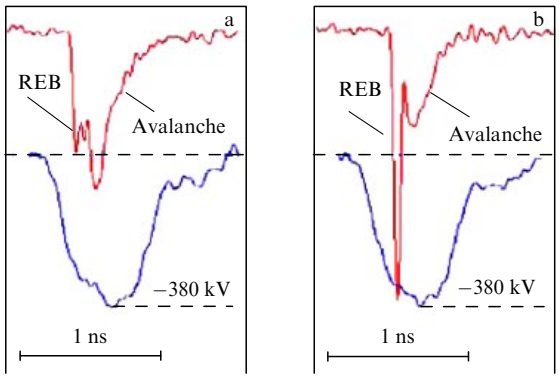

Figure 21. Pulses of the applied voltage $U(t)$ and electron current $I_e(t)$ on the collector downstream of the anode without mutual $U(t)$ and $I_e(t)$ timing. The filter between the anode and collector is absent. In case (a), the RE beam was emitted 0.15 ns earlier than in case (b) [119].

breakdown voltage U_{self} generate subnanosecond pulses of high-energy REs [11, 12, 17–26]. A discharge of exactly such a class [19, 20] was used in experiment [119]. The discharges were implemented in a gas-discharge gap bounded by a solid conic insulator with the interelectrode spacing in the centimeter range and sophisticated cathode geometry (Fig. 20a). It was supposed that along the symmetry axis far away from the cathode, the provided potential distribution was close to uniform (Fig. 20b), which is convenient for the interpretation of the obtained results, as in this case the overvoltage δ depends only on time due to the changing voltage. A grid with a transparency of 50% was used as an anode. The electron current was detected behind the anode by a collector with an area of $S_{coll} \approx 1$ cm^2. In the framework of the experiment concept developed in [119], it was expected that the primary RE beam, while passing through the gas, would generate a secondary RE avalanche through which runaway breakdown would be demonstrated.

Two experimental configurations were implemented: in one of them the field domain was separated from the collector only by a 1-mm-thick air gap, cutting off electrons with energies of less than 6–7 keV, and in the second, additionally by a 60-μm-thick aluminum foil cutting off electrons with energies below 95 keV [119]. At $\delta \geqslant 100$, an RE pulse was observed having a picosecond duration and consisting of a peak (runaway electron beam (REB) [119]), which in the configuration without the filter was followed by a secondary peak ('avalanche current' [119]) observable in the oscilloscope traces in Fig. 21. The secondary peak is interpreted according the GMR mechanism as an RE avalanche, initiated by the primary peak, and a manifestation of the runaway breakdown.

Such an interpretation is unexpected, as the energy of the electrons in the RE avalanche (see Table 3) exceeds by several times the magnitude eU_{max} in the experiment [119] (see Fig. 21). To verify this interpretation [119] of the experimental results, a numerical analysis was carried out [97, 98]. It was necessary to clarify whether the secondary peak of the RE pulse is really produced by the preceding peak.

Setting of the numerical experiment. According to the experimental configuration in [119], it was assumed in [97, 98] that in the super-strong nonuniform field near the cathode the primary RE beam (REB [119]) is formed. The beam continues its motion in the weaker uniform field towards the anode and further to the collector. The 3D simulation was executed with the ELIZA code. Trajectories of $N_{inj} = 2.25 \times 10^6$ electrons with initial energy $\varepsilon_{inj} = 10$ keV were traced. The electrons were 'injected' at point $x = 0$ (the cathode top) along the electric force $-e\mathbf{E}$ into the air gap $d = 1.9$ cm in length (see Fig. 20a). The beam current pulse was approximated by an isosceles triangle with the half-height

duration $\Delta t_{1/2} = 70$ ps, corresponding to experiment [119], and a maximum at the varied moment of time t_m. Electrons with energies above 1 keV were taken into account. The field strength was calculated as $E(x,t) = G(x)U(t)/d$, $x \in [0,d]$, where $G(x)$ describes the field strength distribution along the gap symmetry axis, as illustrated in Fig. 20b. The voltage oscilloscope traces were approximated as follows (cf. Fig. 21):

$$U(t) = U_{\max}\begin{cases} \dfrac{t}{t_1}, & t < t_1, \\ 1, & t_1 \leqslant t < t_2, \\ 1 - \dfrac{t - t_2}{t_1}, & t_2 \leqslant t < t_1 + t_2, \end{cases} \qquad (84)$$

where $t_1 = 0.4$ ns, $t_2 = 0.9$ ns, and $U_{\max} = 500$ kV (according to Fig. 20b). Both experimental configurations, with the filter and without it, were simulated. As the primary RE beam was generated at the leading edge of the voltage pulse [119], the limitation $t_m \leqslant t_1$ was imposed.

Results of the numerical experiment. are a temporal dependence of the RE current dN_e/dt on the 'collector' with an infinite surface and time-integrated electron energy distributions $dN_e/d\varepsilon$ on the collector.

The dependence dN_e/dt at $t_m = 0.3$ ns is presented in Fig. 22a. If the aluminum filter is absent, the integral of the beam current is 99.7% of N_{inj} for primary electrons and 33.2% for secondary ones. In the option with the filter, the integral equals 99.4% and 26.9%, respectively. Hence, the fractions of the primary and secondary electrons which passed the filter equal, respectively, $99.4/99.7 \approx 1$ and $26.9/33.2 = 0.81$. It is seen that the current pulse width at half-maximum $\Delta t_{1/2}$ is almost equal to the initial width of 70 ps and the pulse base widened by less than 50 ps at the expense of the secondary electrons. These results do not agree with the experimental data [119] where the 'tail' duration exceeds 160 ps, and either the integrals of currents for the primary peak and the 'tail' without the filter are close to each other, as in Fig. 3 of Ref. [119], or the integral of the 'tail' is greater (see Fig. 21).

The energy distributions $dN_e/d\varepsilon$, normalized to N_{inj}, are illustrated in Fig. 22b. Without the filter, 94% of the primary electrons are in the energy range above 400 keV; 86% and 95% of the secondary electrons are, respectively, in the ranges of > 100 keV and > 40 keV. Therefore, the filter that according to [119] cuts off electrons with energies of < 95 keV should not significantly affect the registered RE current, which contradicts the oscilloscope traces in Figs 3 and 4 of Ref. [119], where the 'tail' is observed in the absence of the filter.

Variation of t_m, ε_0, and $G(x)$ with fixed amplitude $U_{\max}$ did not essentially affect the computed results. Being reduced to the real collector area $S_{coll} \approx 1$ cm^2, the fraction of secondary electrons decreases, because the spectrum of secondary electrons is significantly softer than that of primary electrons, and they experience stronger angular scattering, thus forming, in the opinion of the authors of Ref. [119], a strongly diverging flux. Moreover, considering the attenuation in the anode will somewhat reduce the fraction of secondary electrons. And, finally, the accepted value of $U_{\max}$ greatly exceeds the voltage amplitude in the experiment (cf. Fig. 21).

Thus, the strongly expressed 'tail' of the picosecond RE pulse (see, e.g., Fig. 21), interpreted as an RE avalanche initiated by the primary pulse (REB [119]), was not revealed in

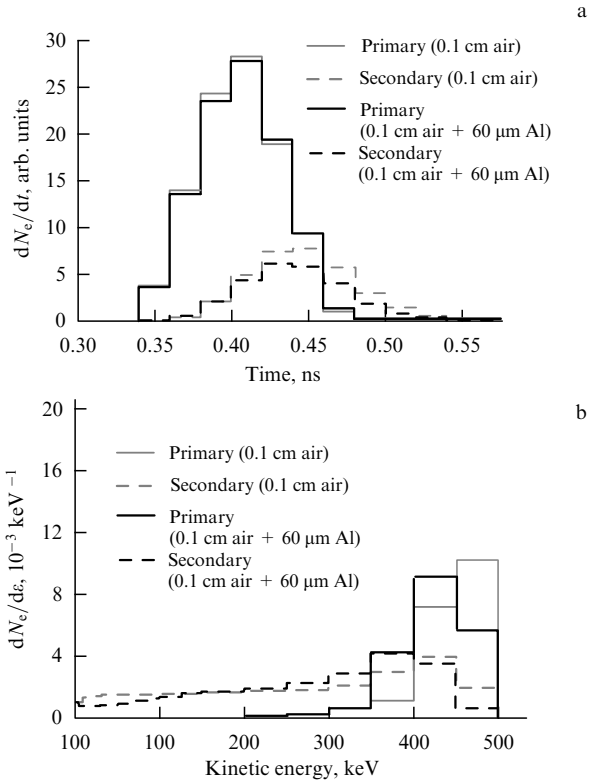

Figure 22. Calculated electron current dN_e/dt (arbitrary units) ($\varepsilon \geqslant 1$ keV) on the 'collector' (a) and electron energy distributions $dN_e/d\varepsilon$ on the 'collector' (b); energy of the 'injected' electrons $\varepsilon_{inj} = 10$ keV, $t_m = 0.3$ ns [97, 98].

the numerical experiment. The calculated pulse of secondary electrons is poorly expressed; it practically merges with the pulse of primary electrons, and the fraction of secondary electrons on the collector relative to the number of primary electrons is $\approx 30\%$. Therefore, under the experimental conditions in [119], it was possible to observe the initial stage of the RE avalanche as a weak enhancement of the primary electron pulse, but the portion of secondary REs is too small to significantly affect the development of the breakdown, in comparison with the contribution of the primary pulse.

Nature of the secondary peak. The results of numerical simulations of the discharge at multiple overvoltages in the self-consistent field at 1 atm [128], which showed that REs greatly contribute to the total current, prove the importance of the runaway of low-energy electrons ('thermal runaway' [129] or, more precisely, 'high-field runaway' [108]). However, an attempt to explain the secondary peak by the acceleration of the secondary low-energy electrons ($\ll 1$ keV), disregarded in the ELIZA code, in the prolonged domain with undisturbed uniform field ($E \approx 160$ kV cm^{-1} [119]) was unsuccessful: in 0.1 ns, one electron of the primary peak does not generate even a single secondary RE in the gap [97, 98].

The passage of the primary beam through the gas-discharge gap is accompanied by the polarization of the secondary plasma, in particular, by the displacement of the field towards the anode, so that the field strength can locally increase in the anode vicinity by orders of magnitude. The secondary peak in [119] can then be explained by the runaway of low-energy electrons in the near-anode domain. The characteristic time of the field redistribution (Maxwellian relaxation time) estimated as

$\tau_M \approx 50$ ps [97, 98] agrees rather well with the experiment [119] (see Fig. 21).

It should also be kept in mind that there is a difference in the electrodynamics of the configurations with and without the filter, in particular, "...the sagging out of the electric field from a gas-discharge gap into the drift space through the holes in the grid," to which Bokhan and Sorokin [130] paid attention in connection with the studies of the so-called open discharge (see, e.g., [22, 130–132] and references therein). As a result of the 'sagging out' of the field into the space outside the grid anode, a breakdown between the grid and collector can occur, manifesting itself as a secondary peak in the configuration without a filter. In the experiments with the filter, the latter shields the collector from the plasma formed in the domain with the field sagged out.

10. Conclusion

The present review is restricted to publications on the relativistic runaway electron avalanche (RREA): discussed are the genesis of the avalanche concept, the avalanche average characteristics, the methods and history of their calculation, and attempts to observe the avalanche in the laboratory. The results of studies of high-energy processes in a thunderstorm atmosphere and their interpretation within the RREA concept are available in reviews [37–40] and references therein.

The classical Townsend avalanche of low-energy electrons is amplified via ionizing collisions of electrons with energies above the ionization threshold of atomic particles, but is populated with electrons of all energies. The development of an avalanche series (low pressures) or single streamers (high pressures, including the open atmosphere) is causal to the electric breakdown in gases [1–5]. However, thunderstorm fields are too weak for the development of the Townsend multi-avalanche or single-channel streamer mechanisms of the breakdown [1–5]. To overcome this difficulty, the GMR mechanism of runaway breakdown in the atmosphere [30] was proposed for relatively weak thundercloud fields. The mechanism allows for rare events producing high-energy electrons, thanks to which the RREA is formed as a process of the exponential rise in the number of high-energy electrons accompanied by the exponential growth of the low-energy electron population.

The genesis of the RREA concept and the runaway breakdown in atmosphere should be rigorously presented as follows: (1) the Wilson hypothesis on the possibility of acceleration of electrons in thundercloud electric fields [14] and the snowball effect owing to the impact reproduction of electrons [133, 134]; (2) the term 'runaway electrons' introduced by Eddington in connection with the Wilson hypothesis [27] and later borrowed by the authors of fusion studies (e.g., [135–137]); (3) the first experiments intended to check the Wilson hypothesis [138–148] (see also [11, 37, 39]); (4) Gurevich's theory of electron runaway in weakly ionized plasma with the dominance of electron-neutral interactions [51]; (5) discovery and investigation of the electron runaway phenomenon in open atmosphere discharges in strong and super-strong electric fields [11, 12, 17–26]; (6) successful registration of X-rays inside thunderclouds [34, 35] and neutron flux enhancements on Earth's surface in correlation with the lightning electromagnetic pulse [149]; (7) Gurevich–Milikh–Roussel-Dupré theory of the avalanche-like amplification of runaway electrons in thunderstorm fields [30]; (8) relativistic positive feedback RFB [42, 73, 107] as an extension of the classical streamer mechanism [1–5] into the relativistic energy range.

In fact, however, paper [30] is based on the Wilson hypothesis [14], the Gurevich theory [51], and the experiment by McCarthy and Parks [35]. The authors of the first publications on the RE and X-ray generation by discharges in the open atmosphere [13, 15–17] were familiar with neither the Wilson hypothesis [14] nor the Gurevich theory [51], though Noggle et al. [15], who observed X-rays from discharges in helium at atmospheric pressure, cite Wilson's paper. Similarly, the authors of the report of 1994 about the penetrating radiation from lightning discharges [150] were not familiar with the already published concept of runaway breakdown in thunderclouds [30].

Like the Townsend avalanche, the RREA is characterized, first of all, by the time t_e and length l_e of enhancement by e times. The values of l_e, analytically calculated in the pioneering article [30] without allowing for angular scattering, are underestimated by less than two times relative to the values calculated finally by the MC [58, 65, 71, 72, 74, 97–99] and KE [65] techniques. For weak fields, typical of thunderclouds, the underestimation does not exceed 1.5 times (see Table 2). Surprisingly, in the improved analysis [76] and the first calculations using the KE method, aimed to correct the results of [30], strongly underestimated values of t_e and l_e were obtained. As emphasized by the authors of [58], within the previous kinetic and analytical models [43, 44, 85–88], the RREA development rate was overestimated by almost an order of magnitude, which greatly reduced the requirements regarding the thunderstorm field strength and length l_e at which an RE number sufficiently large for the adequate interpretation of observational results on the high-energy and optical processes in a thunderstorm atmosphere could be provided.

Values of t_e close to the final ones calculated using the full MC code ELIZA (see the first line of Table 2) were first obtained with the simplified MC code [68, 77]. Later, errors due to the 'human factor' [43–45, 63, 65, 69, 70] were corrected, and different groups calculated quite close values with the MC and KE methods [58, 65, 71, 72, 74, 97–99]. Depending on the 'overvoltage' δ of the electric field relative to the electron drag force, those RREA parameters required for the numerical simulations of the high-energy atmospheric processes and electric discharges, driven by the RREAs, under the fluid approximation, were calculated, namely, t_e, the directed velocity v_{re}, $l_e = v_{re} t_e$, the electron energy and angular distributions, the average electron energy $\langle \varepsilon \rangle$, the runaway threshold ε_{th}, and the coefficients of the longitudinal $D_\parallel$ and transverse $D_\perp$ diffusion.

With the introduction of relativistic feedback (RFB) [73] (by analogy with the positive feedback in the streamer mechanism of the breakdown), the discharges with RREA participation became self-sustained [42, 73, 99, 107]. Although the RFB mechanism limits the RREA enhancement factor to about 10^5, RE flux magnitudes of about 10^{19} m^{-2} s^{-1} can be attained during the development of discharges driven by the RFB [42]. In Dwyer's opinion, "... the feedback can increase the flux of runaway electrons and the accompanying X-ray emission by factors of trillions, resulting in large charge motion, an increase in the conductivity, and ultimately, the collapse of the ambient electric field under conditions for which ordinary runaway breakdown has a completely negligible effect" [42].

After introducing the RREA concept into the physics of atmospheric electricity and using it to interpret the results of explorations of high-energy processes in thunderstorm atmospheres, it was of interest to create the RREA in the laboratory. The 'corrected' values of length l_e [43, 44] (see Table 2) gave hope to achieve an overvoltage magnitude sufficient for producing at least one enhancement length l_e under laboratory conditions. However, because the real l_e values turned out to be extremely large, the restricted dimensions of the setup allowed observing in the laboratory experiment only an initial RREA stage — under conditions which do not differ drastically from those in a thundercloud (open atmosphere, weakly nonuniform electric field with the strength significantly less than the self-breakdown magnitude $E_{self} \approx 3$ MV m^{-1} in a volume with characteristic dimensions at least of the meter scale) — as an increase ($\approx 12\%$) in the number of injected electrons with energies higher than the runaway threshold [118, 119], which testifies in favor of the GMR mechanism [30].

Acknowledgments

The present review is a consequence of the studies executed under the ISTC project nos. 339, 490, 1480, and 3993. The author expresses his deepest gratitude to S Gitomer, the former USA scientific advisor for the ISTC; to C Haldoupis, T Neubert, R A Roussel-Dupré, E M D Symbalisty, collaborators from the USA and the EU in these projects; to N Crosby, S Cummer, A van Deursen, J R Dwyer, R A Roussel-Dupré, D Smith, H Tsuchiya, and E Williams for their support of a proposal on project no. 3993, the last one in the ISTC program. The author is sincerely grateful to E I Bochkov, E N Donskoy, A V Gurevich, C Haldoupis, I M Kutsyk, T V Loiko, T Neubert, R A Roussel-Dupré, E M D Symbalisty, K P Zybin, and other participants in studies executed under these projects, for their long-term collaboration. The author is especially grateful to R I Il'kaev who, as the VINNEF director, supported in 1995–1996 research in the field of high-energy atmospheric electricity in the framework of the VNIIEF–LANL–Lebedev Physical Institute collaboration via the ISTC and to the Head of the VNNIEF Office for International Relations O S Vorontsova who, in spite of difficulties, approved the start of project no. 3993. The author is grateful to the anonymous reviewer from *Physics–Uspekhi* whose comments allowed the article to be significantly improved.

Readers can access the data from the paper via the author by email: leonid.babich52@gmail.com.

References

1. Loeb L B, Meek J M *The Mechanism of the Electric Spark* (Stanford, CA: Stanford Univ. Press, 1941)
2. Meek J M, Craggs J D *Electrical Breakdown of Gases* (Oxford: Clarendon Press, 1953); Translated into Russian: *Elektricheskii Proboi v Gazakh* (Moscow: IL, 1960)
3. Raether H *Electron Avalanches and Breakdown in Gases* (Washington, DC: Butterworths, 1964); Translated into Russian: *Elektronnye Laviny i Proboi v Gazakh* (Moscow: Mir, 1968)
4. Brown S C *Introduction to Electrical Discharges in Gases* (New York: Wiley, 1966)
5. Lozanskii E D, Firsov O B *Teoriya Iskry* (Spark Theory) (Moscow: Atomizdat, 1975)
6. Mesyats G A, Bychkov Yu I, Kremnev V V *Sov. Phys. Usp.* **15** 282 (1972); *Usp. Fiz. Nauk* **107** 201 (1972)
7. Raizer Yu P *Gas Discharge Physics* (Berlin: Springer-Verlag, 1991); Translated from Russian: *Fizika Gazovogo Razryada* (Moscow: Nauka, 1987); *Gas Discharge Physics* (Berlin: Springer, 1997); Translated from Russian: *Fizika Gazovogo Razryada* (Moscow: Nauka, 1992)
8. Korolev Yu D, Mesyats G A *Fizika Impul'snogo Proboya Gazov* (The Physics of Pulsed Breakdown in Gases) (Moscow: Nauka, 1991)
9. Bazelyan E M, Raizer Yu P *Spark Discharge* (Boca Raton, FL: CRC Press, 1998); Translated from Russian: *Iskrovoi Razryad* (Moscow: Izd. MFTI, 1997)
10. Bazelyan E M, Raizer Yu P *Lightning Physics and Lightning Protection* (Bristol: IOP Publ., 2000); Translated from Russian: *Fizika Molnii i Molniezashchity* (Moscow: Fizmatlit, 2001)
11. Babich L P *High-Energy Phenomena in Electric Discharges in Dense Gases: Theory, Experiment, and Natural Phenomena* (Arlington, VA: Futurepast, 2003)
12. Babich L P, Loiko T V, Tsukerman V A *Sov. Phys. Usp.* **33** 521 (1990); *Usp. Fiz. Nauk* **160** (7) 49 (1990)
13. Frankel S et al. *Nucl. Instrum. Meth.* **44** 345 (1966)
14. Wilson C T R *Proc. Cambr. Philos. Soc.* **22** 534 (1924)
15. Noggle R C, Krider E P, Wayland J R *J. Appl. Phys.* **39** 4746 (1968)
16. Stankevich Yu L, Kalinin V G *Sov. Phys. Dokl.* **12** 1042 (1967); *Dokl. Akad. Nauk SSSR* **177** (1) 72 (1967)
17. Tarasova L V, Khudyakova L N *Sov. Phys. Tech. Phys.* **14** 1148 (1969); *Zh. Tekh. Fiz.* **39** 1530 (1969)
18. Tarasova L V et al. *Sov. Phys. Tech. Phys.* **19** 351 (1975); *Zh. Tekh. Fiz.* **44** 564 (1974)
19. Yalandin M I et al. *Tech. Phys. Lett.* **37** 371 (2011); *Pis'ma Zh. Tekh. Fiz.* **37** (8) 56 (2011)
20. Mesyats G A et al. *Plasma Phys. Rep.* **38** 29 (2012); *Fiz. Plazmy* **38** 34 (2012)
21. Bokhan P A, Kolbychev G V *Sov. Phys. Tech. Phys.* **26** 1057 (1981); *Zh. Tekh. Fiz.* **51** 1823 (1981)
22. Vasilyak L M et al. *Phys. Usp.* **37** 247 (1994); *Usp. Fiz. Nauk* **164** 263 (1994)
23. Babich L P *AIP Conf. Proc.* **363** 156 (1996)
24. Babich L P, in *Electron Kinetics and Applications of Glow Discharges. Proc. of the NATO Advanced Research Workshop on Electron Kinetics and Applications of Glow Discharges, St. Petersburg, Russia, May 19–23, 1997* (NATO Science Series, Ser. B, Vol. 367, Eds U Kortshagen, L D Tsendin) (Boston, MA: Springer, 1998) p. 199
25. Tarasenko V F, Yakovlenko S I *Phys. Usp.* **47** 887 (2004); *Usp. Fiz. Nauk* **174** 953 (2004)
26. Babich L P *Phys. Usp.* **48** 1015 (2005); *Usp. Fiz. Nauk* **175** 1069 (2005)
27. Eddington A S *Nature* **117** 25 (1926)
28. Kunhardt E E, Tzeng Y *Phys. Rev. A* **38** 1410 (1988)
29. McCarthy M P, Parks G K *J. Geophys. Res.* **97** 5857 (1992)
30. Gurevich A V, Milikh G M, Roussel-Dupré R *Phys. Lett. A* **165** 463 (1992)
31. Marshall T C, McCarthy M, Rust W D *J. Geophys. Res. D* **100** 7097 (1995)
32. Marshall T C et al. *Geophys. Res. Lett.* **32** L03813 (2005)
33. Rakov V A, Uman M A *Lightning: Physics and Effects* (Cambridge: Cambridge Univ. Press, 2003)
34. Parks G E et al. *Geophys. Res. Lett.* **8** 1176 (1981)
35. McCarthy M, Parks G K *Geophys. Res. Lett.* **12** 393 (1985)
36. Dwyer J R et al. *J. Plasma Phys.* **81** 475810405 (2015)
37. Dwyer J R, Smith D M, Cummer S A *Space Sci. Rev.* **173** 133 (2012)
38. Gurevich A V, Zybin K P *Phys. Usp.* **44** 1119 (2001); *Usp. Fiz. Nauk* **171** 1177 (2001)
39. Lidvansky A S *J. Phys. G* **29** 925 (2003)
40. Babich L P *Phys. Usp.* **62** 976 (2019); *Usp. Fiz. Nauk* **189** 1044 (2019)
41. Kuzhevskii B M *Moscow Univ. Phys. Bull.* **59** (5) 17 (2004); *Vestn. Mosk. Univ. Ser. 3 Fiz. Astron.* (5) 14 (2004)
42. Dwyer J R *Phys. Plasmas* **14** 042901 (2007)
43. Roussel-Dupré R A et al. "Kinetic theory of runaway air breakdown and the implications for lightning initiation", Report LA-12601-MS (Los Alamos, NM: Los Alamos Natl. Lab., 1993) p. 51
44. Roussel-Dupré R A et al. *Phys. Rev. E* **49** 2257 (1994)
45. Gurevich A V, Zybin K P, Roussel-Dupre R A *Phys. Lett. A* **254** 79 (1999)

46. Babich L P, Bochkov E I, Kutsyk I M *J. Exp. Theor. Phys.* **112** 902 (2011); *Zh. Eksp. Teor. Fiz.* **139** 1028 (2011)
47. Babich L P et al. *J. Geophys. Res.* **117** A09316 (2012)
48. Babich L P et al. *J. Geophys. Res.* **118** 2573 (2013)
49. Bochkov E I, PhD Thesis (Phys. Math. Sci.) (Sarov: Russian Federal Nuclear Center All-Russian Research Institute of Experimental Physics, 2013)
50. Landau L D, Lifshitz E M *Quantum Mechanics: Non-Relativistic Theory* (Oxford: Pergamon Press, 1977); Translated from Russian: *Kvantovaya Mekhanika. Nerelyativistskaya Teoriya* (Moscow: Nauka, 1989)
51. Gurevich A V *Sov. Phys. JETP* **12** 904 (1961); *Zh. Eksp. Teor. Fiz.* **39** 1296 (1960)
52. Heitler W *The Quantum Theory of Radiation* (Oxford: Clarendon Press, 1954)
53. Bethe H A, Ashkin J, in *Experimental Nuclear Physics* Vol. 1, Pt. 2 (Ed. E Segrè) (New York: John Wiley and Sons, 1953) p. 166; Translated into Russian: in *Eksperimental'naya Yadernaya Fizika* Vol. 1, Pt. 2 (Ed. E Segrè) (Moscow: IL, 1955) p. 141
54. Akhiezer A I, Berestetskii V B *Quantum Electrodynamics* (New York: Interscience Publ., 1965); Translated from Russian: *Kvantovaya Elektrodinamika* (Moscow: GIFML, 1959)
55. Kunhardt E E, Tzeng Y, Boeuf J P *Phys. Rev. A* **34** 440 (1986)
56. Kunhardt E E, Byszewski W W *Phys. Rev. A* **21** 2069 (1980)
57. Bakhov K I, Babich L P, Kutsyk I M *IEEE Trans. Plasma Sci.* **28** 1254 (2000)
58. Lehtinen N G, Bell T F, Inan U S *J. Geophys. Res.* **104** (A11) 24699 (1999)
59. Babich L P *High Temp.* **33** 653 (1995); *Teplofiz. Vys. Temp.* **33** 659 (1995)
60. Gurevich A V et al. *Phys. Lett. A* **275** 101 (2000)
61. Peterson L R, Green A E S *J. Phys. B* **1** 1131 (1968)
62. Khaerdinov N S, Lidvansky A S, in *Proc. of the Symp. Thunderstorms and Elementary Particle Acceleration, TEPA-2015, Nor Amberd, Armenia, October 5–9, 2016* (Ed. A Chilingarian) (Yerevan, 2016) p. 35
63. Symbalisty E M D et al. *EOS Trans. AGU* **78** 4760 (1997)
64. Symbalisty E M D, Roussel-Dupré R A, Yukhimuk V A *IEEE Trans. Plasma Sci.* **26** 1575 (1998)
65. Babich L P et al. *IEEE Trans. Plasma Sci.* **29** 430 (2001)
66. Babich L P *J. Exp. Theor. Phys.* **98** 707 (2004); *Zh. Eksp. Teor. Fiz.* **125** 808 (2004)
67. Solovyev A A et al. *Phys. Rev. E* **60** 7360 (1999)
68. Babich L P, Kutsyk I M, in *Proc. of the XXIII Intern. Conf. on Phenomena in Ionized Gases, Toulouse, France, July 17–22, 1997* (Journal de Physique. III, No. 10, Supplement, Eds M C Bordage, A Gleizes) (Les Ullis: EDP Sciences, 1997) p. I-8, Contributed papers, Pt. 1
69. Babich L P et al. *Phys. Lett. A* **245** 460 (1998)
70. Babich L P et al. *Dokl. Phys.* **379** 536 (2001); *Dokl. Ross. Akad. Nauk* **379** 606 (2001)
71. Babich L P et al. *Dokl. Phys.* **394** 35 (2004); *Dokl. Ross. Akad. Nauk* **394** 320 (2004)
72. Babich L P et al. *Plasma Phys. Rep.* **30** 616 (2004); *Fiz. Plazmy* **30** 666 (2004)
73. Dwyer J R *Geophys. Res. Lett.* **30** 2055 (2003)
74. Coleman L M, Dwyer J R *Geophys. Res. Lett.* **33** L11810 (2006)
75. Donskoy E N *Vopr. Atom. Nauki Tekh. Ser. Matem. Model. Fiz. Protsessov* (1) 3 (1993)
76. Gurevich A V, Milikh G M, Roussel-Dupre R *Phys. Lett. A* **187** 197 (1994)
77. Babich L P, Kutsyk I M, Kudryavtsev A Yu, in *Proc. of the XXIII Intern. Conf. on Phenomena in Ionized Gases, Toulouse, France, July 17–22, 1997* (Journal de Physique. IV, Supplement, Eds M C Bordage, A Gleizes) (Les Ullis: EDP Sciences, 1997) p. IV-2, Contributed Papers, Pt. 4
78. Kudryavtsev A Yu, PhD Thesis (Phys. Math. Sci.) (Sarov: Russian Federal Nuclear Center All-Russian Research Institute of Experimental Physics, 2006)
79. Holstein T *Phys. Rev.* **70** 367 (1946)
80. Longmire C L, Longley H J "Improvements in the treatment of Compton current and air conductivity in EMP problems", Report No. 3192T (Springfield, VA: Defense Nuclear Agency, 1973)
81. Babich L P, Donskoy E N, Roussel-Dupré R A *Geomagn. Aeron.* **47** 515 (2007); *Geomagn. Aeronom.* **47** 548 (2007)
82. Dwyer J R *Geophys. Res. Lett.* **32** L20808 (2005)
83. Jackson J D *Classical Electrodynamics* (New York: Wiley, 1975)
84. Mott N F, Massey H S W *The Theory of Atomic Collisions* (Oxford: Clarendon Press, 1965)
85. Taranenko Yu, Roussel-Dupré R *Geophys. Res. Lett.* **23** 571 (1996)
86. Lehtinen N G et al. *Geophys. Res. Lett.* **24** 2639 (1997)
87. Yukhimuk V et al. *J. Geophys. Res.* **103** 11473 (1998)
88. Roussel-Dupre R et al. *J. Atmos. Solar-Terr. Phys.* **60** 917 (1998)
89. Celestin S, Pasko V P *J. Geophys. Res.* **116** A03315 (2011)
90. Celestin S, Wei Xu, Pasko V P *J. Geophys. Res.* **117** A05315 (2012)
91. Kim Y-K, Santos J P, Parente F *Phys. Rev. A* **62** 052710 (2000)
92. Celestin S, Pasko V P *J. Phys. D* **43** 315206 (2010)
93. Dwyer J R *J. Geophys. Res.* **115** A00E14 (2010)
94. Babich L P, Bochkov E I, Kutsyk I M *J. Exp. Theor. Phys.* **112** 902 (2011); *Zh. Eksp. Teor. Fiz.* **139** 1028 (2011)
95. Babich L P et al. *J. Geophys. Res.* **117** A09316 (2012)
96. Babich L P, Bochkov E I *J. Exp. Theor. Phys.* **112** 494 (2011); *Zh. Eksp. Teor. Fiz.* **139** 568 (2011)
97. Kutsyk I M et al. *JETP Lett.* **95** 631 (2012); *Pis'ma Zh. Eksp. Teor. Fiz.* **95** 712 (2012)
98. Kutsyk I M et al. *Plasma Phys. Rep.* **38** 891 (2012); *Fiz. Plazmy* **38** 969 (2012)
99. Dwyer J R, Babich L *J. Geophys. Res.* **116** A09301 (2011)
100. Smirnov B M *Iony i Vozbuzhdennye Atomy v Plazme* (Ions and Excited Atoms in Plasma) (Moscow: Atomizdat, 1974)
101. Lowke J J *J. Phys. D* **25** 202 (1992)
102. Lowke J J et al. *J. Geophys. Res.* **117** D19107 (2012)
103. Babich L P et al. *Geomagn. Aeron.* **44** 254 (2004); *Geomagn. Aeronom.* **44** 697 (2004)
104. Milikh G, Roussel-Dupré R *J. Geophys. Res.* **115** A00E60 (2010)
105. Milikh G, Roussel-Dupré R *J. Geophys. Res.* **116** A08313 (2011)
106. Dwyer J R, Rassoul H K *J. Geophys. Res.* **116** A08312 (2011)
107. Babich L P et al. *Geophys. Res. Lett.* **32** L09809 (2005)
108. Dwyer J R *J. Geophys. Res.* **113** D10103 (2008)
109. Koch H W, Motz J W *Rev. Mod. Phys.* **31** 920 (1959)
110. Daniel R R, Stephens S A *Rev. Geophys. Space Phys.* **12** 233 (1974)
111. Gurevich A V, Milikh G M *Phys. Lett. A* **262** 457 (1999)
112. Gurevich A V, Medvedev Yu V, Zybin K P *Phys. Lett. A* **321** 179 (2004)
113. Carlson B E, Ph.D. Thesis (Stanford: Leland Stanford Junior Univ., 2009)
114. Kutsyk I M, Babich L P, Donskoi E N *JETP Lett.* **94** 606 (2011); *Pis'ma Zh. Eksp. Teor. Fiz.* **94** 647 (2011)
115. Grefenstette B W et al. *Geophys. Res. Lett.* **35** L06802 (2008)
116. Gurevich A V et al. *Phys. Lett. A* **260** 269 (1999)
117. Babich L P et al. *Dokl. Phys.* **47** 1 (2002); *Dokl. Ross. Akad. Nauk* **382** 31 (2002)
118. Babich L P et al. *High Temp.* **42** 1 (2004); *Teplofiz. Vys. Temp.* **42** 5 (2004)
119. Gurevich A V et al. *Phys. Lett. A* **375** 2845 (2011)
120. Rieke F F, Prepejchal W *Phys. Rev. A* **6** 1507 (1972)
121. Cheng G, Liu L *IEEE Trans. Plasma Sci.* **39** 1067 (2011)
122. Gonzáles-Iglesias D et al. *IEEE Electron Device Lett.* **36** 1085 (2015)
123. Townsend J S *Motion of Electrons in Gases* (Oxford: Clarendon Press, 1925)
124. Zelenskii K F et al. *Prib. Tekh. Eksp.* (4) 175 (1969)
125. Zelenskii K F et al. *Sov. Phys. Tech. Phys. Lett.* **5** 95 (1979); *Pis'ma Zh. Tekh. Fiz.* **5** 239 (1979)
126. Babich L P et al. *Prib. Tekh. Eksp.* (4) 8 (2000)
127. Pavlovskaya N G et al. *Prib. Tekh. Eksp.* (5) 29 (1978)
128. Babich L P, Kutsyk I M *High Temp.* **33** 190 (1995); *Teplofiz. Vys. Temp.* **33** 191 (1995)
129. Gurevich A V, Zybin K P, Medvedev Yu V *Phys. Lett. A* **361** 119 (2007)
130. Bokhan P A, Sorokin A R *Sov. Phys. Tech. Phys.* **30** 50 (1985); *Zh. Tekh. Fiz.* **55** 88 (1985)
131. Bokhan P A, Zakrevsky D E *Appl. Phys Lett.* **81** 2526 (2002)
132. Bokhan A P, Bokhan P A, Zakrevsky D E *Appl. Phys. Lett.* **86** 151503 (2005)
133. Wilson C T R *Proc. R. Soc. Lond. A* **236** 297 (1956)
134. Williams E R *J. Geophys. Res.* **115** A00E50 (2010)

135. Dreicer H *Phys. Rev.* **115** 238 (1959)
136. Dreicer H *Phys. Rev.* **117** 329 (1960)
137. Trubnikov B A "Particle collisions in fully ionized plasma", in *Reviews of Plasma Physics* Vol. 1 (Ed. M A Leontovich) (New York: Consultants Bureau, 1965) p. 105; Translated from Russian: "Stolknoveniya chastits v polnost'yu ionizovannoi plazme", in *Voprosy Teorii Plazmy* Issue 1 (Ed. M A Leontovich) (Moscow: Gosatomizdat, 1963) p. 98
138. Schonland B F J *Proc. R. Soc. Lond. A* **118** 252 (1928)
139. Schonland B F J *Proc. R. Soc. Lond. A* **130** 37 (1930)
140. Schonland B F J, Viljoen J P *Proc. R. Soc. Lond. A* **140** 314 (1933)
141. Appleton E V, Bowen K G *Nature* **132** 965 (1933)
142. Macky W A *Proc. Cambr. Philos. Soc.* **30** 70 (1934)
143. Halliday E G *Proc. Cambr. Philos. Soc.* **30** 206 (1934)
144. Clay J, Jongen H F, Aarts A J *Physica* **18** 801 (1952)
145. Hill R D *J. Geophys. Res.* **68** 6261 (1963)
146. Shaw G E *J. Geophys. Res.* **72** 462 (1967)
147. Fleisher R L *J. Geophys. Res.* **80** 5005 (1975)
148. Whitmire D P *Lett. Nuovo Cimento* **26** 497 (1979)
149. Shah G N et al. *Nature* **313** 773 (1985)
150. Babich L P, Kutsyk I M, in *VII Konf. po Fizike Gazovogo Razryada. Samara, 21 – 24 Iyunya 1994 g., Tezisy Dokladov* (Proc. of VII Conf. on Physics of Gas Discharges, Samara, RF, 21–24 June, 1994) (Samara, 1994) p. 23